

Rebuttal: 'Sea-level response to melting of Antarctic ice shelves on multi-centennial time scales with the fast Elementary Thermomechanical Ice Sheet model (f.ETISh v1.0)' by Frank Pattyn

I would like to thank both referees for their thorough assessment of my submitted paper. Thanks to their thoughtful comments, I made several improvements to the model and reran the experiments again. I also added extra experiments in line with the concerns of the referees. The experiments on millennium time scales were omitted, because they did not add anything significant to the paper that would become needlessly too long otherwise. In view of the model changes, the appendices have been adapted as well. The major model changes are:

- The complete temperature field is now calculated (based on SIA shape functions for the different advection terms). Therefore, the temperature field includes now horizontal advection and is also correctly time-dependent. Thermomechanical coupling has not been altered (2d coupling)
- The effective viscosity in the SSA equations has not been approximated, but is now iteratively solved. As a consequence, basal drag is not linearized (made function of driving stress) any longer.
- The Coulomb friction law has been used in conjunction with the TGL flux condition at the grounding line, to make it coherent. This means that the optimization procedure has been adapted and friction coefficients ($\tan(\phi)$) are optimized during initialization.

1 Anonymous Referee 1

Received and published: 26 February 2017

1.1 General comments:

This paper presents a thorough and clear description of a new ice sheet model, akin to hybrid dynamics SIA/SSA models currently used for Antarctica, but with some reasonable and innovative simplifications so it is computationally

fast. The model is implemented in MATLAB and will be a useful tool to engage students in teaching and workshop environments, as well as being capable for many research applications.

In this paper the model is thoroughly tested against established benchmarks (EISMINT, MISMIP) and validated vs. modern Antarctica. Sensitivity experiments of Antarctic retreat for simple warming perturbations are described. One important result is that much larger grounding line retreat is obtained with a Coulomb-friction based parameterization of grounding line flux, compared to that based on power-law sliding, but further testing may be desirable (see below).

I would like to thank the referee for this early and very detailed review, which gave me ample time to check out in more detail the concerns that were raised.

1.2 Specific comments:

(1) The treatment of ice temperatures is based on classic vertical profile equilibrium solutions which allow for vertical ice velocity, and then time lagged with an e-folding relaxation towards these solutions at each grid point. The timescale of the e-folding lag is based reasonably on the local Peclet number (pg. 17, eq. 42). This is probably the most drastic simplification from other 3-D hybrid models, and neglects horizontal advection (which cools mid-level interiors as cold surface ice is advected downwards and outwards, and cools the cores of ice shelves supplied by flow across thick grounding lines. A fairly arbitrary compensation for this lack of cooling is attempted by reducing the strain heating (pg. 17, line 6). This simplified temperature treatment is evident in the benchmark intercomparisons in the Appendices, where basal temperature is the only field with poor results.

As a suggestion, perhaps basic horizontal temperature advection could be added to the model, ust by adding an additional term in Eq. (41): $\dots + u \frac{dT}{dx} + v \frac{dT}{dy}$ with (u,v) given by (12) and T is the column mean temperature. That probably would not require much CPU or slowdown of the model.

The referee is correct that this is probably a drastic simplification. It was also one of the first simplifications I made to the model. However, my major concern was not so much omitting horizontal advection, which it is relatively well counterbalanced by frictional heating, as the EISMINT I experiments show. I admit that this has not so much of a physical basis and the coupled experiments in EISMINT II were not very convincing. My major concern with this approximation is related to the time-dependent evolution of the temperature, which in its current form is not suited for paleo-climatic studies. Therefore, I revised the temperature calculation completely by solving the time-dependent thermodynamic equation in three dimensions, similar to Pattyn (2010). It includes besides vertical diffusion and advection also horizontal advection, internal heating and frictional heating. In order to improve calculation speed, the whole subroutine was optimized and given the stability of the numerical scheme, the temperature field is only updated every 10 to 20 iterations.

Nevertheless, a couple of simplifications remain: (i) the temperature field is calculated using shape functions for both horizontal and vertical velocity (Hindmarsh, 1999) as well as for velocity gradients based on the deforma-

tional SIA velocity for a vertically-integrated value of A ; (ii) the flow parameter A is still determined for a given column fraction. Despite these simplifications, the model is now in agreement with both the EISMINT I (Huybrechts et al, 1996) and EISMINT II (Payne et al, 2000) experiments. Even the 'unstable' basal temperature patterns according to some experiments in EISMINT II are now reproduced (and more results are presented in the Appendix).

Given this concern, I suggest that a map of the models basal temperatures for modern Antarctica be shown, and compared with existing model and data based maps (of which the author is a leader).

It was my mistake not to have shown the basal temperature field for the Antarctic ice sheet, especially since the temperature calculation was a major approximation. The basal temperature field was different from the one given in Pattyn (2010), as it does not include the optimization of geothermal heat flow using observed temperature profiles and subglacial lake distribution. However, it was more in line with other basal temperature fields obtained by other model studies (Pollard and DeConto; Huybrechts, ...), which gave me confidence in the approximation. A comparison between the new basal temperature field and the approximation of the submitted manuscript reveals also the same pattern, which demonstrates that the initial approximation was quite well representing the ice-sheet temperature field. The basal temperature field is now included as a figure in the manuscript.

(2) It is puzzling why the inverse procedure for basal sliding coefficients (p. 23-24, Fig. 5) yields quite large errors in surface elevation (200 m) in some regions of the interior East Antarctic plateau. The inverse procedure should reduce them to 10's m (Pollard and DeConto, 2012b) (even if the bed elevations are in error, model or observed, cf. pg. 24 line 19).

Thanks for remarking this. I have been looking into this in more detail. It seems that the use of the regularization term (smoothing) improves the fit near the borders (compared to Pollard and DeConto, 2012b), but increases the error in the interior. I adapted the regularization scheme so that it only applies for marine boundaries (bedrock below sea level). This way the fit is better in the interior as well as close to the boundaries. This has also been stated in the manuscript.

Perhaps these larger errors are due to regions of the bed erroneously being frozen. In frozen basal regions the inverse procedure cannot reduce the model's surface elevation errors. So this is an additional reason to request a basal-temperature map.

Some errors are due to frozen zones, since the optimization procedure does not perform across these zones. However, as shown by the similarity between the basal temperature fields (old and new), this seems not due to a mismatch of frozen/temperate areas.

nb: "ice thickness", pg.24 line 1, should probably be "ice surface elevation".

Indeed it is. Corrected.

(3) One important result is the greater grounding line retreat with TGL (Coulomb-friction based grounding line flux parameterization, Eq. 25), vs SGL (power-law sliding based, Eq. 23). All experiments shown use power-law sliding (Eq. 15) for the interior grounded ice, and none use Coulomb sliding (Eq. 21). My concern is that the combination of TGL with power-law interior sliding is not compatible, and the mismatch in the physics may lead to spurious behavior

in grounding zone regions. (The discussion on pg. 13, lines 24-27 may be relevant).

To address this concern, I would request additional runs be made with Coulomb friction law (Eq. 21) and the TGL grounding line parameterization. This would ideally also involve re-doing the optimization spin-up for basal properties, which may still be feasible by changing ϕ (till friction angle) instead of A_b in Eq. (55). Alternatively, the combined Eq. (22) could be used instead of (21).

This has been looked into with greater detail. First of all, I don't completely agree with the non-compatibility between the Coulomb boundary condition at the grounding line and the Weertman sliding law inland from it. As shown in Tsai et al (2015), the Coulomb friction leading to vanishing effective pressure at the grounding line is a physically correct condition that can be used independently of the basal characteristics of the inland ice sheet. The crossover from Coulomb conditions at the grounding line to power-law conditions inland is a very narrow transition zones (with exception of perhaps the Siple Coast region where streams experience a very low drag for a wide area). The contact with the ocean will always be influenced by marine sediments (characterized by a till friction angle), which makes the combination of both conditions (power law sliding for the ice sheet and Coulomb friction for the grounding line) valid. To demonstrate this, I carried out different experiments with varying values of till friction angle at the grounding line. Only for high till friction angles $\phi > 50^\circ$ does the grounding-line sensitivity diminish, but still remains more sensitive than the grounding line conditions according to the power-law sliding. Moreover, I also included an optimization scheme for the Coulomb friction law (on the suggestion by the referee). This optimization changes $\tan(\phi)$ (and not ϕ as the referee suggested). The resulting fit is less well than with the power law, but it makes ϕ vary between 2- 70°. Higher/lower values would be really non-physical. The resulting response is obviously less sensitive than with the one where ϕ is prescribed, but still more sensitive than the power-law sliding and Schoof-condition at the grounding line. As a comparison, the combination of Weertman sliding and TGL condition are also presented. This reveals that the most dominant factor in the sensitivity is the TGL condition, not the type of sliding/friction inland.

(4) The use of driving stress instead of basal stress in the basal sliding law to avoid iterations (pg. 10, Eqs. 15,16) is one of the features used to speed up the model. But maybe the 20% of the ice sheet where driving stresses are not essentially balanced by basal stresses (p.10, lines 16-17) are in important regions such as ice streams. This concern could be addressed by one sensitivity test in which the approximation in Eq. (16) is not made (requiring expensive iteration).

Basal sliding with the hybrid model IS a function of basal shear stress (or basal drag). So this effect of driving stresses being balanced by driving stresses is not correct. The equations are correct for $m = 1$. However, for a power law with $m = 2$, for instance, Eqs 15,16 make the sliding law more viscous than plastic by introducing the term τ_{u_d} . However, the revised model now properly calculates the effective viscosity in the SSA equations (see response to referee 2), hence requiring iteration, so that this approximation is not made anymore.

(5) The subglacial water pressure p_w in Eqs. (19) and (20), pg. 11, is assumed to

depend on elevation minus sea level, which is a common step in many models. But it is hard to see how the subglacial water system can sense hydrostatic pressure from the ocean at all, more than 100 or 200 km inland from the grounding line.

I know. That is exactly why I did only use the Coulomb condition at the grounding line, because here the effective pressure is zero by definition. Given the fact that I now have introduced the optimization of the Coulomb friction law for the interior ice sheet, the approximate definition of p_w can be questioned, but has also been used by several other authors. As I already mentioned in the manuscript, a subglacial hydrology model would be more appropriate and physically correct.

Technical points:

p.3, Fig. 1. I suggest indicating in the figure that sea level is at $z = 0$, as seems to be required in Eqs. 18, 19 and 20. And z_{sl} must = 0 (p.7, line 3). Alternatively, replace b throughout p.11 with $b - z_{sl}$.

I replaced b by $b - z_{sl}$ as suggested by the referee

p.7, Eq (2). More correctly, $v_{sia} = v_b + \dots |\tau_d|^{n-1} \tau_d$ p.9, line 7 et seq. To avoid confusion, say explicitly that τ_f is the free-floating stress, used later in Eq. (24) as well as in (3),(4) via eta in (11).

Corrected

p.11, line 3: Why might the friction angle phi be a function of bedrock elevation, physically? p.12, lines 6-7. The sentence " However, expressed as a ..." is unclear to me.

This sentence has been removed.

p.13, lines 7-10. Here, it might be helpful to mention that a staggered grid (Arakawa C) grid is used as shown in Fig. 2.

Done

p.14, Eq. (27). Say that this is only applicable for SIA advection.

Done; I explicitly wrote that for the grounded ice sheet according to the SIA model this equation is written as a diffusion equation for ice thickness.

p.14, lines 11-22: Say whether this 'maximum strain check' is applied everywhere, on ice shelves, or just at the grounding line.

I wrote that this is checked at the grounding line.

p.17, line 24 and Eq.(42). Say that this is vertical advection (not horizontal).

This equation has been removed due to the changes in the temperature calculation.

p.18, line 13. Specify the value of E_f used for ice shelves.

Done. It is 0.5.

p. 19, lines 1 and 10. Say that the equilibrium bed topography and loads (b_{eq} , h_{eq} , hw_{eq}) are taken from modern observed fields (Bedmap2), if that is the case.

Done

p.19, line 18. Say that the local numerical integration is for Eq.(38) (I think).

This equation has been removed due to the changes in the temperature calculation.

p.19, line 24. Iterations are also eliminated due to the approximation of driving = basal stress in Eq. (16).

This doesn't apply anymore.

p.21, line 24. A simple one-valued PDD is ok for modern Antarctica with little surface melt. But the surface melt treatment will need improving (snow vs.

ice, refreezing, etc.) to represent greatly increased surface melt around the Antarctic margins in warm future climates.

I agree. A similar approach was adopted by Pollard and DeConto (2012). However, on the time scales I consider, surface melt has not a decisive impact. Refreezing would lead to a higher retention of the melt water, hence limit the impact of surface melt even more. It will certainly become more important if other ice shelf disintegration processes, such as hydro-fracturing, would be taken into account.

p.22, line 9. Say where ocean temperatures T_{oc} are obtained from. Actually it seems that Eq. (53) and T_{oc} are not used in any experiments here, for which the melt rate M is simply prescribed region by region (p.30, lines 17-19).

This section has been removed. It is mentioned in the manuscript that the mechanism is included in f.ETISh, but that only constant values of melt are applied to the ice shelves in this paper.

p.22, line 16. Eq. (53) produces higher melt rates closest to the grounding line not because it's quadratic, but because the freezing temperature T_{fo} decreases with depth (noting h_b in Eq. (54) is negative below sea level).

This section has been removed (see above).

p.23, line 1. Perhaps change "further constrained by" to "driven by".

Done.

p.25, line 14. Change "back by" to "back to". p.27, line 3. Perhaps change to "of the model and the approximations..."

Done.

p.28, Fig. 9 caption, 2nd line. Remove "(a)".

Done. Replaced by 'years' to make clear what the units are.

p.30, line 8. Perhaps change "provoked" to "applied".

Done.

p.30, line 10. *Why* are TGL runs characterized by higher driving stresses?

Referee 2 made a whole point of the driving stresses and I agree that the reasoning should be the other way around. The origin of the high driving stresses is that for a same ice flux, surface gradients must be larger with TGL. See rebuttal to referee 2 for more details. The figure of driving stresses has been removed.

p.31, Fig. 11 caption, 2nd line. Say "Atmospheric temperature forcing is..."

Done.

p.34, line 22. Mention that the agreement with the benchmark(s) is shown in the Appendices.

Done.

p.34, lines 27-28. Change to "Despite the approximations, the results of thermomechanical coupling of ice sheet flow are also in good agreement with the EISMINT benchmark..."

This has been changed, since the thermodynamical part of the model has been improved.

pg.34, line 29: Perhaps change to "compared to the other benchmarks,"

Rephrased.

pg.35, lines 7-8. Change to "requires membrane stresses at both sides of the grounding line to be resolved with sufficient detail (Schoof 2007a),"

Done.

pg.35, line 10. Mention in parentheses that this rule is that on pg. 13, lines 9-10.

I made a reference to the specific section.

pg.35, lines 28-29. Change to "Direct comparison is not possible with recent studies of Antarctic ice mass loss that are forced by atmosphere-ocean models following so-called RCPs (Representative Concentration Pathways). Direct comparison with the SeaRISE...

Done.

pg.36, line 8. Perhaps describe in a few words what "RCP8.5 amplification" is. **This paragraph in the discussion has been deleted, since the millennium time scales have been left out.**

pg.36, lines 28-29. Perhaps change to "with the exception of grounding-line zones with small-scale bedrock variability, where grounding-line response to atmospheric and oceanic forcing is sensitive to spatial resolution."

Done.

pg.37, line 8. The "dominance of ocean forcing" in this paper relies on the absence of physics such as hydrofracturing that occur due to large increases in surface melting around the margins. With RCP8.5 at least, there will be a huge increase in the latter within ?100 to 200 years, which could affect the ice sheet in unexpected ways.

Indeed. This has been rephrased and at several places in the manuscript it has been mentioned that hydro-fracturing (as atmospheric forcing) may induce a much larger impact.

Appendices, figure captions A2 to A5. It would help to specify the benchmark experiment (EISMINT I or II, MISMIP, etc) in each caption, especially if the figures appear on different pages than the relevant text.

Done.

2 S. L. Cornford (Referee)

Received and published: 3 April 2017

This manuscript presents the details and some experiments carried out with a new ice sheet model code (f.ETISH), which is designed to represent the major process in near future ice sheet dynamics (e.g changes in grounding line flux due to ice shelf thinning) well enough to be meaningful but not requiring fine spatial resolution and the attendant computational cost. The new model is similar in that respect to the model of Pollard and DeConto (sans cliff collapse), but makes some additional approximations for the sake of speed. Is this a useful new model? Perhaps. It could be very well suited to long-term integrations, though that is equally true of Pollard and DeConto. It could be useful in large ensemble construction, where I think it makes a better job of representing the physics than (say) Ritz et al 2015. It does seem to contain new but not really well justified approximations in rheology and temperature structure, but given that these things are largely unknown and must be tuned anyway, that may not be very serious problem. The paper is a bit rambling in parts (maybe this review is too), especially the model description and the discussion. Sometimes it includes expressions that are well known, then ignores them, e.g the effective viscosity is treated this way, and the discussion of Coulomb friction laws seem to be a bit extraneous too. I think it really does need a substantial review and edit.

I should like to thank Stephen for this thorough review and I will try to give a non-rambling response to his queries. A series of improvements to the model have been made and are detailed in my response to Referee 1. I will therefore refer to my response to that referee for points that were already raised and briefly mentioned in my introduction to the rebuttal. Given the changes, the model description has been shortened as well, and unnecessary items have been discarded.

2.1 General Comments

One message of the paper seems to be that treating the flux across the grounding line according to Tsai (TGL) rather than Schoof (SGL) dramatically increases the retreat rate. This could be because Tsai depends on a higher power of flotation thickness (more acceleration of retreat on retrograde slopes), but might to some extent be attributed to the addition of another free parameter ($\tan \phi$). Given that the model is so quick, maybe some runs with larger $\tan(\phi)$? Looking at eq 18, for much of WAIS where bedrock elevation, is < -1 km, $\tan(\phi)$ is around $\tan(\phi_{\min}) = 0.2$. What happens if $\tan(\phi) = \tan(\phi_{\max}) = 0.5$ - presumably we see about half the rate of SLR? On the same note, TGL is double sided - flux increases more quickly with grounding line thickness, which would mean that the grounding line accelerates more readily in unstable configurations (retrograde slopes, without buttressing) but decelerates more readily in stable configurations (prograde slopes) - and the formula for $\tan(\phi)$ should amplify this effect somewhat. The East Antarctic results in section 5 seem to differ from this, with the introduction of TGL leading to retreat over prograde slopes (Totten, Wilkes Basin, Recovery Glacier a little upstream from the present day GL) where there was little in the results with SGL.

See my response to Referee 1. Higher values of ϕ lead to lower sensitivity of grounding line retreat, but it is not half the amount of SLR for a doubling of ϕ . Even for very high values of $\phi > 70^\circ$, this leads still to a mass loss that is significantly higher than for the Schoof-condition. I added this in the text. I included also an optimization of the Coulomb friction law, whereby values of till friction angle are optimized, hence also at the grounding line. All experiments with the TGL condition are now run with the Optimized Coulomb friction law. For the 'ice-shelf removal' experiment, the combination Weertman sliding-TGL was added as a comparison, showing that the higher sensitivity is clearly related to TGL. In that section, it is explained in detail what the origin of the difference is (related to the remarks of the referee on driving stresses).

I am suspicious of approximating the effective viscosity by assuming that the stress that enters it is that of an free floating 1HD shelf (eqs 8 and 9). Can this really be a good approximation in buttressed ice shelves like (e.g) PIG, Amery, Totten, where there are regions with little along flow stretching, but strong lateral strains? To me, the example in appendix D is not especially convincing - cross flow gradients are too low, and the flow field too smooth. This might not be a big error in itself, since at higher melt rates all that will matter is the TGL / SGL with no buttressing, but a more convincing test is needed. Why not re-run a middle melt-rate experiment with the normal nonlinear rheology?

I calculated the effective viscosity now as it should be (according to eq. 5).

It also required iteration, but this doesn't seem to slow down the model as much. The resulting effective viscosity is different (as would be expected), and in few cases the response as well. However, the major sensitivity of the model still remains with the treatment of the boundary conditions at the grounding line (Tsai vs Schoof), and the magnitude of change is comparable to the results presented in the initial manuscript.

Given that there is a well known test - MISMIP+ - with published results that include both the Tsai friction rule and ice shelf buttressing - why not test f.ETISH against that?

It is of course an interesting idea that will require quite some work and also falls outside the scope of the present paper. In term, it is envisaged to perform those tests, but it will require major changes in the model code with respect to the adaptation of the boundary conditions.

2.2 Specific comments

2.2.1 Abstract

(and elsewhere) 'The higher sensitivity [in the case of the Tsai 2] is attributed to higher driving stresses upstream from the grounding line.' I'm not sure this makes sense - and I suggest it is at least partly the other way round. Because $q(\text{TGL})$ is larger than $q(\text{SGL})$, but both are only applied at the GL, dh/dx is going to be bigger at the GL for TGL with all else being equal. The same - plain Weertman - friction law is applied upstream.

I corrected this (here and elsewhere in the manuscript). The higher sensitivity is attributed to higher ice fluxes at the grounding line due to vanishing effective pressure.

2.2.2 Section 1

'The majority of these interactions demonstrate non-linear behaviour due to feedbacks, leading to self-amplifying ice mass change.' -> 'Some of these . . .'

Corrected.

'thicker ice grounded in deeper water would result in floatation, increased ice discharge, and further retreat within a positive feedback loop.' -> thicker ice grounded in deeper water would result in increased ice discharge, and further retreat within a positive feedback loop.'

Corrected.

. . . based on boundary layer theory (...Ritz et al., 2015. . .). I don't think the Ritz et al., 2015 GL is based on boundary layer theory, does it? But imposes retreat rates sampled from some sort of probability distribution.

Indeed, you are right. The use of the BLT in Ritz is not in the same way as in Pollard. I removed the reference.

2.2.3 Section 2.1

'The main advantage of SIA is that the velocity is completely determined from the local ice-sheet geometry.' That might be called the main disadvantage too.

Well, it makes the computation rather simple for a rather large domain (interior ice sheet) for which this approximation is valid. Anyway, I removed the sentence.

SSA+SIA : 'a simple addition still guarantees a smooth transition' - why wouldn't it? SIA isn't smooth in the same way as SSA, but so long as the surface elevation is smooth, it will be. More to the point, is this a good approximation? How about at the ice shelf calving front, where $\text{grad}(s)$ is large, there is no basal stick and SIA makes no sense? I don't think Schoof and Hindmarsh 2010 gives us a reason to think that SSA+SIA is any more sensible than plain SSA.

I don't understand this quite well. The addition of both is done for the grounded ice sheet alone. The difference with the Schoof and Hindmarsh approach is that the effective strain doesn't take into account vertical shearing. In the ice shelves, the SIA velocity is always kept zero (no shearing). I made this clear to avoid confusion.

'Basal velocities in the hybrid model are defined through a friction power law, where' Basal traction, no? The velocity is related but depends also on viscous stress at least close to the GL in the SSA+SIA case.

2.1.7. The Coulomb friction law plays no part in the results, except for its involvement with the Tsai flux. I suggest cutting this (longish) section 2.1.5 entirely and describing $\tan(\phi)$ in 2.1.7

This has been changed. The experiments are now run with the Coulomb friction law as well. I therefore kept this section in. Given the changes in the model, the description is shortened elsewhere anyway.

'where 'spy' is the number of seconds per year' Why switch units mid-expression? Eq 25: What value does $\tan(\phi)$ tend to take?

I removed this. The units are everywhere added when appropriate.

2.2.4 Section 2.2

eq 28: should be an inequality? $h_{du}/dx \leq AhTf$ (ie the maximum stretching is in free shelves) 'Ritz et al. (2015) use a slightly different prescription, but sensitivity tests showed that the extra terms in the mass conservation equation can be safely dropped, rendering the maximum strain check therefore independent of velocity gradients.' Which terms? The terms that have been dropped are $\partial u/\partial x$ and $\partial v/\partial x$, both of which involve thickness gradients and are typically positive, so in fact $dh/dt \geq a \cdot M \cdot h(du/dx + dv/dy) \leq a \cdot M \cdot 2AhTf$ And you assume dh/dx is negligible?

Given the changes made to the SSA description, this condition has been taken in its original form. Therefore, it is only mentioned in the text and not specified in an equation. The reader is referred to Ritz et al (2015).

'However, to compensate for the absence of horizontal advection in the model, only a fraction $f_s = 0.25$ of the total strain heating amount was added. This value is determined from the EISMINT benchmark experiments (Appendix A).' Should this value not depend at all on ice speed? Is EISMINT a sufficient test of this quite different dynamics?

Given the changes in the thermodynamics, this parameter has become superfluous.

2.2.5 Section 2.3

OK, these expressions come from others. But are they justified in any way.

2.2.6 Section 2.4

Eq 33. Has some horizontal advection - needed to eliminate $T \, dw/dz$ and reduce vertical advection to $w \, dT/dz$, but neglects horizontal temperature variation? An even simpler solution might be possible if the conservative advection $d/dz(wT)$ was used and all horizontal transport neglected. Or did I miss something?

Horizontal advection is now taken into account.

How is eq 41 based on the Peclet number? So τ is advection dominated when Pe is large and diffusion dominated when $Pe \ll 0$, but does the code actually compute some function of Pe ?

This has become obsolete now.

2.2.7 Section 2.6

Why solve eq 46 with BiCGStab? What preconditioner is used? ILU(0)? UMF-pack is MATLAB's default sparse solver, I think, and I guess the matrices are all small (coarse grid), so if there are large ice shelves (so A becomes poorly conditioned) this direct solver might be the better choice (or not)

The standard sparse Matlab solver works very well, but the use of bicgstab enables to speed up the process. I think that many things can be improved in future on behalf of the numerical solvers. I already optimized the initialization with reduced sparse matrix systems (taking into account only the grid points where ice thickness changes over time). I have a PhD student looking into this matter for the moment.

2.2.8 Section 4.

'This further improves the final fit compared to the non-regularized case.' which is not normally the case with regularization - typically regularization results in worse (or no-better) fit to the observations for the sake of a smoother (or more plausible in some other sense) solution.

Referee 1 made the same remark. Indeed, it should give worse results. However, it makes the results worse for the interior ice sheet, but improves it for the marine borders. Therefore, I adapted the algorithm so that regularization is applied in the marine sectors only. I modified this in the text.

2.2.9 Section 5.1:

Sorry to bring this up, but Cornford et al 2016, Annals of Glaciology <https://doi.org/10.1017/aog.2016.13> does a rather similar experiment (all-Antarctic response to sustained ice shelf removal), with a sub-km model, and the Weertman sliding results could be compared.

Thank you very much for pointing me to that paper (with the unfortunate typo). Indeed, the results of that paper are somehow comparable to removing ice shelves, although that not all ice shelves are removed (once ice thickness smaller than 100m, the shelves remain). I ran these experiments as well and added the results in the paper under the section 'sub-shelf melting'. I made sure that I corrected the typo and ran the model with the melt rates that were actually used (not the ones that are described in the experimental description). A comparison with the results in Cornford et al (2016)

is made at the end of the section of sub-shelf melting. The SGL experiments are quite comparable to this study, albeit that the timing of retreat in the different drainage basins is different in some places. It is explained why.

Is the rate of SLR labelled incorrectly in fig 10?

Figure has been removed.

2.2.10 Section 5.2

'Melting is not allowed to be spread out across the grounded part of the 20 ice sheet near the grounding line as is done in some models (Feldmann et al., 2014; Golledge et al., 2015)'. Note that Feldmann and Golledge are not really trying to spread the melting about, they are just applying some melt to finite area grid cells whose centers are grounded but whose neighbours are floating, estimating a floating fraction by interpolating the thickness above flotation. This sounds pretty innocuous - even sensible - in which context the sentence above sounds like the wrong choice. Of course we know it is not the wrong choice, but maybe say something about why?

I rephrased this: "Melting is only applied to fully floating grid cells, without taking into account the fractional area of grounded grid points that are actually afloat, as done in a few studies (refs)." Whether this is wrong or not, I leave inbetween. I just stated that what the difference is in melt treatment compared to other models.

'[SLR] determined from the change in ice volume above flotation, hence do not represent the total grounded ice mass loss' Seems like an odd comment - how else would it be computed ? It makes me wonder if the section 5.1 SLR is from total mass loss (indeed the text of section 5.1 suggests that, 'the total mass loss for TGL is three times as large compared to SGL, i.e., a contribution to sea-level rise of 12 m ...'), when I assumed it had been computed from VAF

I agree it is ambiguous. I corrected this at the different places. I also abbreviated sea-level rise to SLR at the different places in the manuscript.

Fig 11. Although the 'thick lines (SGL), thin lines (TGL)' plot works for the large delta M, I can't make so well out what is going on at small delta M. how about thin lines with a few symbols (say, circles, squares). Or drop the $dM = 10$ m/a results?

It has been made easier now, since fewer experiments have been made.

Fig 12. To my mind, at least one more grid spacing (there are some runs 16km. right?) to be able to say much about mesh dependence. You can't test convergence at all with just two, you need to show that results are getting closer to one another as $dx \rightarrow 0$

This is a very good remark. The new series of experiments show that spatial resolution influences the timing of grounding line retreat in the different drainage basins, less so the total amount of SLR (at least over longer periods and for high forcings). However, it is not expected that convergence should be obtained when resolution increases, unless one uses the same bedrock data set at each time (i.e., at high resolution an interpolated bedrock map of the low resolution experiment). Since at higher resolutions the bedrock shows a different variability (small bed rises, for instance), grounding-line migration will be influenced by this. However, having said this, I carried out 4 new experiments with melt perturbations (without dT) at 16km resolution. The results are extremely similar to 25 km, showing that the model

has reached convergence. At very high resolutions (<5 km), however, the results could be different for the reason I explained above, but the purpose of the f.ETISH model is to provide model runs at lower spatial resolution that capture the essence in marine ice dynamics.

2.2.11 Section 6

'Another major difference pertains to the marine boundary, with a novel implementation of the grounding-line flux condition according to Tsai et al. (2015), based on a Coulomb friction law (TGL)' 'novel' seems a bit strong, given that Tsai derived the flux formula, and the implementation replaces a very similar formula (SGL) in an overall method to modify the Schoof flux to include buttressing due to Pollard.

I rephrased this.

p35 'unless sub-grid grounding-line parametrizations are used that generally allow for grid sizes of 10 km (Feldmann et al., 2014).' Personally I think this claim in Feldmann 2014 is not supported by the results, which are better with the sub-grid scheme, but still need $dx = 1$ km. Why should we believe that results in one idealized problem should be widely true?

True. I removed the claim of 10 km.

'Nevertheless, comparison with high-resolution SSA and hybrid models show that while differences in transient response exist, results are in overall agreement with the other models (Pattyn and Durand, 2013).' That really was not the message I took from Pattyn and Durand 2013, at least regarding the transient.

I removed this sentence.

'as the ice-sheet profiles 'taper off' towards a flattening upper surface, contrary to the power-law case,' - this happens to some extent in the power law case too, depending on the scale length for viscous stresses transmission.

But for TGL, it is always the case, even for small transition zones.

'(so-called 'aggressive' grounding line in PISM).' Does Gollede really call it 'aggressive' in that paper. I remember him saying it in a talk. Anyway, why not say what it is: a type of numerical error (aggression $\rightarrow 0$ as $dx \rightarrow 0$) rather than something that could be seen as physics.

No, Gollede does not call it aggressive in the paper, but mentions it in presentations. I removed this now. In any case, this section has been removed since the experiments on longer time spans have been omitted.

Sea-level response to melting of Antarctic ice shelves on multi-centennial time scales with the fast Elementary Thermomechanical Ice Sheet model (f.ETISh v1.0)

Frank Pattyn¹

¹Laboratoire de Glaciologie, Department of Geosciences, Environment and Society, Université libre de Bruxelles, Av. F.D. Roosevelt 50, B-1050 Brussels, Belgium

Correspondence to: Frank Pattyn (fpattyn@ulb.ac.be)

Abstract. The magnitude of the Antarctic ice sheet's contribution to global sea-level rise is dominated by the potential of its marine sectors to become unstable and collapse as a response to ocean (and atmospheric) forcing. This paper presents Antarctic sea-level response to sudden atmospheric and oceanic forcings on multi-centennial time scales with the newly developed *fast Elementary Thermomechanical Ice Sheet* (f.ETISh) model. The f.ETISh model is a vertically integrated hybrid ice sheet/ice shelf model with ~~an approximate implementation of ice sheet thermomechanics~~ vertically-integrated thermomechanical coupling, making the model two-dimensional. Its marine boundary is represented by two different flux conditions, coherent with power-law basal sliding and Coulomb basal friction. The model has been compared to ~~a series of~~ existing benchmarks.

Modelled Antarctic ice sheet response to forcing is dominated by sub-ice shelf melt and the sensitivity is highly dependent on basal conditions at the grounding line. Coulomb friction in the grounding-line transition zone leads to significantly higher mass loss in both West and East Antarctica on centennial time scales, leading to 21.5 m sea level rise after 500 year for a ~~moderate-limited~~ melt scenario of 20-10 m a⁻¹ under freely-floating ice shelves, up to 6 m for a 50 m a⁻¹ scenario. The higher sensitivity is attributed to higher ~~driving stresses upstream from ice fluxes at~~ the grounding line due to vanishing effective pressure.

Removing the ice shelves altogether results in a disintegration of the West Antarctic ice sheet and (partially) marine basins in East Antarctica. After 500 years, this leads to a 4.55 m and a ~~12.2~~16 m sea level rise for the power-law basal sliding and Coulomb friction conditions at the grounding line, respectively. The latter value agrees with simulations by DeConto and Pollard (2016) over a similar period (but with different forcing and including processes of ~~hydrofracturing~~ hydro-fracturing and cliff failure).

The chosen parametrizations make model results largely independent of spatial resolution, so that f.ETISh can potentially be integrated in large-scale Earth system models.

1 Introduction

Projecting future sea-level rise (SLR) requires ice sheet models capable of exhibiting complex behaviour at the contact of the ice sheet with the atmosphere, subglacial environment and the ocean. ~~The majority~~ Some of these interactions demon-

strate non-linear behaviour due to feedbacks, leading to self-amplifying ice mass change. For instance, surface mass balance interacts with ice sheets through a powerful melt–elevation feedback, invoking non-linear response as a function of equilibrium line altitude, such as a positive feedback on ablation that can be expected as the ice-sheet surface becomes lower (Levermann and Winkelmann, 2016). This feedback is also the main reason for the threshold behaviour of the Greenland ice sheet on multi-millennial time scales (e.g., Ridley et al., 2010). Typical for these self-amplifying effects is that they work both ways: the melt–elevation feedback equally allows for ice sheets to grow rapidly once a given threshold in positive accumulation is reached, resulting in hysteresis (Weertman, 1976).

Another powerful feedback relates to the contact of ice sheets (especially marine ice sheets with substantial parts of the bedrock lying below sea level) with the ocean. Mercer (1978) and Thomas (1979) identified marine ice sheet instability for ice sheets where the bedrock dips deeper inland from the grounding line (retrograde bed slopes), so that increased (atmospheric/oceanic) melting leads to recession of the grounding line. This would result in the glacier becoming grounded in deeper water with greater ice thickness. Since ice thickness at the grounding line is a key factor in controlling ice flux across the grounding line, thicker ice grounded in deeper water would result in ~~floatation~~, increased ice discharge, and further retreat within a positive feedback loop. Early numerical ice sheet models failed to reproduce this feedback due to the lack of physical complexity (e.g., neutral equilibrium; Hindmarsh, 1993) and the poor spatial resolution to resolve the process of grounding line migration (Viel and Payne, 2005; Pattyn et al., 2006). A major breakthrough was provided by an analysis of grounding line dynamics based on boundary layer theory (Schoof, 2007a, b, 2011), mathematically confirming the earlier findings by Weertman (1974) and Thomas (1979), i.e. that grounding line positions are unstable on retrograde bedrock slopes in absence of (ice shelf) buttressing. Schoof (2007a) showed that numerical ice-sheet models need to evaluate membrane stresses across the grounding line, hence resolving them on a sufficiently fine grid of less than a kilometre, which was further confirmed by two ice sheet model intercomparisons (Pattyn et al., 2012, 2013). Since then several marine ice sheet models of the Antarctic ice sheet have seen the light, with varying ways of treating the grounding line, i.e. by increasing locally spatial resolution at the grounding line (Favier et al., 2014; Cornford et al., 2015), by making use of local interpolation strategies at the grounding line (Feldmann et al., 2014; Feldmann and Levermann, 2015; Gollledge et al., 2015; Winkelmann et al., 2015) or by parametrizing grounding line flux based on boundary layer theory (~~Pollard and DeConto, 2009; Pollard et al., 2015; Ritz et al., 2015; DeConto and Pollard, 2016~~)([Pollard and DeConto, 2009](#); [Pollard et al.](#)

Other feedbacks relate ice sheet dynamics to basal sliding through thermo-viscous instabilities, which may lead to limit-cycle behaviour in ice sheets (Payne, 1995; Pattyn, 1996) as well as ice stream development in absence of strong basal topographic control (Payne and Dongelmans, 1997; Payne et al., 2000; Hindmarsh et al., 2009). More elaborate subglacial water flow models have since been developed, exhibiting similar feedback mechanisms in ice discharge (Schoof, 2010). For marine portions of ice sheets, the major subglacial constraint is governed by till deformation and observations have led to new insights in subglacial till deformation based on Coulomb friction controlled by subglacial water pressure (Tulaczyk et al., 2000a, b). In contact with the ocean, subglacial water pressure may therefore stem from the depth of the bed below sea level, which led to new characterizations of grounding line dynamics (Tsai et al., 2015).

In this paper, I present a new ice sheet model that reduces the three-dimensional nature of ice sheet flow to a two-dimensional problem, while keeping the essential (or elementary) characteristics of ice sheet thermomechanics and ice stream flow. ~~Furthermore, a number of non-linear numerical problems have been linearised in order to increase both numerical stability and improve computational speed, while making sure that the processes modelled are preserved to the level of accuracy needed. Finally, processes~~ Processes controlling grounding line motion are adapted in such a way that they can be represented at coarser resolutions. This way, the model can more easily be integrated within computational-demanding Earth-system models. A ~~novel~~ new grounding-line algorithm based on the zero effective pressure conditions reigning at the contact with the ocean has been implemented (Tsai et al., 2015), which leads to a more sensitive grounding-line response, ~~without necessarily taking into account other mechanisms of accelerating mass loss, such as ice-cliff failure and hydro-fracturing~~ (Pollard et al., 2015; DeConto and Pollard, 2016).

I start by giving a detailed overview of the model and its components. The initialisation procedure for the Antarctic ice sheet is then given, and finally, the sensitivity of the Antarctic ice sheet to sudden atmospheric and ocean warming is presented on centennial time scales. The appendices further describe results of known benchmarks for grounded ice flow (Huybrechts et al., 1996; Payne et al., 2000), ~~floating ice shelves~~ (MacAyeal et al., 1996; Rommelaere and Ritz, 1996), and marine ice sheet dynamics (Pattyn et al., 2012).

2 Model description

The model consists of diagnostic equations for ice velocities, and three prognostic equations for the temporal evolution of ice thickness, ice temperature, and bedrock deformation beneath the ice. Prescribed boundary fields are equilibrium bedrock topography, basal sliding coefficients, geothermal heat flux, and sea level. Present-day mean surface air temperatures and precipitation are derived from data assimilation within climate models. Ablation ~~can be~~ is determined from a Positive Degree-Day model. A list of model symbols is provided in Tables 1–3. A general overview of the Cartesian geometry used is given in Fig. 1.

For the coupled ice sheet/ice shelf system the surface elevation h_s is defined as

$$h_s = \max \left[b + h, \left(1 - \frac{\rho_i}{\rho_w} \right) h + z_{sl} \right], \quad (1)$$

where h is the ice thickness, b is the bedrock elevation, z_{sl} is the sea-level height with respect to the chosen datum, ρ_i and ρ_w are the ice and seawater density, respectively. It follows that the bottom of the ice sheet equals $h_b = h_s - h$, and that $h_b = b$ holds for the grounded ice sheet.

Symbol	Description	Units	Value
\dot{a}	Surface mass balance (SMB)	m a^{-1}	
A	Glen's flow law factor	$\text{Pa}^{-n} \text{a}^{-1}$	
A_b, A'_b	Basal sliding factor in power-law sliding	$\text{Pa}^{-m} \text{m a}^{-1}$	
A_{froz}	Basal sliding factor for frozen conditions	$\text{Pa}^{-m} \text{m a}^{-1}$	10^{-10}
b	Bedrock elevation	m	
b_f	Buttressing factor		0–1
c_p	Specific heat of ice	$\text{J kg}^{-1} \text{K}^{-1}$	2009
c_{po} Specific heat of seawater $\text{J kg}^{-1} \text{K}^{-1}$ 3974 C_r	Calving rate	m a^{-1}	
C_s	Friction coefficient in Schoof (2007a)	$\text{Pa m}^{-m_s} \text{sa}^{m_s}$	$(A'_b/spy)^{-m_s} A'_b^{-m_s}$
c_0	Till cohesion	Pa	0
d	Diffusion coefficient of grounded ice sheet flow	$\text{m}^2 \text{a}^{-1}$	
D	Flexural rigidity of lithosphere	N m	10^{25}
E_f	Adjustment factor in Arrhenius equation		0.035 <u>0.1–1</u>
F_{melt}	Adjustment factor for sub-shelf melt rates		1–8 <u>0.125–1</u>
f_g	Fractional area of shelf grid cell in contact with bed		0–1
f_s Scaling term for strain heating g	Gravitational acceleration	m s^{-2}	9.81
G	Geothermal heat flux	W m^{-2}	
h	Ice thickness	m	
h_b	Bottom of ice sheet/ice shelf	m	
h_e	Subgrid ice thickness on ice shelf edge	m	
h_f Ice thickness in effective viscosity m h_g	Interpolated ice thickness at grounding line	m	
h_{max}	Maximum neighbouring ice thickness	m	
h_s	Ice sheet surface	m	
h_w	Water column thickness under ice shelf	m	
K	Thermal conductivity	$\text{J m}^{-1} \text{s}^{-1} \text{K}^{-1}$	2.1
L Latent heat of fusion J kg^{-1} 3.35×10^5 L_w	Flexural length scale of the lithosphere		
m	Exponent in basal sliding law		2
m_s	Basal sliding exponent in Schoof (2007a)		1/ m
M	Basal melting rate under ice shelves	m a^{-1}	
n	Glen's flow law exponent		3
n_x, n_y	Outward pointing normal vectors in x and y		
<u>O_b</u>	<u>Optimization parameter for Coulomb friction law</u>		
P	Precipitation rate (accumulation)	m a^{-1}	

Table 1. Model symbols, units and nominal values

Symbol	Description	U
p_w	Subglacial water pressure	Pa
P_w	Point load on bedrock	Pa
q	Exponent in Coulomb friction law	
q_b	Bedrock load	Pa
q_g	Ice flux at the grounding line	m
Q_o	Numerical coefficient in Tsai et al. (2015)	
r	Scaling factor in sliding law	
R	Gas constant	J
S	Surface melt rate	m
S_o	Ocean salinity psu 35	psu
s	Seconds per year $s a^{-1}$ 31,556,926	T
T^{eq}	Steady-state temperature K	K
T_{fo}	Ocean freezing temperature K 271.03	T_m
T_{oc}	Ocean temperature	$^{\circ}C$
T_r	Temperature at which basal sliding starts	$^{\circ}C$
T_s	Surface temperature	K
T^*	Homologous temperature	K
ΔT	Background temperature forcing	$^{\circ}C$
δT	Scaling factor in mass balance forcing	$^{\circ}C$
u	Horizontal ice velocities in x direction	m
u_b	Basal velocity in x direction	m
u_g	Velocity at the grounding line (Schoof, 2007a; Tsai et al., 2015)	m
u_0	Limit velocity in Coulomb friction law	m
v	Horizontal ice velocities in y direction	m
v_b	Basal velocity in y direction	m
\mathbf{v}	Vertical mean horizontal velocity	m
\mathbf{v}_b	Horizontal basal velocity	m
\mathbf{v}_d	Horizontal deformational velocity	m
w_b	Lithospheric deflection	
w_c	Weighting factor in calving law	
w_p	Response to point load on bedrock	
x, y	Orthogonal horizontal coordinates	m
z	Vertical elevation, increasing upwards from reference plane	m
z_{sl}	Sea level elevation	m

Table 2. Model symbols, units and nominal values (continued)

Symbol	Description	Units	Value
β^2	Basal friction coefficient		
β_0 Inverse of Péclet number γ	Atmospheric lapse rate	$^{\circ}\text{C m}^{-1}$	0.008
γ_T Thermal exchange velocity $\text{m s}^{-1} \text{K}^{-1} 5 \times 10^{-7} \Delta$	Grid cell size, equal in x and y directions	m	
$\dot{\epsilon}_{xx}, \dot{\epsilon}_{yy}$ Normal strain rate in x and y direction $\text{a}^{-1} \dot{\epsilon}_0$	Minimum strain rate in effective viscosity	a^{-1}	10^{-20}
η	Effective viscosity	Pa a	
κ	Thermal diffusivity	$\text{m}^2 \text{s}^{-1}$	1.1487×10^{-6}
λ_p	Scaling factor in pore water pressure		
ρ_b	Bedrock density	kg m^{-3}	3370
ρ_i	Ice density	kg m^{-3}	910
ρ_w	Sea water density	kg m^{-3}	1028
ω Scaled vertical velocity ϕ	Till friction angle	deg	
ϕ_{\min}	minimum till friction angle	deg	8–12
ϕ_{\max}	maximum till friction angle	deg	30
σ_b	Standard deviation of bedrock variability		
Θ	Buttressing at grounding line		[0, 1]
θ	Ice temperature	K	
θ_b	Basal temperature	K	
θ_b^s	Basal temperature of the ice shelf	K	
τ_b	Basal drag	Pa	
τ_c	Coulomb stress	Pa	
τ_d	Driving stress	Pa	
τ_f	Free-water tensile stress	Pa	
τ_{xx}, τ_{yy}	Longitudinal stress in x and y	Pa	
τ_t Relaxation time for temperature τ_w	Relaxation time for lithospheric response	a	3000
ζ	Scaled vertical coordinate		[0, 1]

Table 3. Model symbols, units and nominal values (continued)

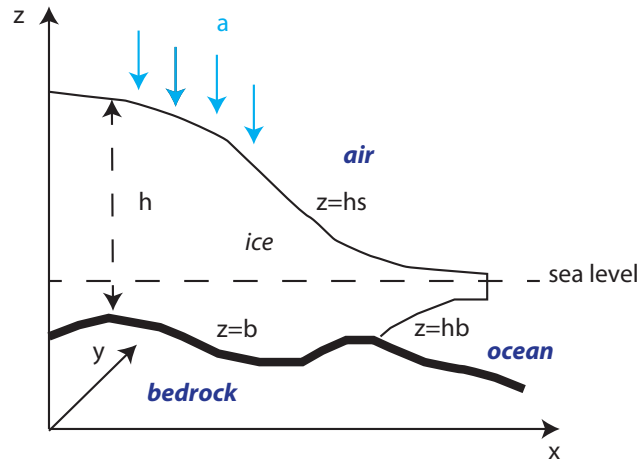


Figure 1. General Cartesian geometry of the f.ETISh model.

2.1 Ice velocities

2.1.1 Approximations

The ice sheet/ice shelf model has several modes of operation, depending on the boundary conditions that are applied. The most elementary flow regime of the grounded ice sheet is according to the Shallow-Ice approximation (SIA; Hutter, 1983), extended with either a Weertman-type (or power-law) function or a linear/plastic Coulomb friction law for basal sliding. Ice shelf flow is governed by the Shallow-Shelf approximation (SSA; Morland, 1987; MacAyeal, 1989), defined by zero basal drag and extended by a water-pressure condition at the seaward edge. The transition between both systems is given by a flux-condition at the grounding line (Pollard and DeConto, 2009, 2012a), either derived from boundary layer theory based on SSA (SGL; Schoof, 2007a) or given by a flux-condition based on Coulomb friction at the grounding line (TGL; Tsai et al., 2015).

10 A second mode of operation is the hybrid mode, in which the flow regime of the grounded ice sheet is governed by a combination of SIA, responsible for ice-deformational flow, and SSA for basal sliding (Bueler and Brown, 2009; Martin et al., 2011; Winkelmann et al., 2011). The hybrid model ~~can be is~~ used in combination with power-law sliding or linear/plastic Coulomb friction underneath the ice sheet. All components of the flow model are detailed in the sections below.

2.1.2 Shallow-Ice Approximation (SIA)

15 The Shallow-Ice approximation (SIA; Hutter, 1983) is commonly used in ice sheet modelling. This approximation is valid for ice sheets of small aspect ratios $h \ll L$, where L is the horizontal length scale of the ice sheet domain, and further characterized by a low curvature and low sliding velocities. The approximation is, however, not valid near grounding lines nor for ice shelf

flow, for which other approximations are applied (see below). According to SIA, the vertical mean horizontal velocity in an ice sheet is given by

$$\mathbf{v}_{\text{SIA}} = \mathbf{v}_b + \frac{2A}{n+2} h \left| \tau_d \right|^{n-1} \tau_d, \quad (2)$$

where $\tau_d = -\rho_i g h \nabla h_s$ is the driving stress, A is the flow parameter in Glen's flow law (with $n = 3$), $\mathbf{v}_b = (u_b, v_b)$ is the basal sliding velocity and $\mathbf{v}_{\text{SIA}} = (u, v)$ is the vertical mean horizontal velocity according to SIA. The flow parameter A is a function of ice temperature (see Sect. 2.4). ~~The main advantage of SIA is that the velocity is completely determined from the local ice-sheet geometry.~~

2.1.3 Hybrid Shallow-Shelf/Shallow-Ice approximation (HySSA)

The flow velocity in an ice shelf or an ice stream characterized by low drag is derived from the Stokes equations (Stokes, 1845) by neglecting vertical shear terms and by integrating the force balance over the vertical. The resulting equations are (Morland, 1987; MacAyeal, 1989):

$$2 \frac{\partial}{\partial x} \left(2\eta h \frac{\partial u}{\partial x} + \eta h \frac{\partial v}{\partial y} \right) + \frac{\partial}{\partial y} \left(\eta h \frac{\partial u}{\partial y} + \eta h \frac{\partial v}{\partial x} \right) - \tau_{b_x} = -\tau_{d_x}, \quad (3)$$

$$2 \frac{\partial}{\partial y} \left(2\eta h \frac{\partial v}{\partial y} + \eta h \frac{\partial u}{\partial x} \right) + \frac{\partial}{\partial x} \left(\eta h \frac{\partial v}{\partial x} + \eta h \frac{\partial u}{\partial y} \right) - \tau_{b_y} = -\tau_{d_y}, \quad (4)$$

where

$$\eta = \frac{A^{-1/n}}{2} \left[\left(\frac{\partial u}{\partial x} \right)^2 + \left(\frac{\partial v}{\partial y} \right)^2 + \frac{\partial u}{\partial x} \frac{\partial v}{\partial y} + \frac{1}{4} \left(\frac{\partial u}{\partial y} + \frac{\partial v}{\partial x} \right)^2 + \varepsilon_0^2 \right]^{(1-n)/2n}, \quad (5)$$

and where $\tau_{d_x} = \rho_i g h (\partial h_s / \partial x)$ (similar for τ_{d_y}). $\varepsilon_0 = 10^{-20}$ is a small factor to keep η finite, hence to prevent singularities when velocity gradients are zero. For the ice shelf, $\tau_b = 0$, while for the grounded ice sheet the basal drag is a function of the friction at the base. The SSA stress-equilibrium equations (3) and (4) require boundary conditions to be specified along the contour which defines the boundary to the ice-shelf domain, which is taken as the edge of the computational domain, irrespective of whether or not calving is considered. Dynamic conditions (specification of stress) are applied at this seaward edge, so that the vertically-integrated pressure balance then reads

$$2\eta h \left[\left(2 \frac{\partial u}{\partial x} + \frac{\partial v}{\partial y} \right) n_x + \frac{1}{2} \left(\frac{\partial u}{\partial y} + \frac{\partial v}{\partial x} \right) n_y \right] \\ = n_x \frac{1}{2} \rho_i g h^2 \left(1 - \frac{\rho_i}{\rho_w} \right), \quad (6)$$

$$2\eta h \left[\left(2 \frac{\partial v}{\partial y} + \frac{\partial u}{\partial x} \right) n_y + \frac{1}{2} \left(\frac{\partial u}{\partial y} + \frac{\partial v}{\partial x} \right) n_x \right] \\ = n_y \frac{1}{2} \rho_i g h^2 \left(1 - \frac{\rho_i}{\rho_w} \right), \quad (7)$$

5 where n_x, n_y are the outward-pointing normal vectors in the x and y direction, respectively.

The ice shelf velocity field is needed for determining the effect of buttressing in the grounding line flux conditions (see below), as well as for the thickness evolution of the ice shelf. For the purpose of buttressing, velocity gradients downstream from the grounding line are used to determine the longitudinal stretching rate, which is compared to the stretching rate of a freely-floating ice shelf to determine a so-called buttressing factor. ~~This does not require a full solution of the non-linear system of ice shelf equations, and velocity gradients can be approximated from a linearised solution of the ice shelf equations. This is done by simplifying the effective viscosity Eq. (5) of the ice shelf, while keeping the essential strain-enhanced effect in the effective viscosity. For the flow-line case, the only non-zero strain rate is the stretching rate in the direction of the flow so that~~

$$\underline{\varepsilon_{xx} = \frac{\partial u}{\partial x} = A \tau_f^n},$$

~~where~~

$$15 \quad \underline{\tau_f = \frac{1}{2} \rho_i g h_f \left(1 - \frac{\rho_i}{\rho_w} \right)}.$$

~~where h_f is defined by~~

$$\underline{h_f = \max [\min(h, 1000), 100]}$$

~~in order to limit the variability of the effective viscosity, especially in areas with highly varying basal topography. Inserting Eq. (??) in Eq. (5) then results in~~

$$20 \quad \underline{\eta = \frac{\tau_f^{1-n}}{2A}}.$$

~~This way, the effective viscosity becomes independent of the velocity components, which significantly increases the calculation efficiency. Despite this approximation, the general behaviour of the flow field is only slightly affected, as is shown in Appendix ??.~~

Both SIA and SSA velocities are combined to obtain the velocity field of the grounded ice sheet according to the hybrid
 5 model (HySSA; Bueler and Brown, 2009). While Bueler and Brown (2009) use a weighing function to ensure a continuous
 solution of the velocity from the interior of the ice sheet across the grounding line to the ice shelf, Winkelmann et al. (2011)
 have demonstrated that a simple addition (for the grounded ice sheet velocities) still guarantees a smooth transition. Thus basal
 velocities for the grounded ice sheet are SSA velocities $\mathbf{v}_b = \mathbf{v}_{SSA}$ and

$$\mathbf{v} = \mathbf{v}_{SIA} + \mathbf{v}_{SSA} \quad (8)$$

10 for the velocity field in the grounded ice sheet. In the ice shelf, the SIA velocity is kept zero throughout.

2.1.4 Power-law basal sliding

Basal sliding is introduced as a Weertman sliding law, i.e.,

$$\mathbf{v}_b = A'_b |\tau_b|^{m-1} \tau_b, \quad (9)$$

where τ_b is the basal shear stress ($\tau_b \sim \tau_d$ for SIA), A'_b is a basal sliding factor, and m is the basal sliding law exponent. The
 15 basal sliding factor A'_b is temperature dependent and allows for sliding within a basal temperature range between -3 and 0°C .
 It further takes into account sub-grid sliding across mountainous terrain (Pollard et al., 2015):

$$A'_b = (1 - r)A_{\text{froz}} + rA_b, \quad (10)$$

where $r = \max[0, \min[1, (T^* - T_r)/(-T_r)]]$, A_{froz} is the sliding coefficient in case of frozen bedrock (chosen to be very
 20 small but different from zero to avoid singularities in the basal friction calculation), T^* is the temperature corrected for the
 dependence on pressure (see Sect. 2.4.3) and $T_r = \min[-3 - 0.2\sigma_b]$, where σ_b is the standard deviation of bedrock elevation
 within the grid cell (Pollard et al., 2015). Basal sliding factors A_b are either considered constant in space/time or are spatially
 varying and obtained through optimization methods (see Sect. 4.1). Basal velocities in the hybrid model are defined through a
 friction power law, where

$$\tau_b = \beta^2 \mathbf{v}_b = A_b'^{-1/m} |\mathbf{v}_b|^{1/m-1} \mathbf{v}_b. \quad (11)$$

25 ~~Since Eq. (11) introduces another dependency on \mathbf{v} in Eq. (3) and Eq. (4), the friction coefficients β^2 are approximated
 by combining $|\mathbf{v}_b|$ with Eq. (9). Furthermore, as for 80% of the Antarctic ice sheet, driving stresses are almost completely
 balanced by basal shear stress (Morlighem et al., 2013), $\tau_b \approx \tau_d$, so that~~

$$\beta^2 = A_b'^{-1/m} |v_b|^{1/m-1} \approx \frac{|\tau_d|^{1-m}}{A_b'}$$

2.1.5 Coulomb friction law

Basal friction within the HySSA equations can also be calculated based on a model for plastic till (Tulaczyk et al., 2000a). Several variations of a basal till model can be found in the literature (Schoof, 2006; Gagliardini et al., 2007; Bueler and Brown, 2009; Winkelmann et al., 2011). Deformation of saturated till is well modelled by a plastic (Coulomb friction) or nearly plastic rheology (Truffer et al., 2000; Tulaczyk et al., 2000a; Schoof, 2006). Its yield stress τ_c satisfies the Mohr–Coulomb relation:

$$\tau_c = c_0 + O_b \tan \phi (\rho_i g h - p_w), \quad (12)$$

where the term between brackets is the effective pressure of the overlying ice on the saturated till (Cuffey and Paterson, 2010), or the ice overburden pressure minus the water pressure p_w , c_0 is the till cohesion ($c_0 = 0$ is further considered), and ϕ is the till friction angle. The latter can be either taken as a constant value or vary as a function of bedrock elevation (Maris et al., 2014):

$$\phi = -\phi_{\min} \frac{b}{10^3} \frac{b - z_{sl}}{10^3} + \left(1 + \frac{b}{10^3} \frac{b - z_{sl}}{10^3} \right) \phi_{\max}, \quad (13)$$

and limited by $\phi = \phi_{\min}$ for $b \leq -10^3$ m and $\phi = \phi_{\max}$ for $b \geq 0$. O_b is a spatially-varying parameter used to optimize the basal friction field, in a similar way as A_b in Eq. (10). Without optimization, it takes the value of $O_b = 1$.

The most comprehensive approach to solve for the subglacial water pressure in Eq. (12) is due to Bueler and van Pelt (2015) by considering a hydrological model of subglacial water drainage within the till. However, Martin et al. (2011) propose to relate major till characteristics to bedrock geometry and allow till friction angle and basal water pressure to be a function of the bed elevation compared to sea level. This leads to zones of weak till and saturation in subglacial basins that are well below sea level (Martin et al., 2011; Maris et al., 2014). Following their analysis, the subglacial water pressure is defined by

$$p_w = 0.96 \lambda_p \rho_i g h. \quad (14)$$

Here, λ_p is a scaling factor such that the pore water pressure is maximal when the ice is resting on bedrock at or below sea level. Below sea level, the pores in the till are assumed to be saturated with water so λ_p is then equal to 1. The factor λ_p is scaled with the height above sea level up until 1000 m. At and above 1000 m, λ_p is equal to 0 (Maris et al., 2014). While there

is no direct physical evidence for such water-pressure distribution in the interior of ice sheets, near grounding lines in direct contact with the ocean, subglacial water pressure of saturated till may also be approximated by (Tsai et al., 2015):

$$p_w = -\rho_w g \hat{b} \left(\frac{b - z_{sl}}{b} \right), \quad (15)$$

which is valid for $b - z_{sl} \leq 0$, otherwise $p_w = 0$. By definition, $p_w = \rho_i g h$ at the grounding line and underneath floating ice shelves, so that the effective pressure becomes zero. Bueler and Brown (2009) consider the pore water pressure locally as at most a fixed fraction (95%) of the ice overburden pressure $\rho_i g h$. Winkelmann et al. (2011) use a fraction of 0.96, which is applied in Eq. (14).

To link Coulomb friction to basal drag, the formulation proposed by Bueler and van Pelt (2015) is opted for, where τ_c and v_b combine to determine τ_b through a sliding law, i.e.,

$$\tau_b = \tau_c \frac{v_b}{|v_b|^{1-q} u_0^q}, \quad (16)$$

where $0 \leq q \leq 1$, and u_0 is a threshold sliding speed (Aschwanden et al., 2013). The Coulomb friction law, Eq. (16), includes the case $q = 0$, leading to the purely plastic (Coulomb) relation $\tau_b = \tau_c v_b / |v_b|$. At least in the $q \ll 1$ cases, the magnitude of the basal shear stress becomes nearly independent of $|v_b|$, when $|v_b| \gg u_0$. Equation (16) could also be written in a generic power-law form $\tau_b = \beta^2 |v_b|^{q-1} v_b$ with coefficient $\beta^2 = \tau_c / u_0^q$; in the linear case $q = 1$, $\beta^2 = \tau_c / u_0$ (Bueler and van Pelt, 2015).

Alternatively, both the power-law sliding law Eq. (9) and the Coulomb friction law Eq. (16) can be combined (Tsai et al., 2015; Asay-Davis et al., 2015), by taking the lowest friction value of both. Since at the grounding line basal sliding velocities are considered highest, this equally implies high basal drag in a traditional power-law sliding law. ~~However, expressed as a basal friction law, Eq. (11) enables to derive high sliding velocities at low and near-zero basal drag. Nevertheless, As a consequence,~~
power law sliding/friction still leads to a relatively sharp transition in τ_b at the grounding line (Tsai et al., 2015). Coulomb basal conditions imply that basal drag vanishes towards the grounding line, thus ensuring a smooth transition between the ice stream and ice shelf. Expressing the basal traction as

$$\tau_b = \min \left[\beta^2 v_b, \frac{\tau_c v_b}{|v_b|^{1-q} u_0^q} \right] \quad (17)$$

ensures that it is continuous (though not differentiable) across the grounding line (Asay-Davis et al., 2015). ~~The Coulomb friction law has been implemented in f.ETISH, but substantial tests have not been carried out in the scope of this paper.~~

2.1.6 Grounding-line flux condition for power-law sliding (SGL)

Previous studies have indicated that it is necessary to resolve the transition zone/boundary layer at sufficiently fine resolution in order to capture grounding-line migration accurately (Durand et al., 2009; Pattyn et al., 2012, 2013; Pattyn and Durand,

2013; Durand and Pattyn, 2015). In large-scale models, this can lead to unacceptably small time-steps and costly integrations. Pollard and DeConto (2009, 2012a) incorporated the boundary layer solution of Schoof (2007a) directly in a numerical ice-sheet model at coarse grid resolution, so the flux, q_g , across model grounding lines is given by

$$q_g = \left[\frac{A(\rho_i g)^{n+1} (1 - \rho_i / \rho_w)^n}{4^n C_s} \right]^{\frac{1}{m_s+1}} \Theta^{\frac{n}{m_s+1}} h_g^{\frac{m_s+n+3}{m_s+1}}. \quad (18)$$

This yields the vertically averaged velocity $u_g = q_g/h_g$ where h_g is the ice thickness at the grounding line. Θ in Eq. (18) accounts for back stress at the grounding line due to buttressing by pinning points or lateral shear, and is defined as

$$\Theta = \frac{b_f \tau_{xx} + (1 - b_f) \tau_f}{\tau_f}, \quad (19)$$

where τ_{xx} is the longitudinal stress just downstream of the grounding line, calculated from the viscosity and strains in a preliminary SSA solution without constraints given by Eq. (18), and τ_f the free-water tensile stress defined in Eq. (20) by

$$\tau_f = \frac{1}{2} \rho_i g h \left(1 - \frac{\rho_i}{\rho_w} \right). \quad (20)$$

b_f is an additional buttressing factor to control the buttressing strength of ice shelves and varies between 0 (no buttressing) and 1 (full buttressing). As in Pollard and DeConto (2012a), C_s is Schoof's basal sliding coefficient and m_s the basal sliding exponent, so that C_s is related to the sliding coefficients A'_b by $C_s = (A'_b/\text{spy})^{-m_s}$, where 'spy' is the number of seconds per year and $C_s = A'_b{}^{-m_s}$, where $m_s = 1/m$. Grounding-line ice thickness h_g is linearly interpolated in space by estimating the sub-grid position of the grounding line between the two surrounding floating and grounded h -grid points. Therefore, the height above floatation is linearly interpolated on the Arakawa C-grid between those two points to where it is zero. Subsequently, the bedrock elevation is linearly interpolated to that location, and the floatation thickness of ice for that bedrock elevation and current sea level is obtained (Pattyn et al., 2006; Gladstone et al., 2010; Pollard and DeConto, 2012a). The velocity u_g is then calculated at the grounding-line points and imposed as an internal boundary condition for the flow equations, hence overriding the large-scale velocity solution at the grounding line. $u_g = q_g/h_g$ is imposed exactly at the u -grid grounding line point when the flux q_g is greater than the large-scale sheet-shelf equation's flux at the grounding line. This is a slight variant of Pollard and DeConto (2012a)-

Equation (18) applies equally to the y direction, with v_g and τ_{yy} instead of u_g and τ_{xx} . Note that spatial gradients of quantities parallel to the grounding line, which are not included in Schoof's flow-line derivation of Eq. (18), are neglected here (Katz and Worster, 2010; Gudmundsson et al., 2012; Pattyn et al., 2013). This parametrization was also found to yield results comparable to SSA models solving transient grounding line migration at high spatial resolution of the order of hundreds of meters (Pattyn and Durand, 2013; Durand and Pattyn, 2015), despite the fact that Eq. (18) applies to steady-state conditions.

2.1.7 Grounding-line flux condition for Coulomb friction (TGL)

The grounding-line parametrization based on the boundary layer theory by Schoof (2007a) is invalid when Coulomb friction near the grounding line is considered and the effective stress tends to zero. However, Tsai et al. (2015) offers such a solution for vanishing Coulomb friction at the grounding line, and therefore independent of basal sliding coefficients:

$$5 \quad q_g = Q_o \frac{8A(\rho_i g)^n}{4^n \tan \phi} \frac{8A(\rho_i g)^n}{4^n O_b \tan \phi} \left(1 - \frac{\rho_i}{\rho_w}\right)^{n-1} \Theta^{n-1} h_g^{n+2}, \quad (21)$$

where $Q_o \approx 0.61$ is a numerical coefficient determined from the boundary-layer analysis. The flux in the y direction is obtained in a similar fashion. As in Eq. (18), buttressing scales to the same power as $(1 - \rho_i/\rho_w)$, which is $n - 1$. The performance of both flux conditions is tested in Appendix C.

The TGL flux condition can be used in conjunction with power-law basal sliding. Indeed, Tsai et al. (2015) have shown that the crossover from Coulomb to power-law roughly occurs at stresses $\gtrsim 100$ kPa, hence the Coulomb regime occurs within $\lesssim 17$ m above the floatation height. This is a very small height difference, which implies that in most cases —with exception of ice plains— a narrow Coulomb regime exists, within a grid cell of a continental-scale model.

2.2 Ice thickness evolution

Ice sheet thickness evolution is based on mass conservation, leading to the continuity equation. For the general ice sheet/ice shelf system, this is written as:

$$\frac{\partial h}{\partial t} = -\frac{\partial(uh)}{\partial x} - \frac{\partial(vh)}{\partial y} + \dot{a} - M, \quad (22)$$

where \dot{a} is the surface mass balance (accumulation minus surface ablation), and M is the basal melt rate (solely underneath ice shelves, as basal melt rates underneath the ice sheet are not accounted for). The treatments of the various local ice gains or losses (surface mass balance, etc.) are described in later sections. For the [SIA model in the](#) grounded ice sheet, Eq. (22) is written as a diffusion equation for ice thickness (Huybrechts, 1992):

$$\frac{\partial h}{\partial t} = \frac{\partial}{\partial x} \left(d \frac{\partial(h + h_b)}{\partial x} \right) + \frac{\partial}{\partial y} \left(d \frac{\partial(h + h_b)}{\partial y} \right) + \dot{a} - M, \quad (23)$$

where h_b is the bottom of the ice sheet (or the bedrock elevation b for the grounded ice sheet).

It is also ensured that thinning due to grounding line retreat does not exceed the maximum permissible rate, using theoretical knowledge of maximum possible stresses at the grounding line that is called the ‘maximum strain check’. Similar to Ritz et al. (2015), tensile stresses [at the grounding line](#) are ensured to not exceed those from buttressing by water alone, i.e., the free-water tensile stress, and calculate the maximum corresponding strain rate, expressed as a maximum thinning rate. ~~The free-water tensile strain rate then becomes-~~

$$\underline{h \frac{\partial u}{\partial x} = h \frac{\partial v}{\partial y} = Ah\tau_f.}$$

Using the mass conservation equation (22), the condition on maximum strain rate is

$$\begin{aligned} \frac{\partial h}{\partial t} &= \underline{\dot{a} - M - \frac{\partial(uh)}{\partial x} - \frac{\partial(vh)}{\partial y}} \\ &\leq \underline{\dot{a} - M - h \frac{\partial u}{\partial x} - h \frac{\partial v}{\partial y}} = \dot{a} - M - 2Ah\tau_f. \end{aligned}$$

- 5 ~~This is valid for $\partial h/\partial x < 0$ when $u > 0$ and $\partial h/\partial y < 0$ when $v > 0$. Ritz et al. (2015) use a slightly different prescription, but sensitivity tests showed that the extra terms in the mass conservation equation can be safely dropped, rendering the maximum strain check therefore independent of velocity gradients.~~

2.3 Calving and sub-shelf pinning

- Ice-front calving is obtained from the large scale stress field (Pollard and DeConto, 2012a), based on the horizontal divergence
10 of the ice-shelf velocities and which is similar to parametrizations used elsewhere (Martin et al., 2011; Winkelmann et al., 2011; Levermann et al., 2012). The calving rate C_r is defined as

$$C_r = 30(1 - w_c) + 3 \times 10^5 \max\left(\frac{\partial u}{\partial x} + \frac{\partial v}{\partial y}, 0\right) \frac{w_c h_e}{\Delta} \quad (24)$$

where $w_c = \min(1, h_e/200)$ is a weight factor and h_e is the subgrid ice thickness within a fraction of the ice edge grid cell that is occupied by ice (Pollard and DeConto, 2012a), defined by

$$15 \quad h_e = \max\left[h_{\max} \times \max\left(0.25, e^{-h_{\max}/100}\right), 30, h\right] \quad (25)$$

where a minimum ice thickness of 30 m avoids too thin ice shelves. The value of h_{\max} is defined as the maximum ice thickness of the surrounding grid cells (grounded or floating) that are not adjacent to the ocean (Pollard and DeConto, 2012a). The calving rate C_r is then subtracted from the basal melt rate M in Eq. (22).

- Given the relatively low spatial resolution of a large-scale ice-sheet model, small pinning points underneath ice shelves due
20 to small bathymetric rises scraping the bottom of the ice and exerting an extra back pressure on the ice shelf (Berger et al., 2016; Favier et al., 2016) are not taken into account. To overcome this a simple parametrization based on the standard deviation of observed bathymetry within each model cell was accounted for to introduce a given amount of basal friction of the ice shelf

(Pollard and DeConto, 2012a). The fractional area f_g of ice in contact with sub-grid bathymetric high is defined as (modified from Pollard and DeConto, 2012a):

$$f_g = \max \left[0, 1 - \frac{h_w}{\sigma_b} \right] \quad (26)$$

where h_w is the thickness of the water column underneath the ice shelf and σ_b is the standard deviation of the bedrock variability (see above). This factor f_g is multiplied with β^2 in the basal friction. For the grounded ice sheet, $f_g = 1$; for the floating ice shelf in deeper waters, $f_g = 0$, so that the ice shelf does not experience any friction.

2.4 Ice temperature and rheology

~~Ice temperature is calculated in a semi-analytical fashion to provide an estimate of both basal temperature and the mean ice column temperature over a given depth. The former determines regions of potential basal sliding, while the latter is employed to determine the vertically-integrated value of the flow parameter A in Glen's flow law. These simplifications allow for the model to remain two-dimensional, but taking into account the basic mechanisms of major thermodynamic processes, contrary to models employing a linear temperature profile (e.g., Kavanaugh and Cuffey, 2009; Golledge and Levy, 2011). The steady-state temperature profile is a function of vertical diffusion and advection, and extended with frictional and strain heating at the base. This is a variant of derivations due to Hindmarsh (1999) and Pattyn (2010). A solution to the horizontal advection problem was also tested (Glasser and Siegert, 2002), based on the column model due to Budd et al. (1971). However, due to the inherent simplifications, it works best when surface slopes and lapse rates are lowest (Hooke, 2005), which results in an overestimation of horizontal advection at the edges of an ice sheet, cooling down areas that are supposedly at pressure melting point. To compensate for the lack of horizontal advection in the model, strain heating was decreased by a given fraction. Finally, a time-dependency is introduced by treating the evolution of the column-ice temperature as a relaxation equation.~~

2.4.1 Ice-sheet temperature

The ~~steady-state~~ diffusion-advection equation for an ice sheet ~~near its centre (in absence of horizontal advection)~~, is given by [\(Huybrechts, 1992\)](#):

$$\beta_0 \frac{\partial^2 \theta}{\partial \zeta^2} - \omega(\zeta) \frac{\partial \theta}{\partial \zeta} \frac{\partial \theta}{\partial t} = \underbrace{0 \kappa \frac{\partial^2 \theta}{\partial z^2} - u \frac{\partial \theta}{\partial x} - v \frac{\partial \theta}{\partial y} + \frac{\Phi}{\rho_i c_p}}_{\text{diffusion-advection}}, \quad (27)$$

where $\beta_0 = \kappa / h \dot{a}$,

~~where~~ $\kappa = K / \rho_i c_p$ is the thermal diffusivity of ice, K is the thermal conductivity, c_p is the heat capacity of ice, θ is the ice temperature, $\zeta = (h_s - z) / h$ is the scaled vertical elevation, with $\zeta = 0$ at the surface and $\zeta = 1$ at the bottom of the ice sheet, and ω is the vertical velocity normalized by the surface mass balance rate, so that $\omega(\zeta = 0) = -1$. This relation has a first integral [\(Hindmarsh, 1999\)](#)

$$\frac{\partial \theta}{\partial \zeta} \equiv \frac{\partial \theta_b}{\partial \zeta} \exp \left[\frac{W(\zeta)}{\beta_0} \right]$$

$$W(\zeta) \equiv \int_1^{\zeta} \omega(\zeta') d\zeta',$$

where $\partial \theta_b / \partial \zeta$ is the basal temperature gradient. The scaled vertical velocity ω according to the Shallow-ice approximation is a function of the exponent of Glen's flow law (Hindmarsh, 1999):-

$$5 \quad \omega = - \frac{\zeta^{n+2} - \zeta(n+2) + n+1}{n+1}$$

so that its integral transforms to-

$$W = \frac{\zeta^{n+3} - 1}{(n+1)(n+3)} - \frac{(\zeta^2 - 1)(n+2)}{2(n+1)} + \zeta - 1.$$

The scaled temperature is then obtained through vertical integration of Eq. (??):-

$$\theta - T_s = \frac{\partial \theta_b}{\partial \zeta} \int_1^{\zeta} \exp \left[\frac{W(\zeta')}{\beta_0} \right] d\zeta',$$

10 $\Phi = -\rho_i g (h_s - z) \nabla h_s \partial \mathbf{v}_d / \partial z$ represents deformational heating, where T_s is the temperature at the surface of the ice sheet. \mathbf{v}_d is the deformational velocity component ($\mathbf{v}_d = \mathbf{v} - \mathbf{v}_b$). The basal boundary condition is given by

$$\frac{\partial \theta_b}{\partial \zeta} \frac{\partial \theta_b}{\partial z} = - \frac{G + \tau_d (\mathbf{v}_s + f_s \mathbf{v}_d)}{K} \frac{G + \tau_d \mathbf{v}_b}{K}, \quad (28)$$

where G is the geothermal heat flux and the second term represents frictional heating at the base. The last term in Eq. (28) represents strain heating, where \mathbf{v}_d is the deformational velocity component ($\mathbf{v}_d = \mathbf{v} - \mathbf{v}_b$). Recognizing that most of the strain heating occurs near the bed, it can be added to the geothermal heat flux (Hooke, 2005). However, to compensate for the absence of horizontal advection in the model, only a fraction $f_s \approx 0.25$ of the total strain heating amount was added. This value is determined from the EISMINT benchmark experiments. Given the two-dimensional nature of the model, the temperature field employs shape functions for vertical profiles of deformational velocity \mathbf{v}_d , its vertical gradient, and the vertical velocity, based on SIA (Hindmarsh, 1999). Eq. 27 is then solved in scaled vertical coordinates $\zeta = (h_s - z)/h$, with $\zeta = 0$ at the surface and $\zeta = 1$ at the bottom of the ice sheet. The use of shape function allows for a faster calculation of the thermodynamic model. However, since this is an approximation compared to fully solving Eq. 27, the EISMINT-I benchmark experiments (Huybrechts et al., 1996) were performed and results are given in Appendix A).

2.4.2 Ice-shelf temperature

In ice shelves, a simple temperature model is adopted, considering the accumulation at the surface balanced by basal melting underneath an ice shelf and with only vertical diffusion and advection into play (Holland and Jenkins, 1999):

$$\theta(\zeta) = \frac{(T_s - \theta_b^s) \exp(\beta_1) + \theta_b^s - T_s \exp(\beta_2)}{1 - \exp(\beta_2)}, \quad (29)$$

- 5 where $\beta_1 = \dot{a}\zeta h/\kappa$, $\beta_2 = \dot{a}h/\kappa$, and θ_b^s is the ocean temperature at the base of the ice shelf, corrected for ice-shelf depth, i.e., $\theta_b^s = T_{oc} = -1.7 - 0.12 \times 10^{-3} h_b$ (Maris et al., 2014).

2.4.3 Temperature evolution

2.4.3 Thermomechanical coupling

The mean column temperature T is obtained by integrating θ from the base of the ice sheet to a given height in the ice column.

- 10 Since most of the ice deformation is in the bottom layers of the ice sheet, the temperature closest to the bottom determines to a large extent the deformational properties. Compared to full thermomechanically-coupled ice sheet models, satisfactory results were obtained by considering a mean column temperature for the lower most 10-40% of the ice column. This fraction can also be regarded as an extra tuning parameter in an ensemble run, especially given the large uncertainties pertaining to geothermal heat flow underneath major ice sheets. The ~~time evolution of the mean column temperature is introduced as a~~
 15 ~~relaxation equation based on the Péclet number, i.e.,~~

$$\frac{\partial T}{\partial t} = -\frac{1}{\tau_t} (T - T^{\text{eq}}).$$

~~where T^{eq} is the steady-state column temperature as calculated with the above-described procedure. Given that the Péclet number $\text{Pe} = h\dot{a}/\kappa$ is the ratio between the characteristic time scales of advection to diffusion, the time scale of each of the processes will then determine the relaxation time needed to reach a steady-state column temperature, i.e.,~~

$$20 \quad \tau_t = \min \begin{cases} h/\dot{a} & (\text{advection}) \\ h^2/\kappa & (\text{diffusion}) \end{cases}$$

~~The main advantage of this scheme, besides being two-dimensional in nature, is that a steady-state temperature field and rheological parameters are readily obtained, reducing the initialization or spin-up time significantly. Comparison of this temperature evolution scheme with conventional three-dimensional models is given in Appendix A and B.~~

2.4.4 Thermomechanical coupling

The flow parameter A and its temperature dependence on temperature are specified as in Huybrechts (1992) and Pollard and DeConto (2012a):

$$A = E_f \times 5.47 \times 10^{10} \exp\left(\frac{-13.9 \times 10^4}{RT^*}\right) \quad \text{if } T^* \geq 263.15\text{K}, \quad (30)$$

$$A = E_f \times 1.14 \times 10^{-5} \exp\left(\frac{-6.0 \times 10^4}{RT^*}\right) \quad \text{if } T^* < 263.15\text{K}, \quad (31)$$

where $T^* = T - T_m$ is the homologous temperature, with $T_m = -8.66 \times 10^{-4}(1 - \zeta)h$ the pressure melting correction and R the gas constant. Units of A are $\text{Pa}^{-3} \text{yr}^{-1}$ corresponding to $n = 3$. The enhancement factor E_f is set to 1 for the main ice sheet model, ~~but lower for the flow of and to $E_f = 0.5$ for~~ ice shelves. The ratio of enhancement factors represent differences in fabric anisotropy between grounded and ice shelf ice (Ma et al., 2010). ~~Moreover, given the linearisation of the SSA equations, this further requires an adjustment (see Appendix ??).~~ Verification of the thermomechanical coupling scheme using a vertical mean value of A follows the EISMINT-II benchmark experiments (Payne et al., 2000) and is detailed in Appendix B.

2.5 Bedrock deformation

The response of the bedrock to changing ice and ocean loads is solved through a combined time-lagged asthenospheric relaxation and elastic lithospheric response due to the applied load (Huybrechts and de Wolde, 1999; Pollard and DeConto, 2012a). The deflection of the lithosphere is given by

$$D\nabla^4 w_b + \rho_b g w_b = q_b, \quad (32)$$

where D is the flexural rigidity of the lithosphere, and ρ_b is the bedrock density. The load is then defined by

$$q_b = \rho_i g h + \rho_w g h_w - \rho_i g h^{\text{eq}} - \rho_w g h_w^{\text{eq}}, \quad (33)$$

where h_w is the ocean column thickness, and h^{eq} and h_w^{eq} are the values of ice thickness and ocean column thickness in equilibrium, respectively, taken from modern observed fields. Equation (32) is solved by a Green's function (Huybrechts and de Wolde, 1999). The response to a point load P_w ($q_b \times \text{area}$) versus distance from the point load l is then given by

$$w_p(l) = \frac{P_w L_w^2}{2\pi D} \text{kei}\left(\frac{l}{L_w}\right), \quad (34)$$

where kei is a Kelvin function of zeroth order (defined as the imaginary part of a modified Bessel function of the second kind), and $L_w = (D/\rho_b g)^{1/4} \approx 132 \text{ km}$ is the flexural length scale. For any load, the different values of the point loads w_p

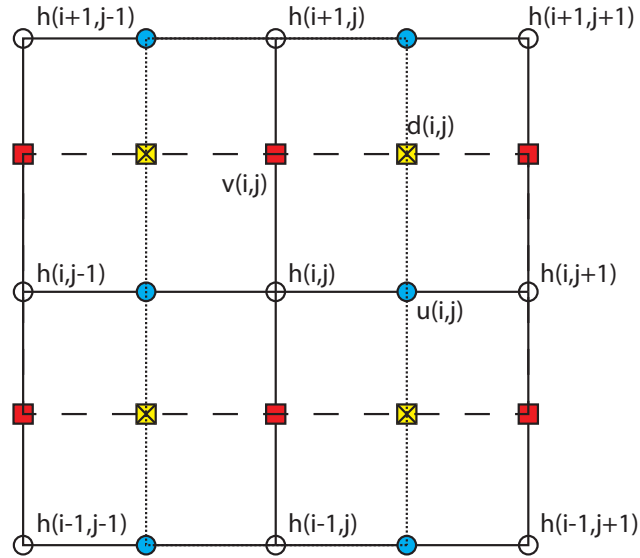


Figure 2. Staggered grids used in the model: the basic grid is the ice-thickness grid (shown in open circles). u and v velocities for the ice shelves (and ice streams) are calculated on two different staggered Arakawa C grids (filled circles and squares, respectively). Diffusion coefficients d in the ice-sheet equation are solved on an Arakawa B grid (crossed squares).

are summed over all grid cells to yield $w_b(x, y)$. Finally, the actual rate of change in bedrock elevation is given by a simple relaxation scheme:

$$\frac{\partial b}{\partial t} = -\frac{1}{\tau_w} (b - b^{\text{eq}} + w_b), \quad (35)$$

where b is the actual bedrock elevation, b^{eq} is the elevation in equilibrium ([taken from modern observed fields](#)), and $\tau_w =$
5 3000 year (Pollard and DeConto, 2012a).

2.6 Numerical grid and solution

The ice sheet-shelf model uses a finite-difference staggered grid, where horizontal velocities (u, v) are calculated on two separate staggered Arakawa C-grids, as is usual for vector fields (Rommelaere and Ritz, 1996), while diffusion coefficients for the ice-sheet equation d are calculated on an Arakawa B-grid, staggered in both x and y direction, since these are scalar quantities (Fig. 2). The f.ETISh model ~~is essentially two-dimensional, with variable coordinates (x, y) in the plane. The ice sheet model uses no vertical coordinate, i. e., the model is vertically-integrated. However, for analytical calculations of the vertical temperature distribution a vertical grid is introduced for the purpose of local numerical integration except for the temperature field calculation. Here, the scaled vertical coordinate system consists of 11 irregularly-spaced layers, with a minimum layer~~

10

thickness of $\Delta\zeta = 0.015$ at the bottom. This way, the number of vertical layers can be greatly reduced, as most of the variability of the vertical temperature profile is situated close to the bed.

The SSA velocity field Eqs. (3–4) is solved as a sparse linear system where both u and v component are solved as once in one matrix \mathbf{A} with size $(2 \times N_x \times N_y)$ by $(2 \times N_x \times N_y)$:

$$5 \quad \begin{pmatrix} \mathbf{A}_{ux} & \mathbf{A}_{vx} \\ \mathbf{A}_{uy} & \mathbf{A}_{vy} \end{pmatrix} \cdot \begin{pmatrix} u \\ v \end{pmatrix} = \begin{pmatrix} b_x \\ b_y \end{pmatrix} \quad (36)$$

where N_x, N_y are the number of grid points in the x, y direction, respectively. The submatrices $\mathbf{A}_{ux}, \mathbf{A}_{vx}$ contain the coefficients for the solution in the x direction for u and v , respectively. $\mathbf{A}_{uy}, \mathbf{A}_{vy}$ are defined in a similar way. Due to the independent nature dependence of the effective viscosity η on u, v , the solution requires no iteration a few iterations to reach convergence. A similar solution approach is taken for solving the continuity equation for ice thickness (Payne and Dongelmans, 10 1997), which was favoured over an Alternating Direct Implicit scheme used in several ice-sheet models (Huybrechts, 1992; Pollard and DeConto, 2012a).

The f.ETISH model is implemented in MATLAB[®]. Computational improvements involved the omission of all *for*-loops by using circular shifts (with exception of the time loop), thereby optimizing the use of matrix operations. The bulk of computational time is devoted to the solution of the sparse matrix systems, which are natively optimized in MATLAB[®] using 15 multi-threading. A preconditioned conjugate gradient method is used for solving the ice sheet/ice shelf continuity equation. The velocity field in the hybrid model is solved using a stabilized bi-conjugate gradients method, which is also preconditioned and further initialized by the velocity field solution from the previous time step. Both numerical solvers are iterative and the preconditioning limits the number of iterations to reach convergence. They are considerably faster compared to the direct solution.

20 The f.ETISH model is compared to other ice sheet models via a series of benchmarks, such as the EISMINT-I benchmark for isothermal ice-sheet models (Huybrechts et al., 1996, Appendix A), the EISMINT-II benchmark for thermomechanically-coupled ice sheet models (Payne et al., 2000, Appendix B), and the MISMIP experiments for marine ice-sheet models (Pattyn et al., 2012, Appendix C). Results show that the f.ETISH model is in close agreement with all of the benchmark experiments.

3 Input and climate forcing

25 3.1 Input data sets

For modelling the Antarctic ice sheet, the bedrock topography is based on the Bedmap2 data (Fretwell et al., 2013), from which ice thickness, present-day surface topography and grounding-line position are derived. Surface mass balance and temperatures are obtained from Van Wessem et al. (2014), based on the output of the regional atmospheric climate model RACMO2 for the period 1979–2011 and evaluated using 3234 *in situ* mass balance observations and ice-balance velocities.

For geothermal heat flux we employ a recent update of Fox-Maule et al. (2005) due to Purucker (2013). It is based on low-resolution magnetic observations acquired by the CHAMP satellite between 2000 and 2010, and produced from the MF-6 model following the same technique as described in Fox-Maule et al. (2005).

All datasets are resampled on the spatial resolution used for the experiments. The experiments shown in this paper employ
5 a grid spacing of 25 (and in a few cases 40 or 16) km.

3.2 Atmospheric and ocean forcing

Atmospheric forcing is applied in a parametrized way, based on the observed fields of precipitation (accumulation rate) and surface temperature. For a change in background (forcing) temperature ΔT , corresponding fields of precipitation P and atmospheric temperature T_s are defined by (Huybrechts et al., 1998; Pollard and DeConto, 2012a)

$$10 \quad T_s = T_s^{\text{obs}} - \gamma(h_s - h_s^{\text{obs}}) + \Delta T, \quad (37)$$

$$P = \dot{a}^{\text{obs}} \times 2^{(T_s - T_s^{\text{obs}})/\delta T}, \quad (38)$$

where $\gamma = 0.008^\circ\text{C m}^{-1}$ is the lapse rate and δT is 10°C (Pollard and DeConto, 2012a). The subscript ‘obs’ refers to the present-day observed value. Any forcing (increase) in background then leads to an overall increase in surface temperature corrected for elevation changes according to the environmental lapse rate γ . The parametrizations of T_s and P can easily be
15 replaced by values that stem from GCMs, with appropriate corrections for surface elevation (e.g., de Boer et al., 2015).

Surface melt is parametrized using a positive degree-day model (Huybrechts and de Wolde, 1999). The total amount of positive degree days (PDD) is obtained as

$$\text{PDD} = \frac{1}{\sigma\sqrt{2\pi}} \int_0^A \left[\int_0^{\bar{T}+2.5\sigma} T \exp\left(-\frac{(T-\bar{T})^2}{2\sigma^2}\right) dT \right] dt, \quad (39)$$

20 where σ is taken as 5°C (Reeh, 1989) and \bar{T} is the mean annual temperature. The annual number of positive degree days represents a melt potential, used to melt snow and (superimposed) ice. This is determined by applying a seasonal cycle to the atmospheric temperatures with a double amplitude of 20°C , linearly increasing to 30°C at an elevation of 3000 m, and kept at 30°C at higher elevations (Pollard and DeConto, 2012a). The PDD melt potential is related to surface melt through a coefficient of 0.005 m of melt per degree day (Pollard and DeConto, 2012a). Although more complex schemes are often used,
25 taking into account refreezing of percolating meltwater in the snow pack and melting of superimposed ice with different melt coefficients (Huybrechts and de Wolde, 1999), which is also confirmed by recent observations (Machguth et al., 2016), surface melt is rather limited for the present-day Antarctic ice sheet. Surface mass balance is then the sum of the different components, i.e., $\dot{a} = P - S$, where $S = 0.005 \times \text{PDD}$ is the surface melt rate.

Melting underneath the floating ice shelves is often based on parametrizations that relate sub-shelf melting to ocean temperature and ice-shelf depth (Beckmann and Goosse, 2003; Holland et al., 2008), either in a linear or a quadratic way (Martin et al., 2011; Pollard and DeConto, 2012a; de Boer et al., 2015; DeConto and Pollard, 2016). This leads to higher melt rates close to the grounding line, as the ice-shelf bottom is the lowest. ~~The While the adaptation by Holland et al. (2008) and Pollard and DeConto~~
 5 (2012a) is implemented in f.ETISh, ~~where the dependence on temperature difference is quadratic:-~~

$$M = F_{\text{melt}} \frac{\rho_w c_{po} \gamma_T}{L \rho_i} |T_{oc} - T_{fo}| (T_{oc} - T_{fo}),$$

~~and where M is the sub-ice-shelf basal melt rate, c_{po} is the specific heat capacity of the ocean, γ_T is the thermal exchange velocity, L is the latent heat of fusion, F_{melt} is a predefined melt factor, depending on the potential for warm ocean currents to access the cavity beneath the ice shelf, T_{oc} is the temperature of the ocean underneath the ice shelf, and T_{fo} is the freezing temperature defined by Beckmann and Goosse (2003) as:-~~
 10

$$T_{fo} = 0.0939 - 0.057S_o + 7.64 \times 10^{-4}h_b,$$

~~where S_o is a mean value for the salinity of the ocean of 35 psu. For determining the only constant values of ice shelf melt were used in the experiments for this paper, scaled by a melt factor F_{melt} a distinction is made between-. This factor distinguishes protected ice shelves (Ross and Ronne-Filchner; Fig. 3), with a melt factor of $F_{\text{melt}} = 1$ and scaling factor of $F_{\text{melt}} = 0.125$, from all other ice shelves with a melt factor of $F_{\text{melt}} = 8$ (Pollard and DeConto, 2012a) that have a scaling factor of $F_{\text{melt}} = 1$. A similar approach has been taken by many other ice-sheet models cited in de Boer et al. (2015). ~~The parametrized melt rate in Eq. (??) follows a quadratic function of ice shelf bottom and thus results in the highest melt rates closest to the grounding line where the ice shelf is thickest, which may not always be the case according to coupled ocean-ice shelf modelling (De Rydt and Gudmundsson, 2016). Favier et al. (2016) used different commonly-used distributions~~
 15 ~~for sub-shelf melting and found significantly different grounding line transient responses. On top of this, recent observations show that the spatial variability in sub-shelf melt rates for the Antarctic ice shelves is quite large and hard to quantify by a simple parametrization (Schodlok et al., 2016). Therefore, a constant value of basal ice-shelf melt was used as a sensitivity parameter in our experiments (independent of ocean temperature), scaled by the spatially-varying factor F_{melt} to account for lower ice-shelf melt rates for the Ross and Ronne-Filchner ice shelves. This way the sensitivity to basal melt rather than the~~
 20 ~~sensitivity to ocean temperature is tested.-~~
 25~~

4 Present-day Antarctic ice sheet simulation

4.1 Initialization

Model initialization to the modern Antarctic ice sheet geometry is based on the method by Pollard and DeConto (2012b) by optimizing basal sliding coefficients in an iterative fashion. This nudging scheme is ~~combined with~~ applied to both the

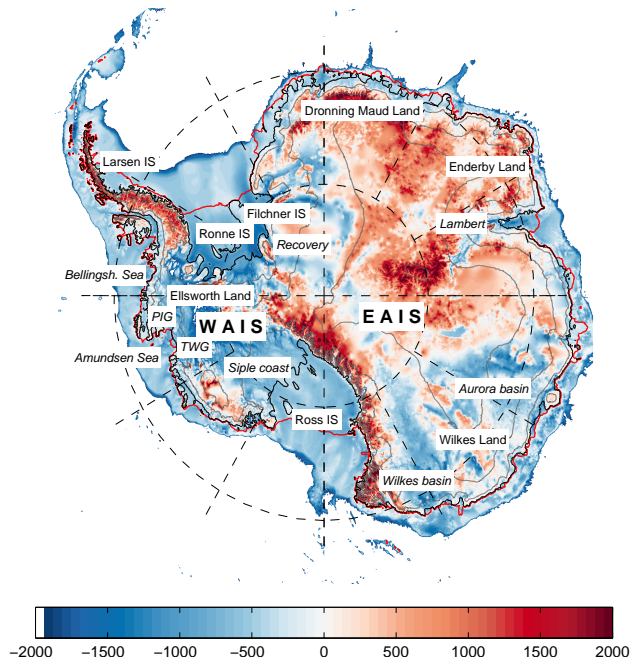


Figure 3. Bedrock topography (colour (m a.s.l.); Fretwell et al., 2013) and surface contours (grey; every 1000 m) of the Antarctic ice sheet, and ice sheet features mentioned in this paper. WAIS = West Antarctic ice sheet; EAIS = East Antarctic ice sheet; PIG = Pine Island Glacier; TWG = Thwaites Glacier; IS = ice shelf. Grounding lines are shown in black; ice shelf edges as a red line.

Weertman-type power law ~~equation for basal sliding but~~ and the Coulomb friction law, so that it can be used in conjunction with the two types of grounding-line flux conditions. The model (with grounding lines and floating ice constrained as described above) is run forward in time, starting from modern observed bed and ice surface elevations and ~~further constrained~~ driven by the observed climatology (surface mass balance and temperature). Full thermomechanical coupling and temperature evolution, isostatic bedrock adjustments ~~as well as~~ calving and sub-grid ice-shelf pinning is equally considered. ~~Basal sliding~~ For the Weertman sliding law, basal sliding coefficients $A_b(x, y)$ are initialized with a constant value ($A_b = 3 \times 10^{-9} \text{ m a}^{-1} \text{ Pa}^{-2}$) for the grounded ice sheet and a higher value ($A_b = 10^{-5} \text{ m a}^{-1} \text{ Pa}^{-2}$) underneath ice shelves and the ocean, to account for slippery saturated marine sediments in case of re-grounding. At intervals of Δt_{inv} years, at each ~~grid point with grounded ice~~ grounded ice grid point, the local basal sliding coefficients $A_b(x, y)$ in Eq. (9) are adjusted by a multiplicative factor

10 (Pollard and DeConto, 2012b):

$$A_b^* = A_b \times 10^{\Delta z}, \quad (40)$$

where

$$\Delta z = \max \left[-1.5, \min \left(1.5, \frac{h_s - h_s^{\text{obs}}}{h_s^{\text{inv}}} \right) \right], \quad (41)$$

and where h_s^{obs} is the observed ice ~~thickness~~ surface elevation and h_s^{inv} is a scaling constant. During the inversion procedure, basal temperature is still allowed to influence sliding. Adjusted $A_b^*(x, y)$ values are also not allowed to exceed $10^{-5} \text{ m a}^{-1} \text{ Pa}^{-2}$, representing the slipperiest deformable sediment. At the grounding line, observed surface velocities (Rignot et al., 2011) are used to define the buttressing factors at the grounding line in the grounding-line flux condition. Values for A_b^* are only updated when $r > 0$ in Eq. (10), so that they are kept unchanged when ice is frozen to the bedrock.

In addition to Pollard and DeConto (2012b) we also introduce a regularization term that essentially smooths high-frequency noise in the basal sliding coefficients by using a Savitsky-Golay filter of degree 3, with a span of 200160 km (surrounding influence matrix). The ~~influence matrix is thus made a function of horizontal distance instead of a fixed cell size.~~ The advantage of such filter is that it keeps lower-frequency variability intact while removing high-frequency noise. ~~This further improves the final fit.~~ The filter is only applied for marine areas ($b - z_{sl} < 0$) as it improves the fit in these areas compared to the non-regularized case and ~~it~~ guarantees a smooth transition between the inland bedrock bed and the more slippery ocean beds under present-day ice shelves.

15 For the Coulomb friction law, optimization starts with a constant field of $O_b = 1$. Eq. 40 then transforms to

$$\underline{O_b^* = O_b \times 10^{-\Delta z}}. \quad (42)$$

Values of O_b are limited between 0.01 and 5 in order to keep $\tan \phi$ between physically plausible values.

Optimized basal sliding coefficients (Fig. ~~??4~~) for the Antarctic ice sheet on a spatial resolution of 25 km were obtained after a forward integration of 10080,000 years with $h_{\text{inv}} = 4000$ and $\Delta t_{\text{inv}} = 500$ $h_{\text{inv}} = 2000$ and $\Delta t_{\text{inv}} = 1000$ year. This results in a small difference (within 100 m) between the observed and the steady-state modelled topographic surface of the interior ice sheet (Fig. ~~??~~). ~~For this run, the SIA model was preferred, as the velocity constraint on the ice shelves does not require the SSA solution. Experiments with the hybrid model resulted in very similar results and a model drift after initialization comparable to the SIA model.~~ 4). The highest sliding coefficients are found in the marginal areas, especially in the Siple Coast sector, as well as under Pine Island and Thwaites Glaciers. Higher values are also encountered in the centre of the ice sheet, which is also obvious in other studies (Pollard and DeConto, 2012b; Bernales et al., 2016). These areas also show larger misfits (Fig. ~~??4~~) and may be attributed to the poor knowledge of bedrock topography, so that uncertainties are translated into a basal friction anomaly.

~~Difference between optimized and observed surface elevation after 100,000 years of integration with $h_{\text{inv}} = 4000$ and $\Delta t_{\text{inv}} = 500$ year.~~

30 ~~Since the temperature field can be determined in steady-state, the time needed to reach a steady-state ice sheet is much shorter than in a conventional thermomechanically-coupled ice-sheet model. This allows for shorter integration times for convergence~~

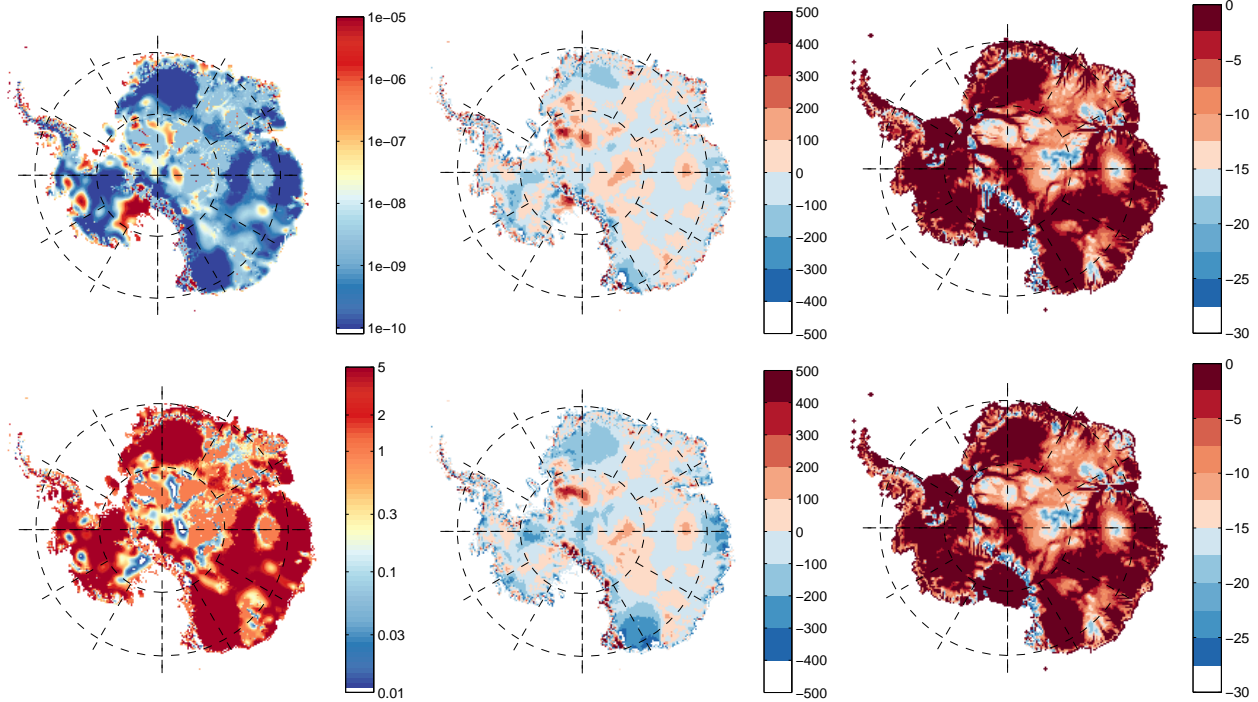


Figure 4. Optimized Top row: optimized basal sliding coefficients $A_b^*(x,y)$ after 10080,000 years of integration with $h_{mv} = 4000$ (left); difference between optimized and $\Delta t_{mv} = 500$ year observed surface elevation (center); basal temperature relative to pressure melting point (right). Bottom row: similar as top row but with optimized friction coefficients $O_b^*(x,y)$ according to the Coulomb friction law.

and updating intervals. The obtained patterns are in general agreement with the results from Pollard and DeConto (2012a, b). The, i.e., the largest errors are found around the major mountain ranges (e.g., Transantarctic Mountains), since outlet glaciers protruding through these mountain ranges are not well represented on coarser grid cells. However, this fit has been improved by including bedrock variability in determining basal sliding coefficients A_b^* in Eq. (10) to allow for basal sliding of smaller outlet glaciers across mountain ranges.

5 The lower row of Fig. 4 displays the result for the Coulomb friction law, in combination with the grounding-line flux condition of Tsai et al. (2015). The pattern of optimized friction parameters is similar to the one obtained for Weertman sliding (but inverse, since it displays friction instead of sliding). The optimization results in a slightly larger misfit (especially near the Wilkes Basin in East Antarctica), and this may be attributed to the rather coarse approach taken here to account for the spatial distribution of subglacial water pressure and till friction angle.

10 The basal temperature fields (Fig 4) for both optimizations are quite similar and in general agreement with basal temperature fields from other Antarctic modelling studies. Differences can easily be attributed to the use of geothermal heat flow datasets, which has the largest impact on basal temperature distribution (Pattyn, 2010).

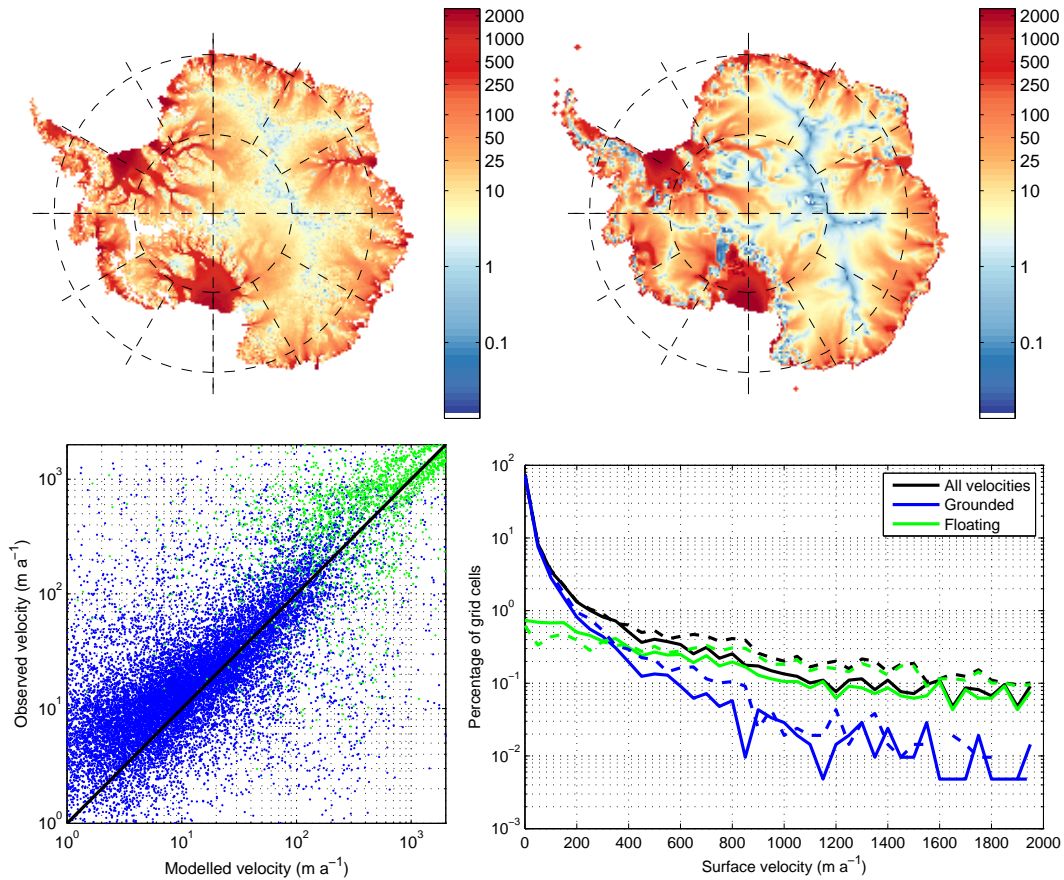


Figure 5. Modelled-Observed (top left) and modelled (top right) ice sheet surface velocities after optimization; point-by-point scatterplot of modelled and observed (Rignot et al., 2011) ice sheet (blue) and ice shelf (green) velocities (bottom left); histogram of velocity distribution of observed (dashed) and modelled (solid) velocities. Each of the bins contains a velocity range of 50 m a⁻¹ (bottom right).

4.2 Model validation

Modelled velocities form an independent check of the model performance, since the optimized basal sliding coefficients are obtained solely from the observed surface topography. The modelled flow field of the Antarctic ice sheet (Fig. 5) compares well to observations of surface velocities due to Rignot et al. (2011), such as the delineation of the different drainage basins and major ice streams discharging into the ice shelves. Some disagreement is found on glaciers discharging through the Transantarctic Mountains in the Ross ice shelf as well as glaciers near the Ellsworth Mountains discharging in the Ronne ice shelf. Those mismatches can be traced back by to the difficulty in resolving those feature during the initialization process.

Point-by-point scatterplot of modelled and observed (Rignot et al., 2011) velocities. The mean difference from modelled to observed velocities for grounded points (blue) is 19 m a^{-1} ($\sigma = 236 \text{ m a}^{-1}$). For floating points (green) a larger difference of 57 m a^{-1} ($\sigma = 549 \text{ m a}^{-1}$) is obtained.

A direct comparison between the present-day velocity field (Rignot et al., 2011) and modelled velocities ~~are shown in Figs. ?? and ??~~ is shown in Fig. 5. The scatterplot (Fig. ??) shows a qualitatively good one-to-one fit for both the grounded ice sheet and the floating ice shelves. Quantitative error analysis shows a mean misfit of 19.11 m a^{-1} with a standard deviation of 236.190 m a^{-1} for the grounded ice flow, and a mean misfit of 57.97 m a^{-1} with a standard deviation of $549.1572 \text{ m a}^{-1}$ for the floating ice shelves. The histogram comparison (Fig. ??) demonstrates a good overall fit of observed and modelled velocity magnitudes. ~~The modelled velocities are slightly higher than the observations, which can be attributed to the vertically-integrated nature of the model the approximation made in ice physics and thermomechanics. Nevertheless, the overall velocities (including ice shelves) map well with the observed ones and the~~ and the result is in line with other model studies (e.g., Martin et al., 2011).

~~Histogram of velocity distribution of observed (dashed) and modelled (solid) velocities. Each of the bins contains a velocity range of 50 m a^{-1} .~~

5 Sensitivity experiments

5.1 Sensitivity to ice-shelf de-buttressing

Ice shelves are the prime gatekeepers of Antarctic continental ice discharge. The breakup of the Larsen B ice shelf (Fig. 3) and the subsequent speed-up of outlet glaciers that previously discharged into the ice shelf witness this important instability mechanism (Scambos et al., 2000, 2004). In West Antarctica, observational evidence (Rignot et al., 2014) as well as modelling studies (Favier et al., 2014; Joughin et al., 2014; Seroussi et al., 2014) show that the reduction in buttressing of ice shelves in the Amundsen Sea embayment may lead to significant inland ice mass loss, and that unstoppable retreat of the grounding line of Thwaites Glacier may already be on its way (Joughin et al., 2014).

Since ice shelf buttressing is a key element in the stability of the Antarctic ice sheet, a useful experiment to understand underlying model buttressing physics is the sudden removal of all floating ice shelves, starting from the initialized model state, and to let the model evolve over time. Over this period ice shelves were not allowed to regrow, which is equivalent to ~~a constant removal of removing~~ removing all floating ice at each time step. This experiment is carried out for ~~the two implemented grounding line physics~~ three cases, i.e., (i) power-law sliding with the flux condition according to Schoof (2007a) (SGL) ~~and~~, (ii) Coulomb friction with flux condition according to Tsai et al. (2015) (TGL), ~~respectively. Both~~ and (iii) power-law sliding with the TGL condition (TGL-1). All experiments result in a sudden ice-mass loss and grounding-line retreat, whereby the West Antarctic ice sheet collapses entirely in less than 200 years according to SGL and less than 100 years according to TGL, respectively (~~Figs Fig. 6 and ??~~). For both. Both TGL experiments lead to a similar mass loss (both in terms of timing and volume). Therefore, the decisive factor governing mass changes is the grounding-line flux condition and not the sliding/friction law that is employed for the grounded ice sheet.

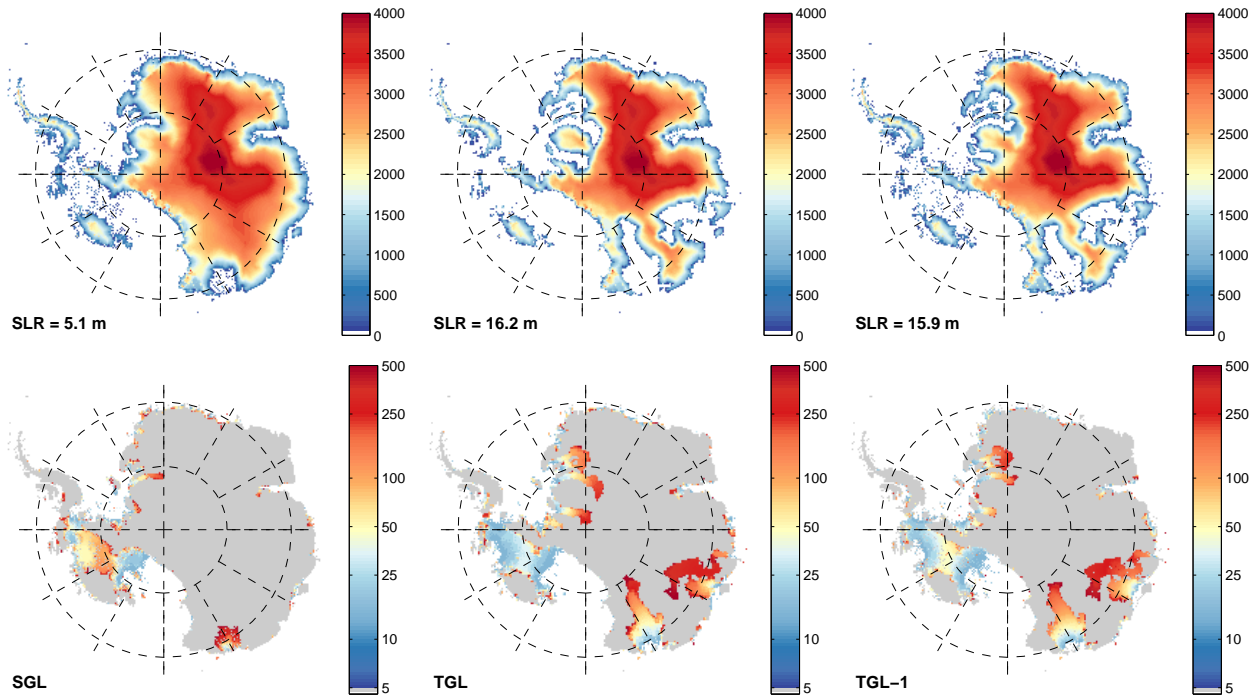


Figure 6. Top: Grounded ice sheet surface elevation (m a.s.l.), 500 years after sudden removal of all ice shelves (left), and Bottom: grounding-line position in time according to the same experiment (right; colour scale is nonlinear and represents time (ain years)) for the Weertman sliding law with SGL condition (top left), Coulomb friction law with TGL condition (center), and Weertman sliding law with TGL condition (bottom right) grounding-line flux conditions. SLR denotes the contribution to sea level rise after 500 years.

For all experiments, grounding-line retreat starts in the marine sections discharging in the Ronne and Ross ice shelves. For the SGL experiment, the retreat from Ellsworth Land leads to thinning in the inland sectors of the Pine Island basin, which after >50 years triggers grounding-line retreat from Pine Island Glacier and subsequently Thwaites Glacier. Grounding-line retreat then spreads rapidly towards the Ross sector of the West Antarctic ice sheet, leading to a complete disintegration of the ice sheet within 150 years. However, for the TGL experiment both TGL experiments, initial grounding-line retreat also occurs in the Amundsen Sea sector, whereby the retreat is much faster and the ice sheet collapses within less than 100 years. Another major difference between both SGL and TGL experiments is that the total mass loss SLR contribution for TGL is three times as large compared to SGL, i.e., a contribution to sea level rise of ~ 1216 m for TGL compared to ~ 4.55 m for SGL after 500 years. The extra mass loss is essentially located in the East Antarctic ice sheet, i.e., Wilkes and Aurora basins (Wilkes Land; Fig. 3), both losing substantial amounts of ice. Despite the presence of a sill at the outlet of Wilkes subglacial basin, grounding-line retreat occurs without invoking any other physical mechanism than the flux condition at the grounding line in combination with complete ice shelf collapse. These results contrast with Mengel and Levermann (2014) who require the removal of a specific

coastal ice volume equivalent to 80 mm of ~~sea-level rise-SLR~~ in order to provoke an unstable grounding-line retreat within Wilkes basin.

~~Evolution of the mean driving stress in the grounding zone—within 50 km upstream of the grounding line after sudden removal of all ice shelves (top) and corresponding ice mass loss—in terms of rate of sea-level rise (bottom) for the SGL and~~

5 TGL experiments.

The higher TGL grounding-line sensitivity must be sought in its underlying physics: at the grounding line the basal shear stress vanishes in a smooth way to reach zero exactly at the grounding line. As shown by Tsai et al. (2015), this is not the case for the SGL algorithm, where a sharp contrast between the inland non-zero basal shear stress and the ocean exists. This boundary becomes smoother with larger sliding velocities, leading to a larger transition zone (Pattyn et al., 2006; Gladstone et al., 2012; Feldmann et al., 2014), but the transition jump does not vanish. ~~For both cases (SGL and TGL), removal of ice shelves leads to an increase in driving stresses.~~ The SGL condition at the grounding line is therefore a function of the friction coefficient A_b , while the TGL condition is related to a single parameter in the friction law, i.e., the till friction angle. The latter is also limited in its range, contrary to A_b ranging across several order of magnitude (from saturated till to nearly frozen bedrock). Furthermore, the TGL condition is a function of ice thickness h to a higher power compared to SGL. Since the TGL ice flux is larger than the SGL flux for similar conditions, the surface gradient at the grounding line is generally higher, ~~mainly due to steeper surface slopes. As shown in Fig. ??, where the mean driving stress in the region within 50 km upstream from the grounding line is plotted in time, driving stresses increase when sudden mass loss is provoked. An increase in driving stress is therefore coincident with the collapse of the West Antarctic ice sheet (note the sudden increase in the rate of sea level rise; Fig. ??). While this is valid for both flux conditions, TGL is characterized by higher driving stresses throughout, hence a more important ice discharge, which facilitates unstable grounding-line retreat. This higher sensitivity hence leading to higher driving stresses. These steeper surface slopes make the grounding line to retreat (and advance) more rapidly than with the power-law condition (SGL). The higher sensitivity for TSL is also demonstrated in the modified MISIP experiments (Appendix C). Additionally, I carried out a series of sensitivity tests by fixing the value of the till friction angle at the grounding line ϕ , ranging from 10 to 60°. Only for $\phi \geq 50^\circ$ did the sensitivity decrease, but the amount of mass loss was still significantly higher than with the SGL condition.~~

5.2 Sensitivity to sub-shelf melt

Antarctic ice sheet sensitivity to sub-shelf melting is investigated with a multi-parameter/multi-resolution forcing ensemble over a period of 500 years. ~~A few experiments were also run over 5000 years.~~ Atmospheric forcing includes changes in background temperature ΔT , ranging from 0 to +8.5°C, affecting both surface temperature, Eq. (37), and surface mass balance, Eq. (38), through the mass balance–elevation feedback. Surface melt is calculated with the PDD model, Eq. (39). Ocean forcing is based on constant forcing values of sub-shelf melting ΔM , ranging from 0 to 50 m a⁻¹ underneath the freely floating ice shelves surrounding the Antarctic ice sheet, and between 0 and 6.25 m a⁻¹ for the Ronne-Filchner and Ross ice shelves (factor 8 less compared to the freely-floating ice shelves). Melting is ~~not allowed to be spread out across the grounded part of the ice sheet near the grounding line as is done in some models only applied to fully floating grid cells, without taking into account the~~

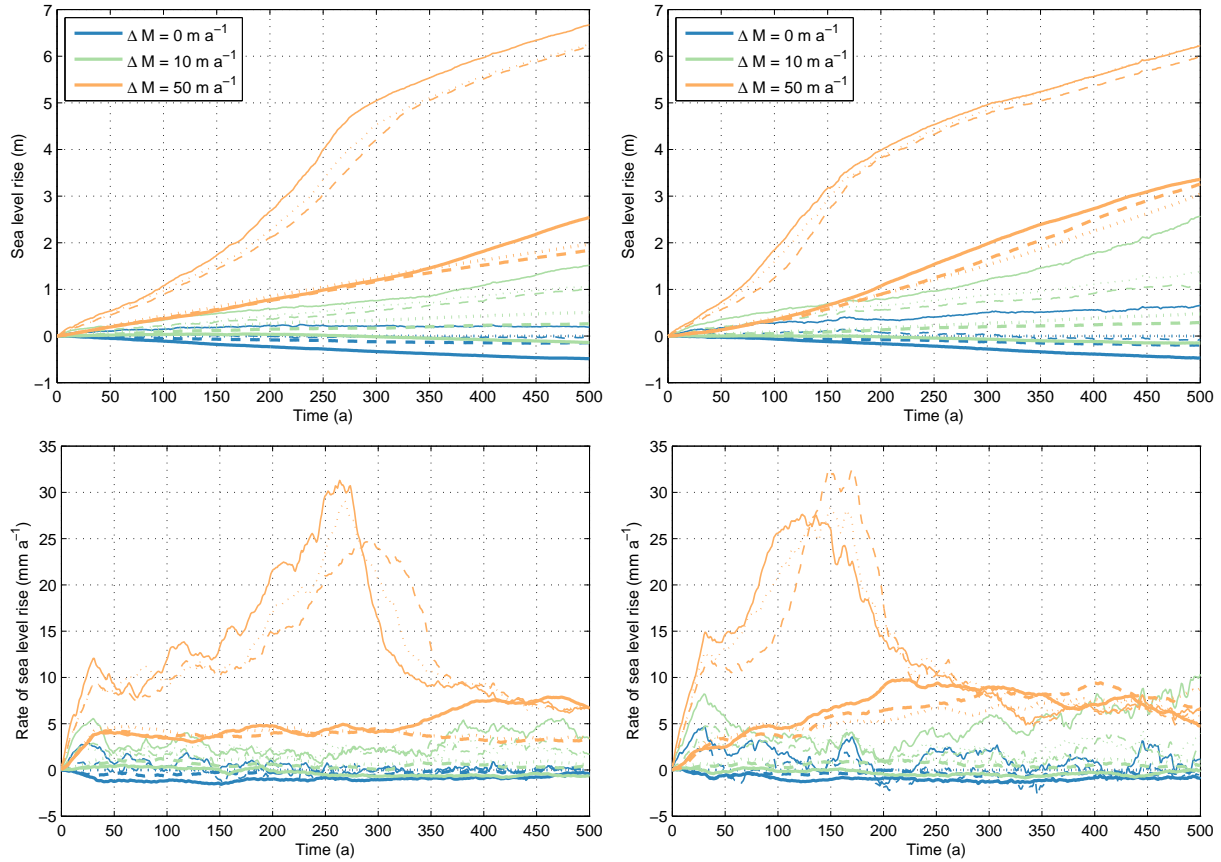


Figure 7. Evolution of sea-level contribution (top) and rate of sea-level rise (bottom) as a function of basal melting underneath ice shelves and background temperature change for the 25 km (left) and 40 km (right) spatial resolutions. **Temperature Atmospheric temperature** forcing is as follows: 0°C (dotted), 2.2°C (dash-dot), 4.5°C (dashed), and 8.5°C (solid line). The thick lines correspond to the SGL grounding-line flux, while the thin lines correspond to the TGL flux.

fractional area of grounded grid points that are actually afloat, as done in a few studies (Feldmann et al., 2014; Golledge et al., 2015). All forcings are applied as a sudden change in temperature/melt rate starting from the initialized model. A background run (without applying the forcing anomaly) is also performed to determine the model drift on the different time scales. The experiments are run for different combinations of sudden changes in background temperature/basal melting rate underneath the ice shelves on a grid size of $\Delta = 25$ km (as well as on a $\Delta = 40$ km grid to test grid-size dependence). A few runs are performed on a grid size of $\Delta = 16$ km for comparison. ~~This gives a total of 40 forcing experiments for the $\Delta = 25, 40$ km grid spacings, and a further 10 experiments (considering only sub-shelf melt forcing) over a time span of 5000 years.~~

Sea-level contribution according to the forcing experiments and rate of change of sea level for the $\Delta = 25, 40$ km spatial resolutions are shown in Fig. 7. These are determined from the change in ice volume above floatation, ~~hence do not represent the total grounded ice mass loss (Bindshadler et al., 2013; Nowicki et al., 2013).~~ Sea-level change (Bindshadler et al., 2013; Nowicki et al., 2013) SLR according to the forcings ranges between -0.5 and 6.57 m after 500 years. ~~Sea-level rise~~ It increases with increasing sub-shelf melt rates and slightly decreases with increasing atmospheric temperature forcing. The latter is due to ~~the increased higher~~ precipitation rates in a warmer climate, leading to an increase in grounded ice mass. However, for larger atmospheric forcing (+8.5°C), mass loss is generally enhanced due to the dominance of surface melt and/or increase in ice flux with increased precipitation rates. The different curves in Fig. 7 are clustered according to sub-shelf melt rate, which is the most decisive process governing mass loss. Atmospheric forcing, however, has only a limited effect, probably because the time scale considered (500 years) is too short to relax the ice sheet to the imposed temperature and precipitation changes, and because weakening of ice shelves through hydro-fracturing is not taken into account. Model drift (zero forcing anomaly) is between 60 and 75 cm of sea level lowering over a period of 500 years, or 0.2–0.3% of the total Antarctic ice sheet volume per Century. This is comparable to other Antarctic model studies (e.g., Nowicki et al., 2013) and shows that the initialization is rather stable and close to steady-state.

The major ~~discrepancy differences~~ in sea-level response ~~is with respect are due~~ to the treatment of grounding-line fluxes. ~~The~~ As shown above, the TGL flux condition systematically leads to significant higher mass losses, making grounding-line migration a more sensitive process ~~as already shown in~~ (Sect. 5.1). The higher sensitivity leads to a rate of change in sea level of up to ~~20–30~~ 20–30 mm a⁻¹. These high values correspond to periods when the marine ice sheet runs into a major instability (MISI). Note, however, that such rates are still significantly lower than those obtained during the ice-shelf removal experiment (~~up to 1 m a⁻¹; Fig. ??~~). For the SGL flux condition, these values are half as much, and major MISIs occur generally at a later stage during the model run. Compared to other studies (Golledge et al., 2015; Ritz et al., 2015; DeConto and Pollard, 2016), the TGL flux conditions puts sea-level contributions at the high end of the spectrum ~~and is comparable to the more ‘aggressive’ grounding-line migration setup in Golledge et al. (2015).~~

Only the higher melt-rate scenarios (~~20–50~~ >10 m a⁻¹) produce significant MISIs over this time period. They first occur in the West Antarctic ice sheet (WAIS), starting from either Pine Island or Thwaites Glacier, progressing inland. Other MISI-prone areas are the Bellingshausen Sea (WAIS) and Wilkes basin (East Antarctic ice sheet – EAIS). Contrary to the de-buttressing experiment in Sect. 5.1, MISIs are not initially triggered in the Siple Coast area, nor through Ellsworth Land. This is probably

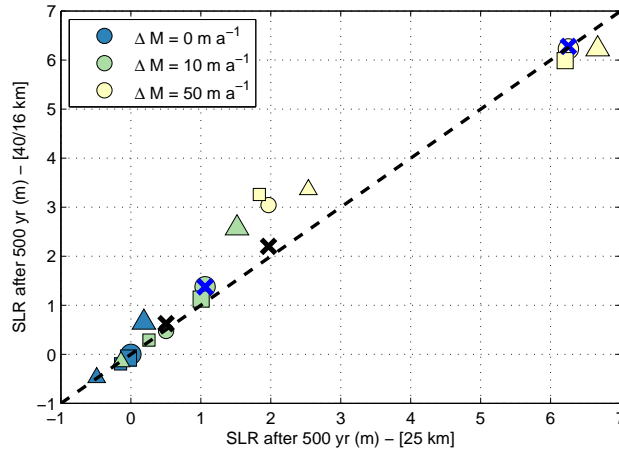


Figure 8. Comparison of sea-level contribution after 500 years as a function of model resolution (25 vs 40 km). Colours denote sub-shelf melt rates; shapes represent background temperature forcing: 0°C (circles), 2.2°C (squares), 4.5°C (triangles), 8.5°C (inverted triangles). Small markers denote the SGL-grounding-line flux condition Weertman-SGL, while large markers the TGL condition Coulomb-TGL. Results for Crosses are the 50 m a⁻¹ melt rate/no forcing anomaly/Tsai flux experiment at a spatial resolution of 16 km is denoted by a red cross comparison between 25 (x-axis) and compared to the 40-16 km results (y-axis) for experiments without atmospheric forcing (only melt); Black = Weertman-SGL; Blue = Coulomb-TGL.

due to the lower imposed melt rates, so that both Ronne and Ross ice shelves remain buttressed for a longer period of time. However, over longer time spans (5000 year), MISs in the West Antarctic ice sheet seem to occur for lower melt rates.

Evolution of sea-level contribution (top) and rate of sea-level rise (bottom) as a function of basal melting underneath ice shelves for 25 km (thick lines) and 40 km (thin lines) spatial resolutions and the TGL flux condition over 5000 year.

5 Atmospheric forcing is not considered.

Sea-level change over millennial time scales (5000 years) is investigated for the TGL flux condition without atmospheric forcing (Fig. ??). Here, only melt rates up to 20 m a⁻¹ were considered, so that rate of sea-level change are lower compared to the previous experiment. Most MISs occur in the first 1000 years (for the highest melt rates) and within 2000 years for the 15 m a⁻¹ rates. MISs occur at later periods (and are also less pronounced) for melt rates of 10 m a⁻¹. However, after 5000 years, sea level contribution is comprised between 7.5 and 10.5 m for all scenarios. They all represent a major destabilisation of the West Antarctic ice sheet. The higher melt scenarios also present significant contributions of the East Antarctic ice sheet (primarily Wilkes and Aurora basins).

The effect of spatial resolution on model result is summarized in Fig. 8 in addition to the data presented in Figs Fig. 7 and ?. Coarser resolutions (40 km) give comparable results to the 25 km grid spacing with an almost one-to-one fit of sea-level contribution after 500 years between both resolutions. Both flux conditions follow this same fit. Larger deviations are observed over longer time spans of several millennia, but the timing of the major MISs is comparable between grid resolutions (Fig. ??)

-, especially for zero melt forcing and the highest melt forcing according to Coulomb-TGL. Those cases correspond to either absence of MISIs (low SLR) or complete disintegration of WAIS (high SLR). The main reason for this relatively good fit must be sought in the grounding line flux conditions (SGL and TGL) that make the model resolution-independent. Models that are not based on such heuristics have to resolve grounding line migration at sub-kilometre resolutions (Pattyn et al., 2013; 5 Pattyn and Durand, 2013).

~~However, Differences in response (medium scenarios) are due to the precise timing of MISIs, that seems to be resolution dependent and some of the MISIs are not completed after 500 years (Fig. 7). However, a spatial resolution of 40 km generally remains to coarse, and results are much improved at 25 km. This is demonstrated by the comparison of 16 km to 25 km resolution for which obtained SLR is almost the same (crosses in Fig. 8), even for the medium scenarios. Nevertheless, it is~~ expected that at very high spatial resolutions (<5 km), grounding-line retreat is influenced by bedrock irregularities as well as the presence of ice-shelf pinning points that are not always properly resolved at coarser resolutions. The parametrization of sub-grid processes, such as basal sliding in mountainous areas and sub-shelf pinning at sub-grid level, have to some extent reduced this dependency in the model. ~~Despite these improvements, higher spatial resolutions (16 km, for instance), systematically lead to a smaller mass loss for a given forcing compared to the coarser resolutions (, but differences remain.~~

15 In order to validate this claim, two more experiments were carried out to make comparison with an existing experimental result at high resolution possible (Cornford et al., 2016). Here, sub-shelf melting is taken as a function of ice thickness (Cornford et al., 2016), i.e.,¹

$$M = \max \left[\min \left(\frac{4}{7}(H - 100), 400 \right), 0 \right]. \quad (43)$$

It limits the melt rate between zero (for ice shelves thinner than 100 m) and 400 m a⁻¹ (for ice shelves thicker than 800 m). Results are shown in Fig. 8)9. The total contribution to SLR after 500 years in the SGL experiment (3.9 m) is comparable to the finest mesh experiment in Cornford et al. (2016). As expected, the TGL experiment gives a much higher mass loss due to its inherent physics. Differences between the model response are sought in the timing of grounding-line retreat within particular drainage basins. For instance, the grounding line in the SGL experiment starts to retreat in the Siple Coast, Ellsworth Land and PIG (as in Cornford et al., 2016), while TWG kicks in at a later time. Here, the effect of bedrock highs starts to play a role in delaying grounding line retreat (Durand et al., 2011). ~~However, the overall contribution to sea level on longer time scales remains comparable to the results at lower spatial resolutions. for the TGL experiment, both PIG and TWG retreat at about the same time at the start of the model run. Such differences in response are to be expected, since both experiments are run on a much coarser resolution (25 km) than in Cornford et al. (2016), hence a different basal topography.~~

¹In Cornford et al. (2016), the applied melt rate differs from its definition in the text; the correct melt rate is given in Eq. 43 (S. Cornford, personal communication, 2017).

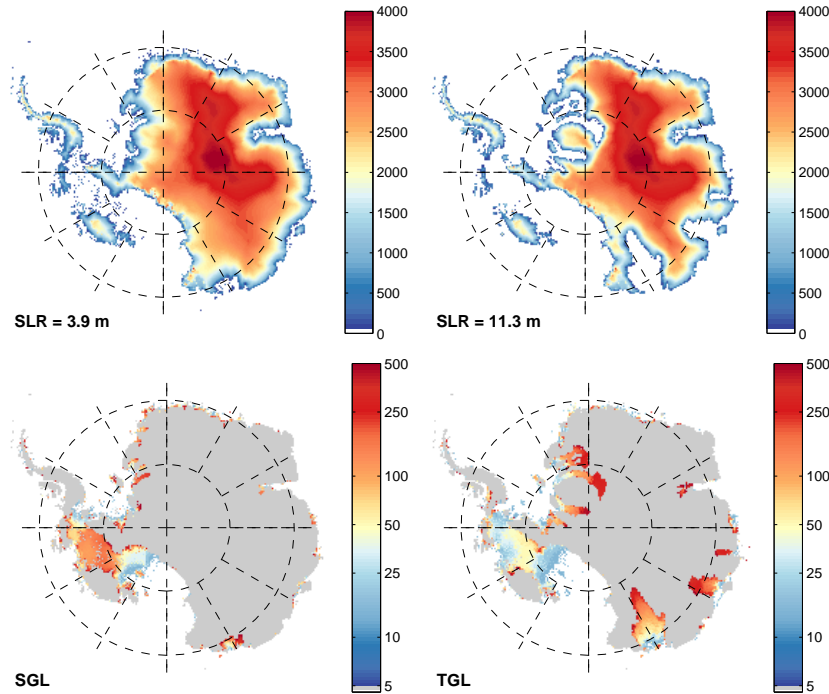


Figure 9. Top: grounded ice sheet surface elevation (m a.s.l.), 500 years after applying melt rates of Cornford et al. (2016). Bottom: grounding-line position in time according to the same experiment (colour scale is nonlinear and represents time in years) for the Weertman sliding law with SGL condition (left) and Coulomb friction law with TGL condition.

6 Discussion

In terms of model complexity, the f.ETISH model is comparable to the Pollard and DeConto (2012a) model. The major difference lies in a number of simplifications that makes the f.ETISH model two-dimensional. This is obtained by approximating the temperature ~~calculation in a semi-analytical fashion (Pattyn, 2010) and by coupling a~~ coupling by relating the mean ice-column temperature to the velocity field via the commonly-used Arrhenius relationship (Cuffey and Paterson, 2010). Another major difference pertains to the marine boundary, with ~~a novel~~ the implementation of the grounding-line flux condition according to Tsai et al. (2015), based on a Coulomb friction law (TGL). ~~This is compared to the traditional Weertman-type boundary condition (SGL) due to Schoof (2007a). Other approximations pertain to linearizations in the SSA equations and basal sliding laws.~~ further extended with a Coulomb friction law for the interior ice sheet. Finally, model initialization based on Pollard and DeConto (2012b) has been further extended with a regularization term that essentially smooths the basal friction field across marine basins and makes the results independent of spatial resolution, since regularization is made a function of horizontal distance instead of number of grid cells. Moreover, the optimization does not involve an optimization of ice-shelf basal mass balance, since observed ice-shelf velocities are used to determine the amount of buttressing at the grounding line.

The resulting initialization is characterized by a small drift once the grounding line is allowed to relax, of the order of 0.2–0.3% of the ice sheet volume in 100 years. Other marine elements such as hydro-fracture and cliff failure (Pollard et al., 2015; DeConto and Pollard, 2016) are not taken into account.

Given the ~~major~~ differences in approach with continental-scale ice-sheet models, such as AISM-VUB (Huybrechts, 1990, 2002), ANICE (de Boer et al., 2013), GRISLI (Ritz et al., 2015), ISSM (Larour et al., 2012), PISM (Bueler and Brown, 2009), PISM-PIK (Martin et al., 2011; Winkelmann et al., 2011; Golledge et al., 2015), PSU-ISM (Pollard and DeConto, 2012a), RIMBAY (Thoma et al., 2014), or SICOPOLIS (Sato and Greve, 2012), verification of the f.ETISh model requires a detailed comparison with existing benchmarks. These are generally based on results of the models cited above. The ~~EISMINT~~ EISMINT-I benchmark (Huybrechts et al., 1996) shows that the ice-dynamical characteristics of f.ETISh are in very close agreement with the ~~benchmark~~ benchmarks shown in Appendix A, despite a different numerical solution scheme. The basal temperature field is also in close agreement ~~and allowed to better define thermal control parameters in the approximation. As is to be expected, the time evolution of the basal temperature field deviates to some extent from the benchmark, with smaller time lags compared to ice thickness variations. This needs to be taken into account when the model is used on longer time scales (glacial–interglacial simulations, for instance). However, as shown in the sensitivity experiments, the thermomechanical effect is not the dominant process in marine ice sheet behaviour, and may only be of importance when focusing on central/divide areas of ice sheets.~~ The results of thermomechanical coupling of ice sheet flow is ~~despite the approximations~~ also in good agreement with the ~~EISMINT benchmark~~ (Payne et al., 2000). ~~Although deviations from the mean are larger compared to the previous benchmark,~~ EISMINT-II benchmark (Payne et al., 2000), albeit that the range of uncertainty between the different participating models on which the benchmark is based, is also much larger.

An important experiment for marine ice sheet models is a test of steady-state grounding-line positions in absence of buttressing (Pattyn et al., 2012). Boundary layer theory indeed predicts that unique grounding line positions exist on a downward sloping bed, while no stable solutions are found on reversed bed slopes (Schoof, 2007a), unless buttressing is significant (Gudmundsson et al., 2012). While the experiments are designed for flowline models, they can be extended to two dimensions to evaluate the behaviour in a qualitative way. Here, the f.ETISh model successfully passes the test independent of model resolution, as grounding-line migration is governed through a heuristic based on the above-mentioned boundary layer theory (Pollard and DeConto, 2009, 2012a) and is extended with a heuristic based on Tsai et al. (2015), that qualitatively gives the same results.

The main advantage of using a grounding-line flux parametrization based on a heuristic rule (Sect. 2.1.6) is that the model can be run at lower spatial resolutions, which is confirmed by the f.ETISh model experiments in Sect. 5.2. Solving the force balance around the grounding line requires ~~to resolve~~ membrane stresses at both sides of the grounding line to be resolved with sufficient detail ~~Schoof (2007a)~~ (Schoof, 2007a), which requires the use of sub-kilometre grid sizes (Pattyn et al., 2012), unless sub-grid grounding-line parametrizations are used that ~~generally allow for grid sizes of ≈ 10 km (Feldmann et al., 2014)~~ may allow for larger grid sizes (Feldmann et al., 2014; Cornford et al., 2016). The main disadvantage of the heuristic rule is that its parametrization is derived from a steady-state solution based on the SSA model. It can therefore be questioned whether the formulation still holds for transients. It also overrules the hybrid model at this particular location. ~~Nevertheless, comparison~~

~~with high-resolution SSA and hybrid models show that while differences in transient response exist, results are in overall agreement with the other models (Pattyn and Durand, 2013).~~

A major finding in this paper is the increased sensitivity of the grounding line based on a Coulomb friction law (Tsai et al., 2015), compared to a power-law sliding condition at the grounding line. Power-law sliding mechanisms near grounding lines have been extensively discussed, since they lead to sudden jumps in basal drag at the grounding line, especially at relatively low sliding speeds (such as in the MISMIP and MISMIP3d experiments Pattyn et al., 2012, 2013). However, sliding velocities in the Antarctic experiments are not preconditioned by a specific sliding coefficient at the grounding line, but determined from the optimization procedure. Therefore, the type of boundary is controlled by the model physics itself. The Coulomb friction condition at the grounding line is consistent with observations, as the ice-sheet profiles ‘taper off’ towards a flattening upper surface, contrary to the power-law case, and basal stresses vanish at the grounding line (Tsai et al., 2015). Moreover, the grounding-line ice flux according to Coulomb friction also depends more strongly on floatation ice thickness, implying higher sensitivity to atmospheric and ocean forcing. Furthermore, grounding is facilitated in shallower water compared to the power-law case, so that smaller perturbations may push the grounding line more easily into regions with a retrograde slope, provoking a grounding-line instability (Tsai et al., 2015). As a result of the higher sensitivity, Antarctic sea-level contribution to a given perturbation is also more than twice as high and rates of sea-level change three times as fast compared to a power-law sliding case.

Direct comparison ~~with other recent study on~~ is not possible with recent studies of Antarctic ice mass loss ~~is less evident, as most comprehensive studies follow~~ that are forced by atmosphere-ocean models following so-called RCPs (Representative Concentration Pathways) ~~that force atmosphere-ocean models~~. Direct comparison with the SeaRISE experiments (Bindschadler et al., 2013; Nowicki et al., 2013) is also hampered due to the lower melt rates applied to the Ross and Ronne-Filchner ice shelves. This differentiation was deliberately chosen, as the de-buttressing experiments show that the highest buttressing stems from those large ice shelves. However, their grounding lines are also farthest from the continental shelf break, hampering the intrusion of warmer waters compared to the smaller ice shelves that are closer to the edge.

However, considering the f.ETISh model with the SGL condition comparable to the PSU-ISM model (Pollard and DeConto, 2009, 2012a), some comparison on sensitivity can be made. For the SeaRISE experiments, the PSU-ISM model predicts a sea-level contribution after 500 years according to a $2 \times$ A1B scenario (without sub-shelf melting) of ~ 0.45 m, while the f.ETISh SGL model results in ~ 0.4 m for similar forcing conditions. One has to note, however, that the initialization of both models is different (spinup versus optimization).

~~Golledge et al. (2015) presents a series of model runs over longer time spans (5000 years) with forcings that are kept constant for a prolonged period of time, which makes comparison possible. For a RCP8.5 scenario they obtain a sea-level contribution of 5.2 m (9.3 m with sub-shelf melting spread out across the grounding line) and 8.6 (11.4) m for a RCP8.5 amplification scenario. Over the same period, f.ETISh covers the range of 8–12 m for moderate melt rates between 10 and 20 m a^{-1} . This shows that even the SGL model is more sensitive than the standard PISM model, but less sensitive when melting is allowed to be spread out across the grounding line (so-called ‘aggressive’ grounding line in PISM). The TGL model, on the other hand, systematically produces a higher contribution to sea level.~~

However, the TGL model is less sensitive than the PSU-ISM model including cliff failure and hydrofracturing (DeConto and Pollard, 2016). These processes potentially lead to a sea level contribution of 12-13 m after 500 years under a RCP8.5 scenario forced by atmosphere/ocean models. This result corresponds remarkably well with the results of the f.ETISh TGL model under complete de-buttressing (without ice-shelf growth), with complete collapse of the West Antarctic ice sheet and major ice loss in the Wilkes and Aurora basins (Fig. 6).

Finally, computational time of f.ETISh largely depends on the spatial resolution, which also governs time steps needed under the CFL condition. A hybrid-model 5000 year run with a grid size of 40 km and a time step of 0.2 year takes approximately 10,000 CPU seconds on a single AMD Opteron 2378 2.4 GHz core of the Hydra cluster (VUB-ULB) and 20,000 CPU seconds for a 500 year run with a grid size of 16 km and time step of 0.02 years on a multicore. Future developments will focus on improving the numerical solution schemes in order to reduce the calculation time (larger time steps), especially at higher spatial resolutions.

7 Conclusions

I developed a new marine ice sheet model, based on common descriptions of ice physics (combined shallow-ice and shallow-shelf approximation) and novel implementation of parametrizations of thermodynamics and grounding line migration. The model has been extensively tested against existing benchmarks and has been shown to be scale-independent, with the exception of high-spatial-resolution-where-detailed-bedrock-variability-may-delay-grounding-zones-with-small-scale-bedrock-variability, where grounding-line response to atmospheric and oceanic forcing is sensitive to spatial resolution. This makes the model extremely attractive to couple within Earth System models.

The model has been initialized to the present-day Antarctic ice sheet conditions in order to obtain initial steady-state conditions as close as possible to the observed ice sheet. Independent validation has been obtained through comparison with observed surface velocities that are not utilised during the optimization phase.

Two forcing experiments over a period of 500 years are carried out, one during which all floating ice shelves are removed, and one during which sudden atmospheric and oceanic forcing is applied. Both experiments show a very high sensitivity to grounding-line conditions, as Coulomb friction in the grounding-line transition zone leads to significantly higher mass loss in both West and East Antarctica, compared to commonly-used power-law sliding laws (such as Weertman-type). For the ice-shelf removal experiment this leads to 4.55 m and 12.2 m sea-level rise-16 m SLR for the power-law basal sliding and Coulomb friction conditions at the grounding line, respectively. This high-end response is of the same order of magnitude as obtained by DeConto and Pollard (2016) using ice-shelf de-buttressing-caused-by-hydrofracture-debuttressing-caused-by-hydro-fracture and cliff failure.

The atmospheric/oceanic forcing experiments clearly show the dominance of ocean forcing in sea-level response, where significant MISIs (Marine Ice Sheet Instabilities) occur under relatively mild sub-shelf melt scenarios over centennial time scales (500 years). Such-MISIs-seem-to-occur-even-for-melt-rates-within-the-range-of-1.25-10 m a⁻¹-over-millennial-time-scales (5000 years)-

8 Data availability

All datasets used in this paper are publicly available, such as Bedmap2 (Fretwell et al., 2013) and geothermal heat flow data (Purucker, 2013). Results of the RACMO2 model were kindly provided by Melchior Van Wessem.

Acknowledgements. I should like to thank Lionel Favier and Heiko Goelzer for the numerous discussions that helped in developing and improving the f.ETISH model and their helpful comments on an earlier version of the manuscript. I am also indebted to my ‘guinea pigs’ Thomas Bogaert, Violaine Coulon and Sainan Sun for revealing a few coding errors as well as for their patience while struggling with initial and non-optimized versions of the model. Finally, I should like to thank Stephen Cornford and an anonymous referee for their very helpful comments that made the manuscript/model improve significantly.

Appendix A: ~~EISMINT-I~~ EISMINT-I benchmark

10 A1 Fixed-margin experiment

The ~~EISMINT-I~~ EISMINT-I benchmark is the first series of ice-sheet model intercomparisons aiming at benchmarking large-scale ice sheet models under idealized and controlled conditions (Huybrechts et al., 1996). The first (fixed margin) experiment considers a square grid of 1500×1500 km with a flat bed at zero elevation. Grid spacing is taken as $\Delta = 50$ km leading to 31×31 regularly-spaced grid points. Starting from zero ice thickness, the model is forced with a constant surface mass balance of 0.3 m a^{-1} and surface temperature according to $T_s = 239 \text{ K} + (8 \times 10^{-8})d_{\text{summit}}^3$, where d_{summit} is defined as $\max(|x - x_{\text{summit}}|, |y - y_{\text{summit}}|)$, expressed in km. Further boundary conditions for the model are zero ice thickness at the edges of the domain and a constant geothermal heat flux of $G = 0.042 \text{ W m}^{-2}$. The ice temperature is not coupled to the ice flow field and a constant value for the flow parameter of $10^{16} \text{ Pa}^{-n} \text{ a}^{-1}$ is considered. ~~The modelled ice sheet reaches a steady state in less than 25,000 years using a time step of 25 years, due to the fact that the temperature field is taken as steady-state (no relaxation applied).~~

The f.ETISH model is a 3d Type I model according to the classification scheme in ~~EISMINT-I~~ EISMINT-I, i.e., diffusion coefficients for the grounded ice sheet are calculated on a staggered Arakawa-B grid. Table A1 lists the comparison with data from other 3d Type I models. Both ice thickness and flux compare very well within error bounds of the sample range (limited to only 2–3 models in the ~~EISMINT-I~~ EISMINT-I benchmark, unfortunately). Also the basal temperature at the divide and along the profile is within the limits given by the ~~EISMINT-I~~ EISMINT-I benchmark. ~~The profile of the basal temperature in agreement with the benchmark (Fig. A1 has been obtained by setting $f_s = 0.25$ in Eq. (28). This way, strain heating at the base of the ice sheet is reduced to implicitly account for horizontal advection. Both processes are a function of the horizontal velocity, but act in opposing ways~~ EISMINT-I benchmark. Differences can be attributed to the use of the shape functions for the velocity field as well as to the use of a staggered grid for the temperature field, whereby the temperature at the divide and along the profile are interpolated values along the central line.

Exp	Variable	Benchmark	f.ETISH
FM	h_{summit}	3419.90 ± 1.70	3421.80 <u>3421.82</u>
	q_{midpoint}	789.95 ± 1.83	790.33 <u>790.43</u>
	T_{summit}^b	-8.84 ± 1.04	-8.38 <u>-7.54</u>
MM	h_{summit}	2997.5 ± 7.4	2986.30 <u>2986.41</u>
	q_{midpoint}	999.24 ± 17.91	994.38 <u>994.49</u>
	T_{summit}^b	-13.43 ± 0.75	-12.68 <u>-11.81</u>

Table A1. Comparison of f.ETISH with the ~~EISMINT-I~~ EISMINT-I fixed (FM) and moving margin (MM) experiment benchmark based on an ensemble of 2–3 models (Huybrechts et al., 1996) for the steady-state experiment.

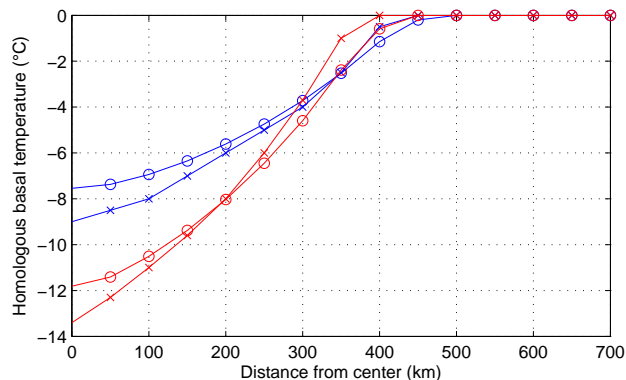


Figure A1. Homologous basal temperatures along the central line according to the ~~EISMINT-I~~ EISMINT-I experiment calculated with f.ETISH (circles) and according to the ~~EISMINT-I~~ EISMINT-I benchmark (crosses) for the fixed margin (blue) and moving margin (red) experiment.

A2 Moving margin experiment

The moving-margin experiment includes ice ablation, hence the presence of an equilibrium line on the ice sheet. This is obtained by defining the climatic conditions by $\dot{a} = \min\{0.5, h_s(R_{\text{el}} - d_{\text{summit}})\}$ and $T_s = 270 - 0.01h$, where d_{summit} is here defined as the radial distance from the centre (in km), and s and R_{el} are $10^{-2} \text{ m a}^{-1} \text{ km}^{-1}$ and 450 km, respectively (Huybrechts et al., 1996). The steady-state ice sheet according to this experiment does not reach the edge of the domain, but is circular in shape. Note that, contrary to the fixed margin experiment, surface temperature is a function of surface elevation and not of the geometrical characteristics of the domain. Surface mass balance, however, remains a function of the distance to the centre of the domain.

Basic characteristics of the experiment are listed in Table A1, and simulated values of ice thickness (h_{summit}) and basal temperature at the divide (T_{summit}^b), as well as ice flux between divide and margin are in good agreement with the benchmark. Also

Exp	Variable	Benchmark	f.ETISH
FM 20ka	h_{summit} (200 ka)	3264.8±5.6	3268.80 <u>3266.02</u>
	Δh_{summit}	563.0±3.7	565.94 <u>566.20</u>
	$\Delta T_{\text{summit}}^b$	2.11±0.09	1.69 <u>2.67</u>
FM 40ka	h_{summit} (200 ka)	3341.7±3.9	3345.98 <u>3344.51</u>
	Δh_{summit}	619.0±3.2	621.60 <u>621.53</u>
	$\Delta T_{\text{summit}}^b$	4.12±0.06	2.71 <u>2.79</u>
MM 20ka	h_{summit} (200 ka)	2813.5±2.0	2806.82 <u>2805.19</u>
	Δh_{summit}	528.6±11.3	533.88 <u>533.66</u>
	$\Delta T_{\text{summit}}^b$	2.54±0.00	4.93 <u>0.95</u>
MM 40ka	h_{summit} (200 ka)	2872.5±6.8	2872.91 <u>2871.85</u>
	Δh_{summit}	591.4±4.6	595.27 <u>595.38</u>
	$\Delta T_{\text{summit}}^b$	7.61±0.05	8.04 <u>6.51</u>

Table A2. Comparison of f.ETISH with the ~~EISMINT-I~~ EISMINT-I fixed (FM) and moving margin (MM) experiment benchmark based on an ensemble of 2–3 models (Huybrechts et al., 1996) for the forcing experiments with a sinusoidal signal of 20 and 40 ka, respectively. Bold values are those outside the range given by the benchmark results.

the basal temperature profile agrees well with the benchmark, ~~for the same value of f_s used in the fixed margin experiment~~ and differences can be attributed to the factors listed in Appendix A1.

A3 Transient experiment

Temporal changes in ice thickness/volume and basal temperature are analysed with a forcing experiment, where the surface temperature and mass balance perturbations are defined as follows (Huybrechts et al., 1996):

$$\Delta T = 10 \sin\left(\frac{2\pi t}{T}\right), \quad (\text{A1})$$

$$\Delta \dot{a} = 0.2 \sin\left(\frac{2\pi t}{T}\right) \quad \text{for fixed margin}, \quad (\text{A2})$$

$$\Delta R_{\text{el}} = 100 \sin\left(\frac{2\pi t}{T}\right) \quad \text{for moving margin}. \quad (\text{A3})$$

The model run starts from the steady-state ice sheet obtained in the previous section and the forcing is applied for a period of 200 ka, with a periodicity of $T = 20$ and 40 ka, respectively. Results are depicted in Fig. A2 for the fixed margin and in Fig. A3 for the moving margin experiment. Table A2 lists the main characteristics of ice thickness and basal temperature amplitude variations, as well as ice thickness at the divide at the end of the experiment (200 ka).

All ice thickness changes (amplitude and phase) as well as the phase in temperature according to the two forcing scenarios are in close agreement with the benchmark. However, amplitude ~~and phase~~ differences for the basal temperatures deviate.

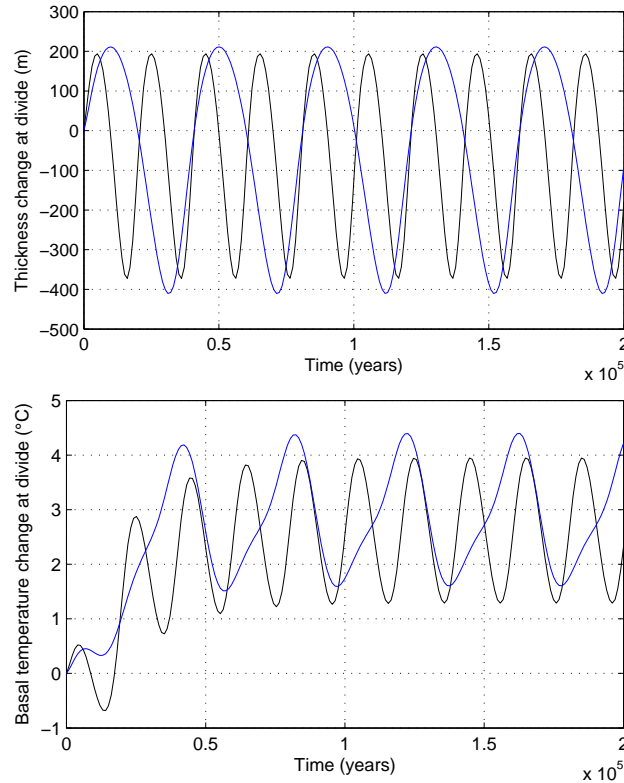


Figure A2. Ice thickness and basal temperature variations for the [EISMINT-I](#) fixed margin experiment with a 20 ka (black) and a 40 ka (blue) forcing.

The phase response of basal temperatures at the ice divide is much shorter for [f-ETISH](#) compared to the full thermodynamic calculation according to the benchmark, due to the approximation of the response time as a relaxation function. We did perform a series of sensitivity experiments (not shown) with varying tuning factors to the relaxation time (defined by the Peclet number), but this affected to a much larger extent the amplitude in response of the basal temperature signal rather than the shift in phase.

- 5 [, but the EISMINT I data sample is rather limited for comparison. The phase of the basal temperature response is in agreement with the benchmark.](#) All other parameters are within the bounds of the benchmark (Table A2).

Appendix B: [EISMINT-II](#) [EISMINT-II](#) benchmark

The [EISMINT-II](#) [EISMINT-II](#) benchmark (Payne et al., 2000) is based on the moving margin experiment of Huybrechts et al. (1996), but includes thermomechanical coupling of the ice flow to the temperature field. Contrary to the [EISMINT-I](#) [EISMINT-I](#) benchmark, inter-model differences are considerably larger, especially with respect to the area of the ice sheet that reaches pressure melting point at the base. The standard experiment consists of a flat bed of the same size as the [EISMINT-I](#) [EISMINT-I](#)

10

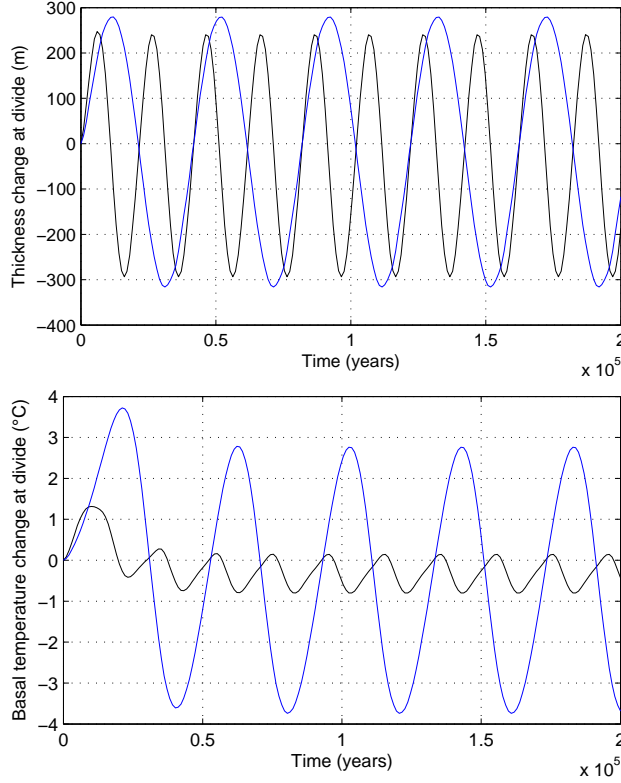


Figure A3. Ice thickness and basal temperature variations for the [EISMINT-I](#) moving margin experiment with a 20 ka (black) and a 40 ka (blue) forcing.

benchmark, but with a spatial resolution of 25 km, leading to 61×61 grid points. The basic experiment ([A in Payne et al. \(2000\)](#)) ([A in Payne et al., 2000](#)) runs the ice sheet in equilibrium starting from zero ice thickness on the domain and with $u_b = 0$. The climatic conditions are defined as:

$$\dot{a} = \min \{ \dot{a}_{\max}, s(R_{\text{el}} - d_{\text{summit}}) \} \quad (\text{B1})$$

$$5 \quad T_s = T_{\min} + s_T d_{\text{summit}}, \quad (\text{B2})$$

where d_{summit} is defined as in the moving margin experiment as the radial distance from the centre (in km), s and R_{el} are taken as in the moving margin experiment ($10^{-2} \text{ m a}^{-1} \text{ km}^{-1}$ and 450 km, respectively), and \dot{a}_{\max} , T_{\min} and s_T are defined as 0.5 m a^{-1} , 238.15K, and $1.67 \times 10^{-2} \text{ K km}^{-1}$, respectively. Contrary to the moving margin experiment, climatic conditions are independent of ice sheet surface elevation, hence the mass-balance elevation feedback is excluded.

10 ~~Four~~ [Six](#) further experiments were carried out, i.e., experiment B, C, ~~D~~ and [F](#), [F](#), [G](#) and [H](#) (in Payne et al., 2000). They consist of a stepwise change in surface temperature, $T_{\min} = 243.15\text{K}$ (B), a stepwise change in surface mass balance $\dot{a}_{\max} = 0.25$,

$R_{el} = 425$ km (C) and a stepwise shift in equilibrium-line altitude $R_{el} = 425$ km. Experiments B, C and D start from the steady-state solution of A. Experiment F is similar to A, but starting with a value of $T_{min} = 223.15$ K (model run starting without ice). Experiment G incorporates basal slip according to a linear sliding law ($m = 1$ and $A_b = 10^{-3} \text{ m a}^{-1} \text{ Pa}^{-1}$) with a similar setup as A. Finally, experiment H is similar to G, but where sliding is limited to areas that are at pressure melting at the base.

Results for experiments ~~A-D~~ A-H are summarized in Table A3. The majority of parameters are within the bounds of the benchmark, but major differences are related to the basal temperature at the divide. All experiments exhibit a radial pattern in basal temperatures that are at pressure melting point for the outer part of the ice sheet, with a cold spike in the center of the ice sheet. In all experiments, our temperature spike is slightly less cold than the one given by the benchmark. However, despite this ~~significant~~ difference, the size of the basal area at pressure melting point is in accord with the benchmark. ~~The~~ Again, the main reason for this ~~large~~ difference is that temperatures in f.ETISh are calculated on a staggered Arakawa-B grid and not exactly at the ice divide, ~~thereby always taking into account a given amount of strain heating due to the non-zero horizontal velocity. The difference is further exacerbated by the large horizontal temperature gradients for these experiments. As a result of the higher temperatures under the ice divide, the simulated divide ice thickness is also lower than the one from the benchmark. Nevertheless, ice.~~ Despite these differences in temperature, ice volume and area coverage are ~~generally in accord~~ totally in agreement with the benchmark mean.

The emblematic ~~experiment F~~ experiments F and H in Payne et al. (2000) displayed an irregular pattern in the basal temperatures of the benchmark for all participating models, leading to cold spikes reaching to the edge of the ice sheet. The pattern was shown to be model-dependent and further investigations traced its origin to an interaction between vertical advection (cooling down the base) and strain heating (Hulton and Mineter, 2000). The pattern was found to be highly dependent on spatial grid resolution due to the lack of membrane ~~stresses~~ stresses in the shallow-ice approximation (Hindmarsh, 2006, 2009). ~~Since~~ Also f.ETISh ~~does not account for vertical advection explicitly, the patterning is not produced by the model, even for a large range of surface temperature perturbations to provoke cooling at the base~~ produces a similar patterning for this particular experiment, despite the approximations in the thermomechanical coupling (using a vertically-integrated temperature) and the use of shape functions (Figure A4).

Appendix C: Modified MISMIP experiments

The capacity of an ice sheet model to cope with the marine boundary, and more specifically migration of the grounding line, is essential in Antarctic ice-sheet modelling. Since grounding-line dynamics were elucidated mathematically based on boundary layer theory (Schoof, 2007a, b, 2011), two intercomparison exercises were established. The first one tested grounding-line migration and stability on downward sloping beds and instability on retrograde slopes for flow-line models (Pattyn et al., 2012), and the second tested the effect of buttressing for two- and three-dimensional ice-sheet models (Pattyn et al., 2013). Given that marine ice sheet instability is a crucial feedback process in marine ice sheet behaviour, we performed the flow-line experiments for a plan-view model setup. Experiments were carried out for both grounding-line flux conditions SGL and TGL.

Exp	Variable	Benchmark	f.ETISH
A	Volume (10^6 km ³)	2.128±0.145	2.007 -2.133
	Area (10^6 km ²)	1.034±0.086	1.041 -1.092
	Melt fraction	0.718±0.290	0.826 -0.703
	H_{summit} (m)	3688.342±96.740	3354.515 3605.157
	T_{summit}^b (K)	-17.545±2.929	-6.500 -11.033
B	Δ Volume (%)	-2.589±1.002	-2.037 -3.628
	Δ Melt fraction (%)	11.836±18.669	12.500 -17.589
	ΔH_{summit} (%)	-4.927±1.316	-3.166 -5.259
	$\Delta T_{\text{summit}}^b$ (K)	4.623±0.518	2.323 4.115
C	Δ Volume (%)	-28.505±1.204	-28.061 -27.739
	Δ Area (%)	-19.515±3.554	-20.180 -21.002
	Δ Melt fraction (%)	-27.806±31.371	-10.044 -45.160
	ΔH_{summit} (%)	-12.928±1.501	-11.896 -12.764
	$\Delta T_{\text{summit}}^b$ (K)	3.707±0.615	-0.117 3.045
D	Δ Volume (%)	-12.085±1.236	-12.565 -12.377
	Δ Area (%)	-9.489±3.260	-10.090 -10.139
	Δ Melt fraction (%)	-1.613±5.745	7.666 -4.848
	ΔH_{summit} (%)	-2.181±0.532	-2.445 -2.168
	$\Delta T_{\text{summit}}^b$ (K)	-0.188±0.060	-0.128 -0.341
<u>G</u>	<u>Volume (10^6 km³)</u>	<u>1.589 ±0.702</u>	<u>1.529</u>
	<u>Area (10^6 km²)</u>	<u>1.032 ±0.071</u>	<u>1.088</u>
	<u>Melt fraction</u>	<u>0.352 ±0.530</u>	<u>0.319</u>
	<u>H_{summit} (m)</u>	<u>2365.206 ±1468.880</u>	<u>2220.538</u>
	<u>T_{summit}^b (K)</u>	<u>-24.016 ±7.681</u>	<u>-17.864</u>
<u>H</u>	<u>Volume (10^6 km³)</u>	<u>1.900 ±0.461</u>	<u>1.807</u>
	<u>Area (10^6 km²)</u>	<u>1.032 ±0.067</u>	<u>1.807</u>
	<u>Melt fraction</u>	<u>0.529 ±0.429</u>	<u>0.496</u>
	<u>H_{summit} (m)</u>	<u>3507.984 ±394.380</u>	<u>3225.787</u>
	<u>T_{summit}^b (K)</u>	<u>-17.925 ±2.977</u>	<u>-12.664</u>

Table A3. Comparison of f.ETISH with the EISMINT-II experiments (Payne et al., 2000).

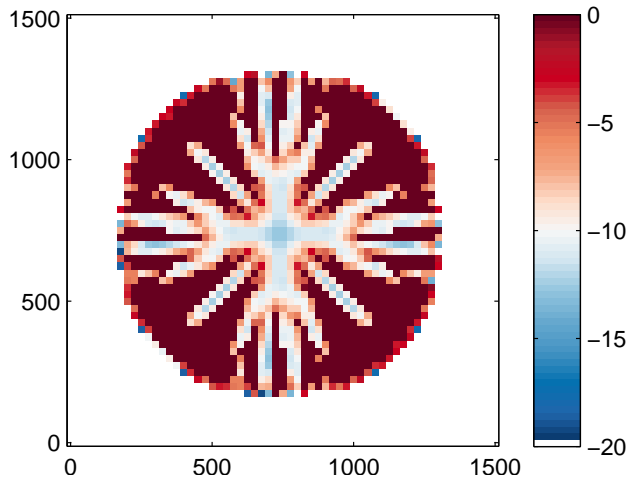


Figure A4. Predicted basal temperatures (corrected for pressure-dependence) according to EISMINT-II experiment H.

Ice shelves are included, but without exerting any buttressing strength, i.e. $\tau_{xx} = \tau_f$. The first experiment is an ice sheet on a seaward-sloping bedrock, which in plan view results in a conic bed, defined by (Pattyn et al., 2012):

$$B = 720 - \frac{778.5}{750} d_{\text{summit}}, \quad (\text{C1})$$

where d_{summit} (km) is the radial distance from the centre of the domain. The second experiment consists of an overdeepened section in the bedrock profile, hence the presence of a retrograde slope, defined by (Pattyn et al., 2012):

$$B = 729 - \frac{2184.8}{750^2} d_{\text{summit}}^2 + \frac{1031.72}{750^4} d_{\text{summit}}^4 - \frac{151.72}{750^6} d_{\text{summit}}^6. \quad (\text{C2})$$

The initial ice sheet is obtained for a constant value of the flow parameter A of $10^{-16} \text{ Pa}^{-n} \text{ a}^{-1}$ and a constant surface mass balance of $\dot{a} = 0.3 \text{ m a}^{-1}$. A grid-size spacing of $\Delta = 50 \text{ km}$ is employed. All other parameters are listed in Tables 1–3. Subsequently, the flow-rate parameter A is altered to a new value to obtain a new steady state, where lower/higher values of A leads to grounding-line advance/retreat, respectively. According to theory, a given set of boundary conditions leads to unique steady state grounding-line positions on a downward sloping bedrock, while the grounding line never reaches a steady-state position on an upward-sloping bedrock, which is depicted in Fig. A5. For the overdeepened bed, this leads to hysteresis, i.e., multi-valued grounding-line positions and ice sheet profiles for the same set of boundary conditions (Figs. A5 and A6). The numerical error was estimated by determining the position of each grounding-line grid cell compared to its radial distance from the centre of the ice sheet (both experiments results in radial ice caps). The mean position of the grounding line and the

standard deviation corresponding to each steady-state are shown in Fig. A6. Interpolation of the exact position within a grid cell was not considered. All errors are smaller than the nominal grid size of 50 km. The lowest numerical error corresponds to the grounding-line treatment according to the power-law sliding law without the presence of ice shelves ($\sigma \sim 20$ km). Including ice shelves makes the ice sheet more rapidly advance across the unstable section, since ice shelf thickness increases for lower values of A . Associated errors are also larger. Finally, the flux condition for Coulomb friction (Tsai et al., 2015) results in a generally smaller ice sheet, as the ice flux across the grounding line is higher than in the previous case. The ice sheet is also more sensitive to changes in A , i.e., small changes make the grounding line advance and retreat more rapidly. Associated errors are smaller for the no-shelf experiment, but significantly larger for the ~~retreat-ice-shelf~~ experiment. Given the larger sensitivity, the numerical solution is also less stable compared to the power-law flux condition SGL of Schoof (2007a) and the use of smaller time steps could probably improve the results.

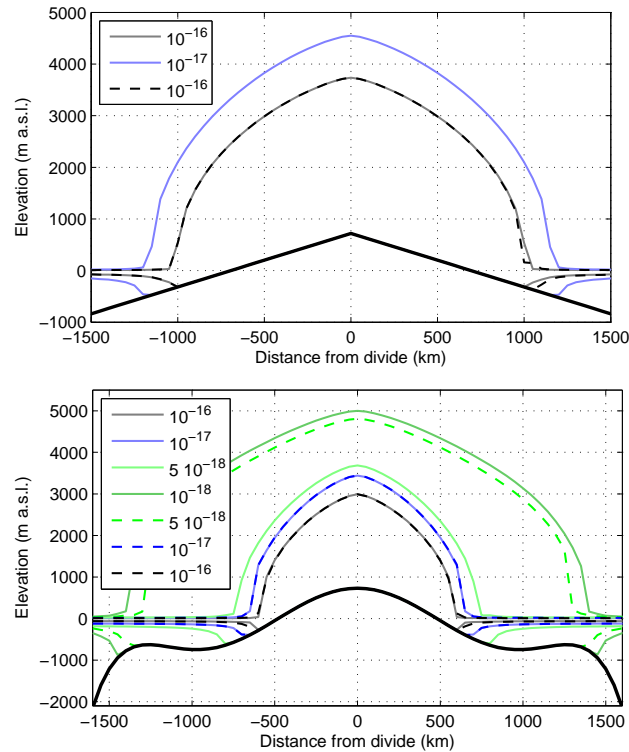
Errors on the advance and retreat grounding-line positions are displayed in the bottom panel of Fig. A6. In all cases, the difference in grounding-line position between advance and retreat is less than 10 km (one-fifth of the spatial resolution of the model). In some cases the error is exactly zero, meaning that the steady state ice sheets (the one obtained during advance compared to the one obtained after retreat) are exactly the same.

15 **Appendix D: Ice-shelf velocity diagnostics**

~~EISMINT also provided ice-shelf test for diagnostic velocities of the Ross ice shelf (MacAyeal et al., 1996), which is repeated here, but compared to interferometrically derived ice shelf velocities (Rignot et al., 2011). For this purpose, the model was run in diagnostic mode at a spatial resolution of 10 km with the Bedmap2 dataset (Fretwell et al., 2013). Ice flow velocities at the grounding line are taken from Rignot et al. (2011) and are calculated for the shelf according to the linearised SSA model equations (3), (4) and (??). The ice shelf velocity field was obtained with an adjustment flow factor of $E_f = 0.05$ (Fig. ??). The magnitude of obtained velocities is also similar for other ice shelves with the same tuning factor (not shown).~~

~~Comparison of modelled (left panel) and observed (right panel) ice shelf velocities (m a^{-1}) for the Ross ice shelf. Observed velocities are taken from Rignot et al. (2011) and resampled at a 10 km resolution.~~

~~The global Ross ice shelf velocity field is well reconstructed in the modelled result and matches the observed velocity magnitude. However, certain details of the flow field are missing, especially in relation to the outlet of Byrd Glacier, entering the Ross ice shelf (Fig. ??). However, this flow feature is also missing in some velocity reconstructions from other models (MacAyeal et al., 1996) and is probably related to an underestimation of the ice flux across Byrd Glacier.~~

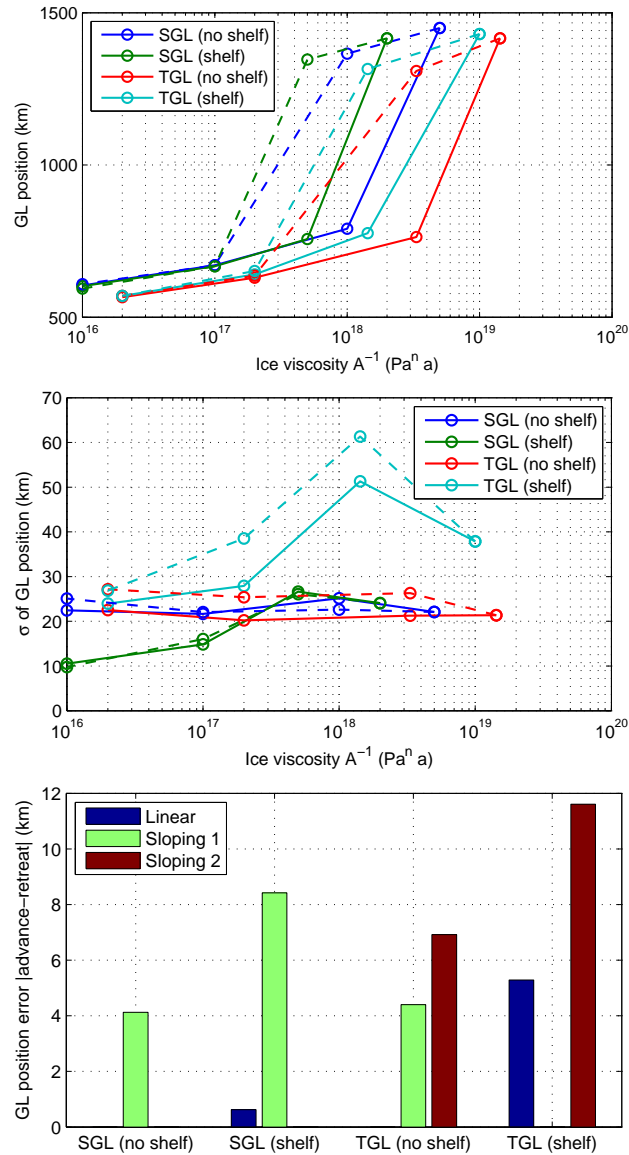


Steady-state ice-sheet/ice-shelf profiles corresponding to different values of the flow parameter A ($\text{Pa}^{-n} \text{a}^{-1}$) along the center-line for the downward-sloping bedrock (upper panel) and the overdeepened bedrock case (lower panel) according to the advance (solid line) and retreat (dashed line) experiments and a grounding-line flux-condition according to Eq. (18).

Figure A5. Steady-state ice-sheet/ice-shelf profiles for the MISIMIP experiments corresponding to different values of the flow parameter A ($\text{Pa}^{-n} \text{a}^{-1}$) along the center-line for the downward-sloping bedrock (upper panel) and the overdeepened bedrock case (lower panel) according to the advance (solid line) and retreat (dashed line) experiments and a grounding-line flux-condition according to Eq. (18).

References

- Asay-Davis, X. S., Cornford, S. L., Durand, G., Galton-Fenzi, B. K., Gladstone, R. M., Gudmundsson, G. H., Hattermann, T., Holland, D. M., Holland, D., Holland, P. R., Martin, D. F., Mathiot, P., Pattyn, F., and Seroussi, H.: Experimental design for three inter-related Marine Ice-Sheet and Ocean Model Intercomparison Projects, *Geoscientific Model Development Discussions*, 8, 9859–9924, doi:10.5194/gmdd-8-9859-2015, 2015.
- 5 Aschwanden, A., Adalgeirsdóttir, G., and Khroulev, C.: Hindcasting to measure ice sheet model sensitivity to initial states, *The Cryosphere*, 7, 1083–1093, doi:10.5194/tc-7-1083-2013, 2013.
- Beckmann, A. and Goosse, H.: A parameterization of ice shelf–ocean interaction for climate models, *Ocean Modelling*, 5, 157 – 170, doi:http://dx.doi.org/10.1016/S1463-5003(02)00019-7, 2003.



Median (upper panel) and standard deviation (lower panel) of steady-state grounding-line positions for a circular ice sheet as a function of the flow parameter A ($\text{Pa}^{-n} \text{a}^{-1}$) for the overdeepened bedrock experiment according to different flux conditions at the grounding line and inclusion/exclusion of ice shelves. Solid lines represent advance and dashed lines represent retreat experiments.

Figure A6. Median (upper panel) and standard deviation (centre panel) of steady-state grounding-line positions according to the MISIP experiments for a circular ice sheet as a function of the flow parameter A ($\text{Pa}^{-n} \text{a}^{-1}$) for the overdeepened bedrock experiment according to different flux conditions at the grounding line and inclusion/exclusion of ice shelves. Solid lines represent advance and dashed lines represent retreat experiments. The lower panel displays the difference in grounding-line position for the steady-state ice sheets obtained during advance with those obtained during retreat (same parameter values) for the linear-sloping bed (Linear) and the overdeepened bed. The latter has two sections with stable steady-state solutions, i.e., a small ice sheet (Sloping 1) and a large one (Sloping 2).

- Berger, S., Favier, L., Drews, R., Derwael, J.-J., and Pattyn, F.: The control of an uncharted pinning point on the flow of an Antarctic ice shelf, *Journal of Glaciology*, 62, 37–45, doi:10.1017/jog.2016.7, 2016.
- Bernales, J., Rogozhina, I., Greve, R., and Thomas, M.: Comparison of hybrid schemes for the combination of Shallow Approximations in numerical simulations of the Antarctic Ice Sheet, *The Cryosphere Discussions*, 2016, 1–32, doi:10.5194/tc-2016-117, 2016.
- 5 Bindschadler, R. A., Nowicki, S., Abe-Ouchi, A., Aschwanden, A., Choi, H., Fastook, J., Granzow, G., Greve, R., Gutowski, G., Herzfeld, U., Jackson, C., Johnson, J., Khroulev, C., Levermann, A., Lipscomb, W. H., Martin, M. A., Morlighem, M., Parizek, B. R., Pollard, D., Price, S. F., Ren, D., Saito, F., Sato, T., Seddik, H., Seroussi, H., Takahashi, K., Walker, R., and Wang, W. L.: Ice-sheet model sensitivities to environmental forcing and their use in projecting future sea level (the SeaRISE project), *Journal of Glaciology*, 59, 195–224, doi:10.3189/2013JG12J125, 2013.
- 10 Budd, W. F., Janssen, D., and Radok, U.: Derived physical characteristics of the Antarctic ice sheet, *ANARE Interim Reports, Series A. Glaciology*, 120, 1971.
- Bueler, E. and Brown, J.: Shallow shelf approximation as a “sliding law” in a thermomechanically coupled ice sheet model, *Journal of Geophysical Research: Earth Surface*, 114, doi:10.1029/2008JF001179, f03008, 2009.
- Bueler, E. and van Pelt, W.: Mass-conserving subglacial hydrology in the Parallel Ice Sheet Model version 0.6, *Geoscientific Model Development*, 8, 1613–1635, doi:10.5194/gmd-8-1613-2015, 2015.
- 15 Cornford, S. L., Martin, D. F., Payne, A. J., Ng, E. G., Le Brocq, A. M., Gladstone, R. M., Edwards, T. L., Shannon, S. R., Agosta, C., van den Broeke, M. R., Hellmer, H. H., Krinner, G., Ligtenberg, S. R. M., Timmermann, R., and Vaughan, D. G.: Century-scale simulations of the response of the West Antarctic Ice Sheet to a warming climate, *The Cryosphere*, 9, 1579–1600, doi:10.5194/tc-9-1579-2015, 2015.
- Cornford, S. L., Martin, D. F., Lee, V., Payne, A. J., and Ng, E. G.: Adaptive mesh refinement versus subgrid friction interpolation in 20 simulations of Antarctic ice dynamics, *Annals of Glaciology*, 57, 1–9, doi:10.1017/aog.2016.13, 2016.
- Cuffey, K. and Paterson, W. S. B.: *The Physics of Glaciers*. 4th ed, Elsevier, New York, 2010.
- de Boer, B., van de Wal, R. S. W., Lourens, L. J., Bintanja, R., and Reerink, T. J.: A continuous simulation of global ice volume over the past 1 million years with 3-D ice-sheet models, *Climate Dynamics*, 41, 1365–1384, doi:10.1007/s00382-012-1562-2, 2013.
- de Boer, B., Dolan, A. M., Bernales, J., Gasson, E., Goelzer, H., Gollledge, N. R., Sutter, J., Huybrechts, P., Lohmann, G., Rogozhina, I., 25 Abe-Ouchi, A., Saito, F., and van de Wal, R. S. W.: Simulating the Antarctic ice sheet in the late-Pliocene warm period: PLISMIP-ANT, an ice-sheet model intercomparison project, *The Cryosphere*, 9, 881–903, doi:10.5194/tc-9-881-2015, 2015.
- De Rydt, J. and Gudmundsson, G. H.: Coupled ice shelf-ocean modeling and complex grounding line retreat from a seabed ridge, *Journal of Geophysical Research: Earth Surface*, 121, 865–880, doi:10.1002/2015JF003791, 2016.
- DeConto, R. M. and Pollard, D.: Contribution of Antarctica to past and future sea-level rise, *Nature*, 531, 591–597, doi:10.1038/nature17145, 30 2016.
- Durand, G. and Pattyn, F.: Reducing uncertainties in projections of Antarctic ice mass loss, *The Cryosphere*, 9, 2043–2055, doi:10.5194/tc-9-2043-2015, 2015.
- Durand, G., Gagliardini, O., Zwinger, T., Le Meur, E., and Hindmarsh, R. C.: Full Stokes modeling of marine ice sheets: influence of the grid size, *Annals of Glaciology*, 50, 109–114, doi:10.3189/172756409789624283, 2009.
- 35 Durand, G., Gagliardini, O., Favier, L., Zwinger, T., and le Meur, E.: Impact of bedrock description on modeling ice sheet dynamics, *Geophysical Research Letters*, 38, doi:10.1029/2011GL048892, l20501, 2011.
- Favier, L., Durand, G., Cornford, S. L., Gudmundsson, G. H., Gagliardini, O., Gillet-Chaulet, F., Zwinger, T., Payne, A. J., and Le Brocq, A. M.: “Retreat of Pine Island Glacier controlled by marine ice-sheet instability”, *Nature Climate Change*, 4, 117–121, 2014.

- Favier, L., Pattyn, F., Berger, S., and Drews, R.: Dynamic influence of pinning points on marine ice-sheet stability: a numerical study in Dronning Maud Land, East Antarctica, *The Cryosphere*, 10, 2623–2635, doi:10.5194/tc-10-2623-2016, 2016.
- Feldmann, J. and Levermann, A.: Collapse of the West Antarctic Ice Sheet after local destabilization of the Amundsen Basin, *Proceedings of the National Academy of Sciences*, 112, 14 191–14 196, doi:10.1073/pnas.1512482112, 2015.
- 5 Feldmann, J., Albrecht, T., Khroulev, C., Pattyn, F., and Levermann, A.: Resolution-dependent performance of grounding line motion in a shallow model compared with a full-Stokes model according to the MISMIP3d intercomparison, *Journal of Glaciology*, 60, 353–360, doi:10.3189/2014JoG13J093, 2014.
- Fox-Maule, C., Purucker, M. E., Olsen, N., and Mosegaard, K.: Heat Flux Anomalies in Antarctica Revealed by Satellite Magnetic Data, *Science*, 309, 464–467, 2005.
- 10 Fretwell, P., Pritchard, H. D., Vaughan, D. G., Bamber, J. L., Barrand, N. E., Bell, R., Bianchi, C., Bingham, R. G., Blankenship, D. D., Casassa, G., Catania, G., Callens, D., Conway, H., Cook, A. J., Corr, H. F. J., Damaske, D., Damm, V., Ferraccioli, F., Forsberg, R., Fujita, S., Gim, Y., Gogineni, P., Griggs, J. A., Hindmarsh, R. C. A., Holmlund, P., Holt, J. W., Jacobel, R. W., Jenkins, A., Jokat, W., Jordan, T., King, E. C., Kohler, J., Krabill, W., Riger-Kusk, M., Langley, K. A., Leitchenkov, G., Leuschen, C., Luyendyk, B. P., Matsuoka, K., Mouginit, J., Nitsche, F. O., Nogi, Y., Nost, O. A., Popov, S. V., Rignot, E., Rippin, D. M., Rivera, A., Roberts, J., Ross, N., Siegert, M. J.,
- 15 Smith, A. M., Steinhage, D., Studinger, M., Sun, B., Tinto, B. K., Welch, B. C., Wilson, D., Young, D. A., Xiangbin, C., and Zirizzotti, A.: Bedmap2: improved ice bed, surface and thickness datasets for Antarctica, *The Cryosphere*, 7, 375–393, 2013.
- Gagliardini, O., Cohen, D., Raback, P., and Zwinger, T.: Finite-element modeling of subglacial cavities and related friction law, *J. Geophys. Res.*, 112, doi:10.1029/2006JF000576, 2007.
- Gladstone, R. M., Payne, A. J., and Cornford, S. L.: Parameterising the Grounding Line in Ice Sheet Models, *The Cryosphere*, 4, 605–619,
- 20 doi:10.5194/tc-4-605-2010, 2010.
- Gladstone, R. M., Payne, A. J., and Cornford, S. L.: Resolution requirements for grounding-line modelling: sensitivity to basal drag and ice-shelf buttressing, *Annals of Glaciology*, 53, 97–105, doi:10.3189/2012AoG60A148, 2012.
- Glasser, N. F. and Siegert, M. J.: Calculating basal temperatures in ice sheets: an Excel spreadsheet method, *Earth Surface Processes and Landforms*, 27, 673–680, doi:10.1002/esp.344, 2002.
- 25 Golledge, N. R. and Levy, R. H.: Geometry and dynamics of an East Antarctic Ice Sheet outlet glacier, under past and present climates, *Journal of Geophysical Research: Earth Surface*, 116, doi:10.1029/2011JF002028, f03025, 2011.
- Golledge, N. R., Kowalewski, D. E., Naish, T. R., Levy, R. H., Fogwill, C. J., and Gasson, E. G. W.: The multi-millennial Antarctic commitment to future sea-level rise, *Nature*, 526, 421–425, 2015.
- Gudmundsson, G. H., Krug, J., Durand, G., Favier, L., and Gagliardini, O.: The Stability of Grounding Lines on Retrograde Slopes, *The*
- 30 *Cryosphere Discuss.*, 6, 2597–2619, doi:10.5194/tcd-6-2597-2012, 2012.
- Hindmarsh, R. C. A.: Qualitative Dynamics of Marine Ice Sheets, in: *Ice in the Climate System*, edited by Peltier, W., NATO ASI Series I (12), pp. 67–99, Berlin, Springer-Verlag, 1993.
- Hindmarsh, R. C. A.: On the Numerical Computation of Temperature in an Ice Sheet, *J. Glaciol.*, 45, 568–574, 1999.
- Hindmarsh, R. C. A.: Stress gradient damping of thermoviscous ice flow instabilities, *Journal of Geophysical Research: Solid Earth*, 111,
- 35 doi:10.1029/2005JB004019, b12409, 2006.
- Hindmarsh, R. C. A.: Consistent generation of ice-streams via thermo-viscous instabilities modulated by membrane stresses, *Geophysical Research Letters*, 36, doi:10.1029/2008GL036877, 106502, 2009.

- Hindmarsh, R. C. A., Leysinger Vieli, G. J. M. C., and Parrenin, F.: A Large-Scale Numerical Model for Computing Isochrone Geometry, *Ann. Glaciol.*, 50, 130–140, 2009.
- Holland, D. M. and Jenkins, A.: Modeling Thermodynamic Ice-Ocean Interactions at the Base of an Ice Shelf, *J. Phys. Oceanogr.*, 29, 1787–1800, 1999.
- 5 Holland, P. R., Jenkins, A., and Holland, D. M.: The response of ice shelf basal melting to variations in ocean temperature., *Journal of Climate*, 21, 2008.
- Hooke, R.: *Principles of Glacier Mechanics*, Principles of Glacier Mechanics, Cambridge University Press, 2005.
- Hulton, N. R. J. and Minster, M. J.: Modelling self-organization in ice streams, *Annals of Glaciology*, 30, 127–136, doi:doi:10.3189/172756400781820561, 2000.
- 10 Hutter, K.: *Theoretical Glaciology*, Dordrecht, Kluwer Academic Publishers, 1983.
- Huybrechts, P.: A 3-D Model for the Antarctic Ice Sheet: a Sensitivity Study on the Glacial-Interglacial Contrast, *Climate Dyn.*, 5, 79–92, 1990.
- Huybrechts, P.: The Antarctic Ice Sheet and Environmental Change: a Three-Dimensional Modelling Study, *Berichte für Polarforschung*, 99, 1–241, 1992.
- 15 Huybrechts, P.: Sea-level Changes at the LGM from Ice-Dynamic Reconstructions of the Greenland and Antarctic Ice Sheets during the Glacial Cycles, *Quaternary Science Reviews*, 21, 203–231, 2002.
- Huybrechts, P. and de Wolde, J.: The dynamic response of the Greenland and Antarctic ice sheets to multiple-century climatic warming, *Journal of Climate*, 12, 2169–2188, 1999.
- Huybrechts, P., Payne, A., and The EISMINT Intercomparison Group: The EISMINT Benchmarks for Testing Ice-Sheet Models, *Ann. Glaciol.*, 23, 1–12, 1996.
- 20 Huybrechts, P., Abe-Ouchi, A., Marsiat, I., Pattyn, F., Payne, A., Ritz, C., and Rommelaere, V.: Report of the Third EISMINT Workshop on Model Intercomparison, European Science Foundation (Strasbourg), 1998.
- Joughin, I., Smith, B. E., and Medley, B.: Marine Ice Sheet Collapse Potentially Under Way for the Thwaites Glacier Basin, West Antarctica, *Science*, 344, 735–738, doi:10.1126/science.1249055, 2014.
- 25 Katz, R. F. and Worster, M. G.: Stability of ice-sheet grounding lines, *Proc. R. Soc. A*, p. 10.1098/rspa.2009.0434, 2010.
- Kavanaugh, J. L. and Cuffey, K. M.: Dynamics and mass balance of Taylor Glacier, Antarctica: 2. Force balance and longitudinal coupling, *Journal of Geophysical Research: Earth Surface*, 114, doi:10.1029/2009JF001329, f04011, 2009.
- Larour, E., Seroussi, H., Morlighem, M., and Rignot, E.: Continental Scale, High Order, High Spatial Resolution, Ice Sheet Modeling using the Ice Sheet System Model, *J. Geophys. Res.*, 117, 10.1029/2011JF002140, 2012.
- 30 Levermann, A. and Winkelmann, R.: A simple equation for the melt elevation feedback of ice sheets, *The Cryosphere*, 10, 1799–1807, doi:10.5194/tc-10-1799-2016, 2016.
- Levermann, A., Albrecht, T., Winkelmann, R., Martin, M. A., Haseloff, M., and Joughin, I.: Kinematic first-order calving law implies potential for abrupt ice-shelf retreat, *The Cryosphere*, 6, 273–286, doi:10.5194/tc-6-273-2012, 2012.
- Ma, Y., Gagliardini, O., Ritz, C., Gillet-Chaulet, F., Durand, G., and Montagnat, M.: Enhancement factors for grounded ice and ice shelves inferred from an anisotropic ice-flow model, *Journal of Glaciology*, 56, 805–812, doi:10.3189/002214310794457209, 2010.
- 35 MacAyeal, D. R.: Large-scale Ice Flow over a Viscous Basal Sediment: Theory and Application to Ice Stream B, Antarctica, *J. Geophys. Res.*, 94, 4071–4087, 1989.

- MacAyeal, D. R., Rommelaere, V., Huybrechts, P., Hulbe, C. L., Determann, J., and Ritz, C.: An Ice-Shelf Model Test based on the Ross Ice Shelf, *Ann. Glaciol.*, 23, 46–51, 1996.
- Machguth, H., MacFerrin, M., van As, D., Box, J. E., Charalampidis, C., Colgan, W., Fausto, R. S., Meijer, H. A. J., Mosley-Thompson, E., and van de Wal, R. S. W.: Greenland meltwater storage in firn limited by near-surface ice formation, *Nature Climate Change*, doi:10.1038/nclimate2899, 2016.
- 5 Maris, M. N. A., de Boer, B., Ligtenberg, S. R. M., Crucifix, M., van de Berg, W. J., and Oerlemans, J.: Modelling the evolution of the Antarctic ice sheet since the last interglacial, *The Cryosphere*, 8, 1347–1360, doi:10.5194/tc-8-1347-2014, 2014.
- Martin, M. A., Winkelmann, R., Haseloff, M., Albrecht, T., Bueller, E., Khroulev, C., and Levermann, A.: The Potsdam Parallel Ice Sheet Model (PISM-PIK) Part 2: Dynamic equilibrium simulation of the Antarctic ice sheet, *The Cryosphere*, 5, 727–740, doi:10.5194/tc-5-727-2011, 2011.
- 10 Mengel, M. and Levermann, A.: Ice plug prevents irreversible discharge from East Antarctica, *Nature Climate Change*, 4, 451–455, doi:10.1038/nclimate2226, 2014.
- Mercer, J.: West Antarctic Ice Sheet and CO₂ Greenhouse Effect: a Threat of Disaster, *Nature*, 271, 321–325, 1978.
- Morland, L.: Unconfined Ice-Shelf Flow, in: *Dynamics of the West Antarctica Ice Sheet*, edited by van der Veen, C. J. and Oerlemans, J., pp. 15 99–116, Kluwer Acad., Dordrecht, Netherlands, 1987.
- Morlighem, M., Seroussi, H., Larour, E., and Rignot, E.: Inversion of basal friction in Antarctica using exact and incomplete adjoints of a higher-order model, *Journal of Geophysical Research: Earth Surface*, 118, 1746–1753, doi:10.1002/jgrf.20125, 2013.
- Nowicki, S., Bindschadler, R. A., Abe-Ouchi, A., Aschwanden, A., Bueller, E., Choi, H., Fastook, J., Granzow, G., Greve, R., Gutowski, G., Herzfeld, U., Jackson, C., Johnson, J., Khroulev, C., Larour, E., Levermann, A., Lipscomb, W. H., Martin, M. A., Morlighem, M., Parizek, 20 B. R., Pollard, D., Price, S. F., Ren, D., Rignot, E., Saito, F., Sato, T., Seddik, H., Seroussi, H., Takahashi, K., Walker, R., and Wang, W. L.: Insights into spatial sensitivities of ice mass response to environmental change from the SeaRISE ice sheet modeling project I: Antarctica, *Journal of Geophysical Research: Earth Surface*, 118, 1002–1024, doi:10.1002/jgrf.20081, 2013.
- Pattyn, F.: Numerical Modelling of a Fast-Flowing Outlet Glacier: Experiments with Different Basal Conditions, *Ann. Glaciol.*, 23, 237–246, 1996.
- 25 Pattyn, F.: Antarctic Subglacial Conditions inferred from a Hybrid Ice Sheet/Ice Stream Model, *Earth Planet. Sci. Lett.*, 295, 451–461, 2010.
- Pattyn, F. and Durand, G.: Why marine ice sheet model predictions may diverge in estimating future sea level rise, *Geophysical Research Letters*, 40, 4316–4320, doi:10.1002/grl.50824, 2013.
- Pattyn, F., Huyghe, A., De Brabander, S., and De Smedt, B.: Role of Transition Zones in Marine Ice Sheet Dynamics, *J. Geophys. Res.*, 111, 10.1029/2005JF000394, 2006.
- 30 Pattyn, F., Schoof, C., Perichon, L., Hindmarsh, R. C. A., Bueller, E., de Fleurian, B., Durand, G., Gagliardini, O., Gladstone, R., Goldberg, D., Gudmundsson, G. H., Huybrechts, P., Lee, V., Nick, F. M., Payne, A. J., Pollard, D., Rybak, O., Saito, F., and Vieli, A.: Results of the Marine Ice Sheet Model Intercomparison Project, MISMIIP, *The Cryosphere*, 6, 573–588, doi:10.5194/tc-6-573-2012, 2012.
- Pattyn, F., Perichon, L., Durand, G., Favier, L., Gagliardini, O., Hindmarsh, R. C., Zwinger, T., Albrecht, T., Cornford, S., Docquier, D., Fürst, J. J., Goldberg, D., Gudmundsson, G. H., Humbert, A., Hütten, M., Huybrechts, P., Jouvét, G., Kleiner, T., Larour, E., Martin, 35 D., Morlighem, M., Payne, A. J., Pollard, D., Rückamp, M., Rybak, O., Seroussi, H., Thoma, M., and Wilkens, N.: Grounding-line migration in plan-view marine ice-sheet models: results of the ice2sea MISMIIP3d intercomparison, *Journal of Glaciology*, 59, 410–422, doi:10.3189/2013JoG12J129, 2013.
- Payne, A. J.: Limit Cycles in the Basal Thermal Regime of Ice Sheets, *J. Geophys. Res.*, 100, 4249–4263, 1995.

- Payne, A. J. and Dongelmans, P. W.: Self-organisation in the Thermomechanical Flow of Ice Sheets, *J. Geophys. Res.*, 102, 12 219–12 234, 1997.
- Payne, A. J., Huybrechts, P., Abe-Ouchi, A., Calov, R., Fastook, J. L., Greve, R., Marshall, S. J., Marsiat, I., Ritz, C., Tarasov, L., and Thomassen, M.: Results from the EISMINT Model Intercomparison: the Effects of Thermomechanical Coupling, *J. Glaciol.*, 46, 227–238, 2000.
- Pollard, D. and DeConto, R. M.: Modelling West Antarctic Ice Sheet Growth and Collapse Through the Past Five Million Years, *Nature*, 458, 10.1038/nature07 809, 2009.
- Pollard, D. and DeConto, R. M.: Description of a Hybrid Ice Sheet-Shelf Model, and Application to Antarctica, *Geosci. Model Dev.*, 5, 1273–1295, doi:10.5194/gmd-5-1273-2012, 2012a.
- Pollard, D. and DeConto, R. M.: A simple inverse method for the distribution of basal sliding coefficients under ice sheets, applied to Antarctica, *The Cryosphere*, 6, 953–971, doi:10.5194/tc-6-953-2012, 2012b.
- Pollard, D., DeConto, R. M., and Alley, R. B.: Potential Antarctic Ice Sheet retreat driven by hydrofracturing and ice cliff failure, *Earth and Planetary Science Letters*, 412, 112 – 121, 2015.
- Purucker, M.: Geothermal heat flux data set based on low resolution observations collected by the CHAMP satellite between 2000 and 2010, and produced from the MF-6 model following the technique described in Fox Maule et al. (2005), <http://websrv.cs.umt.edu/isis/index.php>, 2013.
- Reeh, N.: Parameterization of melt rate and surface temperature on the Greenland ice sheet, *Polarforschung*, 59, 113–128, 1989.
- Ridley, J., Gregory, J. M., Huybrechts, P., and Lowe, J.: Thresholds for irreversible decline of the Greenland ice sheet, *Clim. Dyn.*, 35, 1049–1057, 2010.
- Rignot, E., Mouginot, J., and Scheuchl, B.: Ice Flow of the Antarctic Ice Sheet, *Science*, 333, 1427–1430, 2011.
- Rignot, E., Mouginot, J., Morlighem, M., Seroussi, H., and Scheuchl, B.: Widespread, rapid grounding line retreat of Pine Island, Thwaites, Smith, and Kohler glaciers, West Antarctica, from 1992 to 2011, *Geophysical Research Letters*, 41, 3502–3509, doi:10.1002/2014GL060140, 2014.
- Ritz, C., T. L. Edwards a, d. G. D., Payne, A. J., Peyaud, V., and Hindmarsh, R. C. A.: Potential sea-level rise from Antarctic ice-sheet instability constrained by observations, *Nature*, doi:10.1038/nature16147, 2015.
- Rommelaere, V. and Ritz, C.: A thermomechanical model of ice-shelf flow, *Annals of Glaciology*, 23, 13–20, 1996.
- Sato, T. and Greve, R.: Sensitivity experiments for the Antarctic ice sheet with varied sub-ice-shelf melting rates, *Annals of Glaciology*, 53, 221–228, doi:10.3189/2012AoG60A042, 2012.
- Scambos, T. A., Hulbe, C., Fahnestock, M., and Bohlander, J.: The link between climate warming and break-up of ice shelves in the Antarctic Peninsula, *Journal of Glaciology*, 46, 516–530, doi:doi:10.3189/172756500781833043, 2000.
- Scambos, T. A., Bohlander, J. A., Shuman, C. A., and Skvarca, P.: Glacier Acceleration and Thinning after Ice Shelf Collapse in the Larsen B Embayment, *Geophys. Res. Lett.*, 31, L18 402, 2004.
- Schodlok, M. P., Menemenlis, D., and Rignot, E. J.: Ice shelf basal melt rates around Antarctica from simulations and observations, *Journal of Geophysical Research: Oceans*, 121, 1085–1109, doi:10.1002/2015JC011117, 2016.
- Schoof, C.: Variational methods for glacier flow over plastic till, *Journal of Fluid Mechanics*, 555, 299–320, doi:10.1017/S0022112006009104, 2006.
- Schoof, C.: Ice Sheet Grounding Line Dynamics: Steady States, Stability and Hysteresis, *J. Geophys. Res.*, 112, doi:doi:10.1029/2006JF000664, 2007a.

- Schoof, C.: Marine ice sheet dynamics. Part I. The case of rapid sliding, *J. Fluid Mech.*, 573, 27–55, 2007b.
- Schoof, C.: Ice-sheet acceleration driven by melt supply variability, *Nature*, 468, 803–806, 2010.
- Schoof, C.: Marine ice sheet dynamics. Part 2. A Stokes flow contact problem, *J. Fluid Mech.*, 679, 122–155, 2011.
- Seroussi, H., Morlighem, M., Rignot, E., Mouginot, J., Larour, E., Schodlok, M., and Khazendar, A.: Sensitivity of the dynamics of Pine Island Glacier, West Antarctica, to climate forcing for the next 50 years, *The Cryosphere*, 8, 1699–1710, doi:10.5194/tc-8-1699-2014, 2014.
- Stokes, G.: On the theories of internal friction of fluids in motion, *Trans. Cambridge Philos. Soc.*, 8, 287–305, 1845.
- Thoma, M., Grosfeld, K., Barbi, D., Determann, J., Goeller, S., Mayer, C., and Pattyn, F.: RIMBAY – a multi-approximation 3D ice-dynamics model for comprehensive applications: model description and examples, *Geoscientific Model Development*, 7, 1–21, doi:10.5194/gmd-7-1-2014, 2014.
- Thomas, R. H.: The Dynamics of Marine Ice Sheets, *J. Glaciol.*, 24, 167–177, 1979.
- Truffer, M., Harrison, W. D., and Echelmeyer, K. A.: Glacier motion dominated by processes deep in underlying till, *Journal of Glaciology*, 46, 213–221, doi:10.3189/172756500781832909, 2000.
- Tsai, V. C., Stewart, A. L., and Thompson, A. F.: Marine ice-sheet profiles and stability under Coulomb basal conditions, *Journal of Glaciology*, 61, 205–215, doi:doi:10.3189/2015JoG14J221, 2015.
- Tulaczyk, S. M., Kamb, B., and Engelhardt, H. F.: Basal Mechanics of Ice Stream B, West Antarctica. II. Undrained-Plastic-Bed Model, *J. Geophys. Res.*, 105, 483–494, 2000a.
- Tulaczyk, S. M., Kamb, B., and Engelhardt, H. F.: Basal Mechanics of Ice Stream B, West Antarctica. I. Till Mechanics, *J. Geophys. Res.*, 105, 463–481, 2000b.
- Van Wessem, J., Reijmer, C., Morlighem, M., Mouginot, J., Rignot, E., Medley, B., Joughin, I., Wouters, B., Depoorter, M., Bamber, J., Lenaerts, J., De Van Berg, W., Van Den Broeke, M., and Van Meijgaard, E.: Improved representation of East Antarctic surface mass balance in a regional atmospheric climate model, *Journal of Glaciology*, 60, 761–770, doi:doi:10.3189/2014JoG14J051, 2014.
- Vieli, A. and Payne, A.: Assessing the Ability of Numerical Ice Sheet Models to Simulate Grounding Line Migration, *J. Geophys. Res.*, 110, doi:doi:10.1029/2004JF000202, 2005.
- Weertman, J.: Stability of the Junction of an Ice Sheet and an Ice Shelf, *J. Glaciol.*, 13, 3–11, 1974.
- Weertman, J.: Milankovitch solar radiation variations and ice age ice sheet sizes, *Nature*, 261, 17–20, 1976.
- Winkelmann, R., Martin, M. A., Haseloff, M., Albrecht, T., Bueller, E., Khroulev, C., and Levermann, A.: The Potsdam Parallel Ice Sheet Model (PISM-PIK) Part 1: Model description, *The Cryosphere*, 5, 715–726, 2011.
- Winkelmann, R., Levermann, A., Ridgwell, A., and Caldeira, K.: Combustion of available fossil fuel resources sufficient to eliminate the Antarctic Ice Sheet, *Science Advances*, 1, doi:10.1126/sciadv.1500589, 2015.